THEORETICAL MODELING OF THE ACTUATION MECHANISM IN INTEGRATED INDUCED STRAIN ACTUATOR/SUBSTRUCTURE SYSTEMS
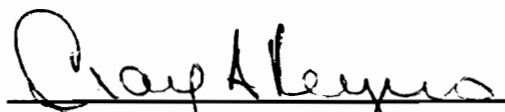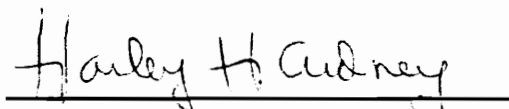
by

Mark Wen-Yih Lin

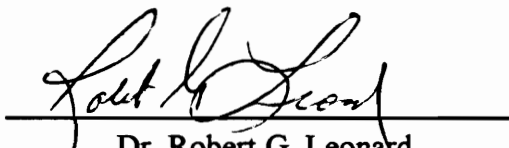Dissertation submitted to the Faculty of the

Virginia Polytechnic Institute and State University

in partial fulfillment of the requirements for the degree of

Doctor of Philosophy

in

Mechanical Engineering

APPROVED:

_____

Dr. Craig A. Rogers, Chairman

_____
Dr. Harley H. Cudney

_____
Dr. O. Hayden Griffin, Jr.

_____
Dr. Robert G. Leonard

_____
Dr. Harry H. Robertshaw

July, 1993

Blacksburg, Virginia

THEORETICAL MODELING OF THE ACTUATION MECHANISM IN INTEGRATED INDUCED STRAIN ACTUATOR/SUBSTRUCTURE SYSTEMS

(Abstract)

Induced strain actuators have been integrated with conventional structural materials to serve as energy input devices or actuating elements in many engineering applications implementing intelligent material systems and structures concepts. In order to use the actuation mechanism produced by the integrated induced strain actuators efficiently, the mechanics of the mechanical interaction between the actuator and the host substructure must be understood and modeled accurately. A refined analytical model has been developed based on the plane stress formulation of the theory of elasticity for a surface-bonded induced strain actuator/beam substructure system. Closed-form solutions of the induced stress field were obtained in an approximate manner using the principle of stationary complementary energy. The model has also been extended to include the presence of adhesive bonding layers and applied external loads. The results of the current model were compared with those obtained by finite element analysis and the pin-force and Euler-Bernoulli models.

It was shown that the current model is capable of describing the edge effects of the actuator on actuation force/moment transfer and interfacial shear and peeling stress distributions that the existing analytical models fail to describe. Good agreement was obtained between the current model and the finite element analysis in terms of predicting actuation force/moment transfer. The interfacial shear stress distribution obtained by the current model satisfies stress-free boundary conditions at the ends of the actuator, which

the finite element model is not able to satisfy. The current model correctly describes the transfer of the actuation mechanism and the resulting interfacial stress distributions; thus, it can be used in designing integrated induced strain actuator/substructure systems.

Moreover, a new induced strain actuator configuration, which includes inactive edges on the ends of the actuators, has been proposed to alleviate the intensity of the interfacial stresses. The effectiveness of the actuator on the interfacial stress alleviation was verified by the current analytical model and finite element analysis. It was shown that the proposed actuator configuration can significantly alleviate intensive interfacial shear and peeling stresses without sacrificing the effectiveness of the actuation mechanism. The chances of interfacial failure of the integrated structural system, fatigue failure in particular, can thus be reduced.

Acknowledgments

I would like to express my gratitude to Dr. Craig Rogers, my major advisor, for his guidance and advice throughout my study. I am also very grateful to all my committee members for the valuable suggestions and comments on this dissertation.

I also wish to thank all the staff and students in the Center for Intelligent Material Systems and Structures for their gracious support at all times. I would especially like to thank Ms. Beth Howell for her help on the writing and meticulous proof-reading of my papers.

My special thanks to my wife, Chi-Ping (Kathy), without her support with love and patience throughout my graduate study, this work would not have been possible. Also, I would like to thank her for the typing of the manuscript for this dissertation. I would also like to express may special gratitude to my parents, my sister, and my brother-in-low for their continued support and financial assistance.

Finally, I would like to gratefully acknowledge the support of the Office of Naval Research.

Table of Contents

List of Figures

List of Tables

Chapter 1

Introduction and Literature Review

1.1 Introduction to Intelligent Material Systems and Structures

Motivated by the performance requirements of the advanced structural systems of the future, structural engineers have been pursuing a new approach to structural and material design. The goal of this new approach is to develop material systems and structures that can rearrange themselves to their most optimum functional capabilities to adapt to external stimuli such as load and environmental disturbance by using inherent or integral functional elements such as sensors, actuators, and controllers. From this effort pursued for the past decade in the structural engineering community, the concept of developing a higher form of material systems and structures that possess 'life' functions of sensing, actuation, control and intelligence has led to a new field of endeavor in advanced technology.

Since the emergence of this new technology, there has been much discussion related to the definition of intelligent material systems and structures. Wada et al. (1990) define intelligent structures as structures that contain highly integrated sensors, actuators, and a control system. The construction of the intelligent structures involves distribution and integration of not only sensing and actuating elements, but also of electronic components involved in signal conditioning, computing, and power regulation.

Takagi (1990) define intelligent materials beyond the primitive functions, i.e., sensor, effector/actuator, and processor capabilities, as intelligent functions and social utility. The intelligent functions indicate that the intelligence is inherent in the materials, i.e., self-learning, self-repair, prediction/notification, etc. The social utility represents the intelligence level from the viewpoint of human beings such as human friendliness, environmental harmony, reliability, etc.

Recently, Rogers (1993) proposed a design philosophy based on a science paradigm to provide guidance on creating such a material system. Rogers states that the objective of the concept is to create artifacts by instilling intelligence in the microstructure to reduce the mass and energy of the system to perform adaptive functions. The vision or guidance of the creation is to learn from nature and living systems and establish a similar or even superior sophisticated architecture of the nerves, muscles and brain networks found in biological systems in the man-made artifacts with inherent or integrating analogous sensors, actuators, and control system.

Engineering applications implementing intelligent material systems and structures concepts have demonstrated many prominent functional capabilities that the integrated sensors, actuators, and control system can achieve. Successful examples have been reported in the areas such as structural vibration and acoustic control, material/structure health monitoring and damage control, nondestructive evaluation, structural shape and motion control, etc. (Rogers, 1990). The prospective evolution of science and technology invoked by the concept of intelligent material systems and structures is enormous. The

2

concept may be applied to such diverse fields of science and technology as aerospace engineering, automobile industry, civil engineering, and biomedical engineering, etc. As stated by Takagi (1990) "the science and technology in the coming twenty-first century, will rely heavily on the development of new materials ... 'intelligent materials' are leading candidates for such new materials."

1.2 Mechanism of Induced Strain Actuation

One of the primitive functions in intelligent material systems and structures is the actuation capability. This includes the ability to actively change material/structural physical and/or chemical characteristics such as geometry, color, mechanical properties, chemical composition, electrical properties, etc. In practice, various desired actuation capabilities require different actuators for the actuating mechanisms they provide. For the purpose of actively altering the material/structural geometrical configurations, mechanical properties, and internal stress/strain distributions, materials which are able to induce noticeable strains by nonmechanical stimuli are natural candidates. These types of actuating materials are usually classified as "induced strain actuators".

Induced strain actuators refer to materials that exhibit coupling of some degree between their geometric configuration and a nonmechanical stimulus. In principle, there are a number of materials possessing induced strain phenomena coupled with various stimuli. Nevertheless, the most commonly used induced strain actuators in intelligent material systems and structures are those of electromechanical, magnetomechanical, or

3

thermomechanical type.   Piezoelectrics and electrostrictors whose induced strains are coupled to an applied electric field, magnetostrictors which couple strains with magnetic fields, and shape memory alloys and thermal actuators which couple strains with applied temperature differentials are examples of commonly used induced strain actuators.

In general, the constitutive relations for induced strain actuators have the form: $\varepsilon = \sigma / E + \lambda$, where λ is termed free induced strain, which is activated by nonmechanical stimuli depending on the coupling characteristics of the actuators, and enters into the equation in a manner analogous to the thermal strains of conventional structural materials.   The characteristic induced strain can be used to achieve desired actuation functionalities in a structure by integrating induced strain actuators, either embedded or surface-bonded, with the structure.

Activation of the induced strain actuators by applying nonmechanical stimuli will cause a mismatch on the strain fields in the actuators and the host substructure, resulting in an alteration of the internal stress state and the apparent strain of the integrated structural system. Figure 1.1 illustrates the deformations of a beam-like structure with symmetrically surface-bonded induced strain actuators activated in pure extension and pure bending modes. This induced strain actuation mechanism can be controlled to purposefully vary the physical characteristics and geometric configurations of the material systems and; consequently, to achieve the desired actuation capability of the structural system.
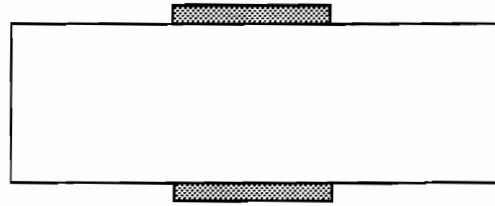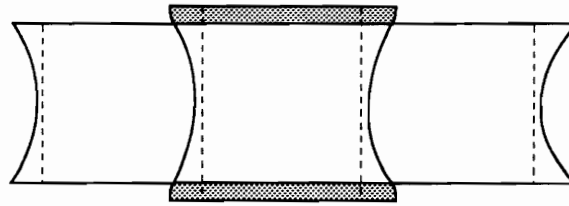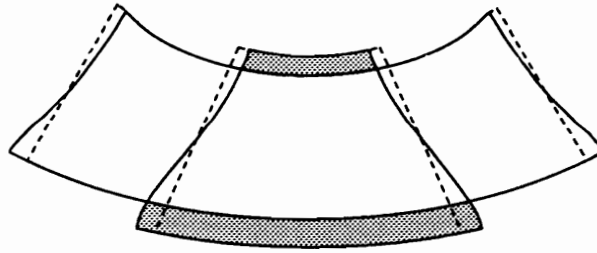
Figure 1.1. Schematic deformation patterns of a beam structure with surface-bonded induced strain actuators: (*a*) undeformed geometry, (*b*) pure extension actuation, (*c*) pure bending actuation.

A number of research work using the induced strain actuation mechanism produced by integrated induced strain actuators has been reported in the area of active structural vibration and acoustic control. Bailey and Hubbard (1985) used piezoelectric polymer film (PVDF) as a distributed actuator to actively damp structural vibration. A substantial increase in baseline damping was reported for the first vibration mode of a cantilever beam with a layer of PVDF film covering all over the beam on one side. Fanson and Chen (1986) demonstrated the control authority using surface-bonded piezoceramic actuators/ sensors in the vibration suppression for large flexible space structures. It was shown that multi-mode vibration suppression can be achieved with dramatic reduction in dynamic response. The effectiveness of using integrated piezoelectric actuators/sensors has also been demonstrated in active torsional and bending control of laminated composite plates (Lee, 1987), in torsional vibrational control of tube type structures (Sung et al., 1990), and in dynamic control of slewing motion of flexible structures (Garcia and Inman, 1990).

Dimitriadis et al. (1991) used piezoceramic actuator patches for distributed noise and vibration excitation of thin plates. It was shown that piezoactuators are effective to either excite or suppress particular modes of the plate. Structural acoustic control using shape memory alloy actuators has also been investigated by Liang et al. (1991) for composite plates. It was demonstrated that with the capability to tune the natural frequency and the mode shapes by activating the shape memory alloy actuators, the directivity pattern, radiation efficiency, and transmission loss of the composite plates can be purposefully modified.

The adaptive structural control techniques using integrated induced strain actuators has been implemented in the control of flight vehicles. Scott and Weisshaar (1991) conducted a feasibility study on the use of integrated piezoceramic actuators to control panel flutter of atmospheric flight vehicles. Librescu et al. (1992) employed distributed piezoelectric actuators to actively control the excessive deflections and large bending moments of aircraft wing structures carrying heavy tip weights. It was shown that the piezoelectric actuators are capable of alleviating, without weight penalties, the undesired deflection and bending effects.

The mechanism of induced strain actuation has also been used for material damage control. Rogers et al. (1991) used embedded or surface-bonded induced strain actuators to reduce stress intensity at the highly-stressed area of a structure. It was demonstrated that the fatigue life span of the materials can be increased using piezoelectric actuators to reduce the amplitude of fatigue stress caused by external fatigue loads and the crack tip stress concentration can be alleviated by activating a shape memory alloy actuator embedded near the crack tip. The concept was also used by Sensharma et al. (1992) to reduce static stress concentration in an isotropic plate with a hole. It was shown that the stress concentration around the hole can be reduced substantially by applying induced strains over a small area around the hole.

Another application using induced strain actuation mechanism is the active shape precision control. Sato et al. (1980) used piezoelectric polymer film (PVDF) bonded on the nonoptical surface of a laminar glass mirror to obtain the desired smooth curves on the

optical surface. Haftka and Adelman (1985) used thermal actuators, the materials which have much higher coefficients of thermal expansion than do the structural materials, to minimize the overall distortion of a large flexible space structure from its ideal shape. It was shown that for a 55-m radiometer antenna reflector subjected to orbital heating, reductions in distortion up to a factor of three can be realized.

1.3 Modeling of Induced Strain Actuation Mechanism

Ensuring the effectiveness and reliability of integrated induced strain actuators requires an understanding of the mechanics of the mechanical interaction between the actuators and the host substructures. One of the most fundamental issues is to determine, a priori, the actuation effects being induced in the substructure and the resulting overall structural response. Another important aspect related to the physical design of the system is the determination of interfacial shear and peeling stresses that, coupled with interfacial bonds of low strength, usually result in the failure of structural integrity. To investigate these issues, a mechanical model capable of describing the mechanical coupling at different levels of actuator excitation is needed.

Modeling of the actuation mechanism in the integrated actuator/substructure system is not an easy task. The presence of the geometric and material discontinuities of the structural system brings about a strong coupling between in-plane and transverse deformation and stresses at the interface near the actuator edges. This, in turn, produces a highly

complicated three-dimensional stress state difficult to model with simple analytical schemes.

Over the past decade, simplified approaches have been suggested in modeling the mechanical interaction between induced strain actuators coupled with host substructures. The first comprehensive analytical model appears in the work by Crawley and de Luis (1987). Two distinct one-dimensional mechanical models were derived for elastic beam structures with induced strain actuator patches that are either bonded to the beam surface or embedded in a laminate composite beam. The first model, dealing with the case of surface-bonded actuators, assumes a uniform through-the-thickness strain in the actuators and an Euler-Bernoulli strain distribution, i.e., uniform strain in pure extension/contraction mode and linear strain in pure bending mode, in the beam substrate. The magnitude of the strains is then determined from the overall force and moment equilibrium of the resulting stress field in each constituent. Figure 1.2 shows the assumed strain distributions for pure extension and pure bending actuation.

This model was subsequently rederived from force transfer considerations and was termed the "pin-force" model (Lazarus and Crawley, 1989). The effect of the actuators, based on the assumed uniform strain field, was effectively replaced by a pair of "pin" forces acting on the interfaces at the edges of the actuators. Figure 1.3 illustrates the pin-force mechanism for pure extension and pure bending actuation. It has been shown that for pure bending actuation this model gives a good approximation when the beam substrate is much thicker than the actuators. However, for relatively thin substrates, the model fails to
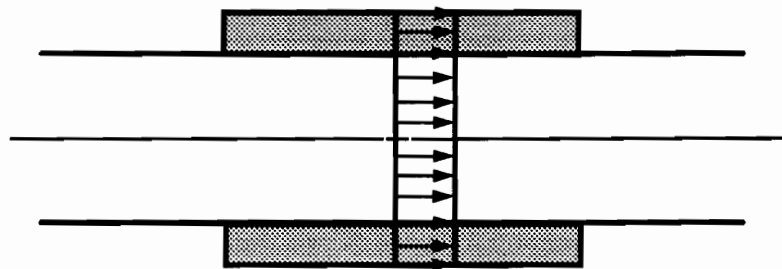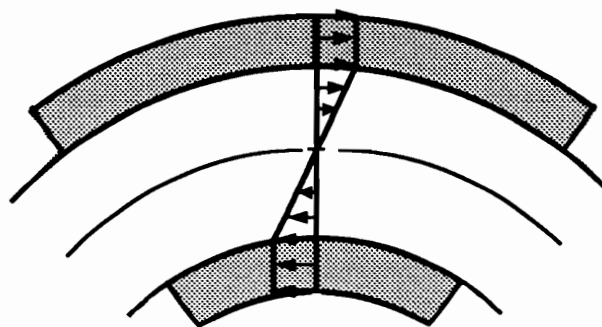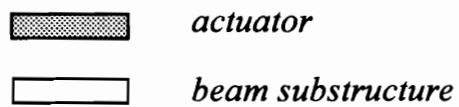
Figure 1.2. Assumed strain distributions in the uniform strain model: (*a*) pure extension mode, (*b*) pure bending mode (Crawley and de Luis, 1987).
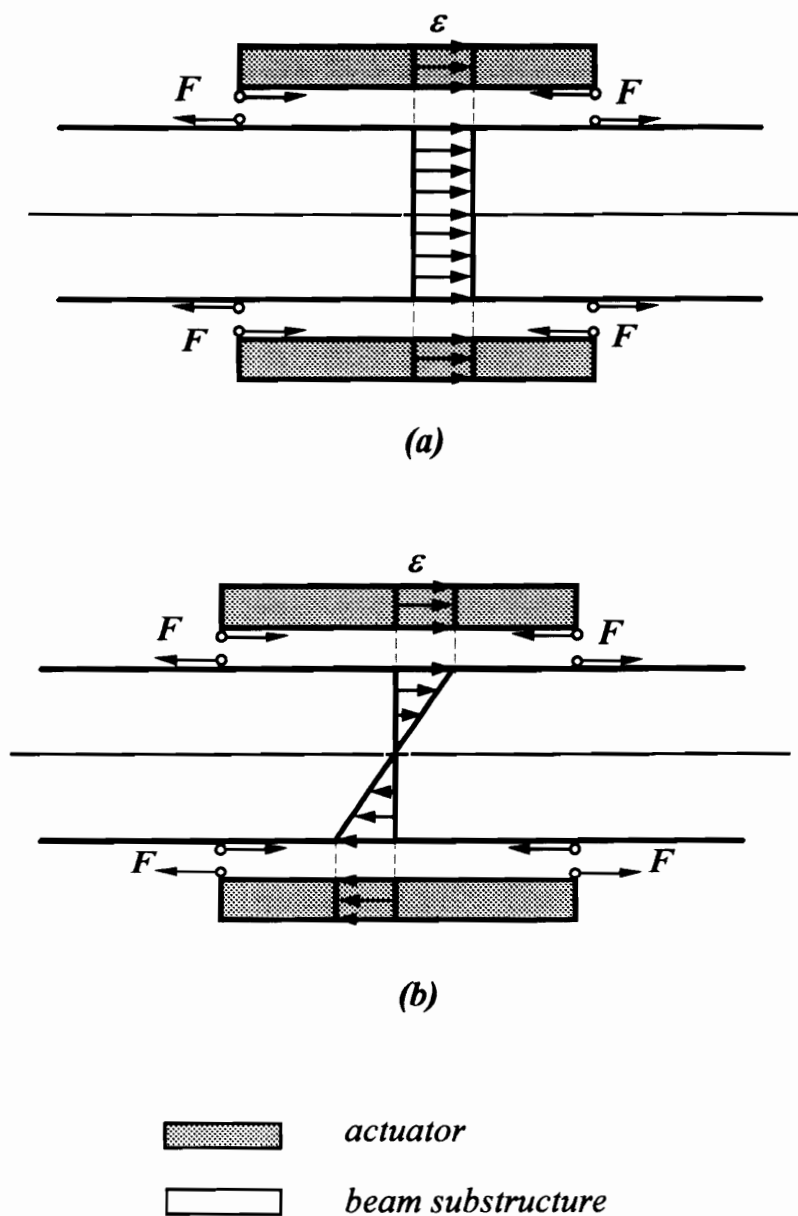
Figure 1.3. Schematic representation of pin-force model: (*a*) pure extension mode, (*b*) pure bending mode (Lazarus and Crawley, 1989).

11

account for the flexural rigidity of the actuators, resulting in an overestimation for the bending strain in the beam substrate.

The second model, dealing with both surface-bonded and embedded actuators, assumes Euler-Bernoulli strain distributions in both the actuator and the beam substrate. Figure 1.4 shows the assumed strain distributions for the cases of surface-bonded and embedded actuators. The strains in the actuators comply with the Euler-Bernoulli strain distribution for the integrated structure in spite of their locations. Explicit solutions for the magnitude of the strains, which results in overall force and moment equilibrium, were obtained in terms of the beam-to-actuator stiffness and thickness ratios and the free induced strain of the actuators.

To account for the influence of adhesive bonding layers, the shear lag theory was employed by Crawley and de Luis (1987). The theory represents the bonding layer with a thin shear lag in which the in-plane shear stress is the only stress component considered. The resulting strains in the beam substrate and the actuators were obtained in terms of the shear lag parameter which involves the thickness and shear stiffness of the bonding layer as well as the substrate-to-actuator stiffness and thickness ratios. This scheme helps explain the transfer of the actuation mechanism from the actuators to the host substructure; yet lacks quantitative accuracy due to the simplified stress state in the bonding layer.
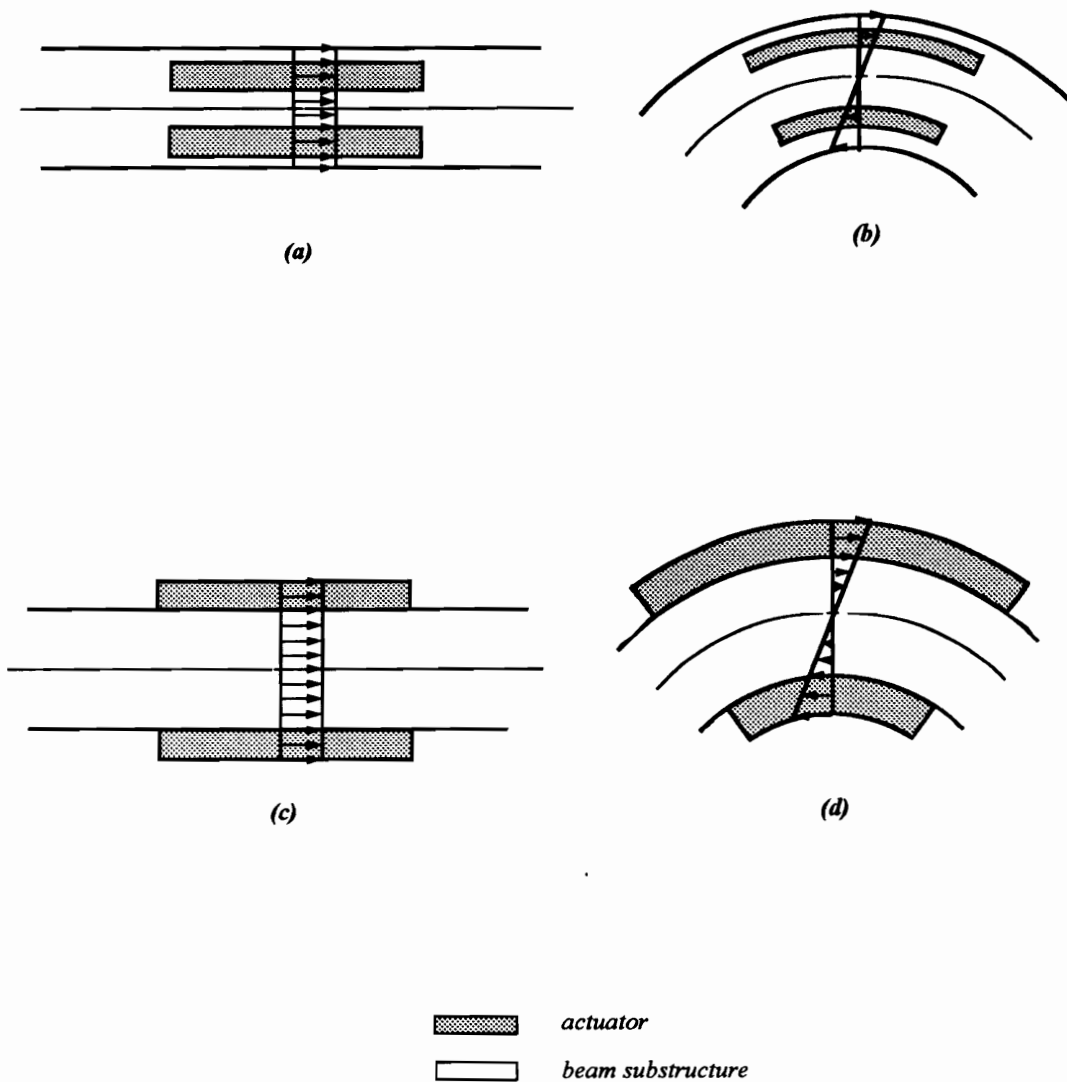
Figure 1.4. Assumed strain distributions in the Euler-Bernoulli model: (*a*) embedded actuators in pure extension mode, (*b*) embedded actuators in pure bending mode, (*c*) surface-bonded actuators in pure extension mode, (*d*) surface-bonded actuators in pure bending mode (Crawley and de Luis, 1987).

Lazarus and Crawley (1989) further extended the one-dimensional pin-force model to the two-dimensional pin-force plate model and the Euler-Bernoulli model to the consistent plate model for plate structures. The consistent plate model was designated because its strain field consists with the kinematic assumption of the classical lamination theory.

The presence of the spatial discontinuity of the actuator patches (surface-bonded or embedded) in a composite laminate, i.e., the patches only cover a portion of the structure, was treated by Wang and Rogers (1990) using classical lamination theory. A Heaviside step function was employed to describe the spatial distribution of the actuator patches. The actuation mechanism of the actuators were consequently represented by point forces and/or point moments acting on the substrate at the location of the actuator's edges. The model was later revised to include the mechanical interaction of the actuator and the host substructure using an assumed linear strain profile to derive the effective forces and moments on the substrate based on the conservation of strain energy (Wang and Rogers, 1991).

The study of the mechanical interaction between the actuators and the host substructure has also been undertaken using numerical approaches, mainly the finite element method. Robbins and Ready (1990) used a finite element approach to investigate the static and dynamic actuation behavior of a piezoelectrically actuated beam. The beam structure analyzed was a unsymmetric, three-layered, laminated beam, i.e., aluminum beam, adhesive layer, and piezoelectric actuator, where the only deformation impetus was an actuation strain induced in the actuator. The finite element models were developed using

14

four different displacement-based one-dimensional beam theories, all of which are derivable from the generalized laminated plate theory of Reddy (1987).

The first two finite element models coincide with classical beam theory and shear deformation beam theory, respectively, and were termed as equivalent single-layer models. The last two finite element models assume piece-wise linear distribution, not only for axial displacement but also for both axial and transverse displacements, respectively, and were termed multi-layer models. It was shown that only the second multi-layer model predicted a static stress distribution which satisfies all the traction boundary conditions of the problem. Nevertheless, the static stress fields predicted by all four models are similar except near the end of the actuator (i.e., within one laminate thickness of the end of the actuator). It was also demonstrated that for higher modes of vibration and/or beam structures with low aspect ratios, the modal amplitudes predicted by the multi-layer models differ significantly from those of the equivalent single-layer models.

The actuation response of a laminated composite plate with distributed piezoelectric actuators subjected to mechanical and/or electrical loadings was also modeled by Ha et al. (1991) using the finite element approach. The finite element model was based on a variational principle by combining the equilibrium equations of motion and the constitutive equation of piezoelectrics. An eight-node three-dimensional composite brick element was adopted for the analysis, and three-dimensional incompatible modes were considered to account for the bending response of the composites due to the deformation of the piezoelectrics. Numerical calculations were performed to simulate the experimental

15

results reported by Lazarus and Crawley (1989). Good agreement was obtained in comparing the results of longitudinal bending, transverse bending, and lateral twisting of cantilevered composite plates with surface-bonded distributed piezoelectric actuators.

Tzou and Tseng (1990a) also used the finite element approach to investigate the distributed dynamic sensing and actuation response of an elastic plate with surface-bonded piezoelectric actuators and sensors. A thin piezoelectric finite solid element with an internal degree of freedom was formulated using a variational method and the Hamilton's principle. Both strain and electrical energies of the piezoelectrics were considered in the formulation. The sensor and actuator equations of an integrated plate structure which consists of an elastic plate with two surface-bonded piezoelectrics (one serves as a distributed sensor and the other as a distributed actuator) were derived based on the framework of the Kirchhoff-Love assumptions. The active vibration control of an integrated plate structure was studied by the proposed finite element model using closed-loop constant-gain negative velocity feedback and constant-amplitude negative velocity feedback control algorithms. The finite element model was later extended for an integrated shell structure by generalizing the piezoelectric finite element to the tri-orthogonal curvilinear coordinate system of the shell (Tzou and Tseng, 1990b).

Recently, a continuum theory for piezoelectric shells was derived by Tzou and Zhong (1991). The electromechanical equations of motion and generalized boundary conditions of the piezoelectric shell subjected to mechanical and electrical excitations were derived using the Hamilton's principle and linear piezoelectric theory. Applications of the theory

were then demonstrated in the investigation of active vibration tuning for a piezoelectric bimorph cantilevered beam and a PVDF cylindrical shell.

The finite element method was also used by Shah et al. (1993) recently to model the mechanical interaction between piezoelectric actuators and substructure to determine static response and stress fields due to application of electric field to the actuator patches. Constitutive equations of the piezoelectrics were incorporated in the finite element formulation for in-plane stress analysis. A technique for evaluating nodal stresses at the patch boundary where material discontinuity is present was also developed to improve the accuracy of nodal stresses obtained by averaging the Gaussian stress conventional scheme.

In summary, many simple analytical schemes have been proposed to model the actuation mechanism to provide information for the purpose of designing integrated induced strain actuator/substructure systems. However, all of these models were developed based on the framework of the mechanics of material method. Since these formulations consider only axial normal stresses, they are not able to describe the complex stress state near the actuators' edges. Therefore, the solutions obtained are valid only in the region away from the edges, and provide no information about the shear and peeling stresses at the interfaces which are usually responsible for the failure in structural integrity.

The induced strain actuation mechanism can be modeled using the finite element method without strenuous effort, and this method offers a high degree of flexibility for different

geometric configurations. However, this method is inconvenient for parametric studies and the relatively time-consuming computation of the finite element analysis generally cannot fulfill the effective real-time adaptability or control required in most applications of intelligent structures.

Therefore, a refined model with a closed-form solution which can more accurately describe the mechanical interaction between the actuator and the host substrate, in particular the edge effect and the interfacial shear and peeling stress distribution, is in a great demand for efficient and reliable designs of the integrated induced strain actuator/substructure systems..

1.4 Research Objective

The primary objective of the present research is to develop a refined analytical model which is capable of describing the edge effects due to the presence of the free edges of the actuators and determining the interfacial shear and peeling stress distribution. The effective forces/moments induced by the actuator in the host substrate and the resulting interfacial stress intensity will be investigated. Parametric studies for different actuator-to-substrate geometry and material property ratios on the resulting actuation effect will be performed. Moreover, the influence of bonding layers which provide adhesion to the constituents and applied external loads on the actuation mechanism will also be modeled. It is expected that understanding the mechanics of the induced strain actuation mechanism and being able to model it correctly will provide more accurate information for designing

such an integrated structural system and will lead to the design of more effective induced strain actuators for use in intelligent material systems and structures.

In Chapter 2, the detailed formulation of the proposed analytical model for a beam structure with surface-bonded induced strain actuator patches is presented. The capability of the model is then demonstrated with numerical examples and the results are compared with finite element analyses. Chapter 3 expands the model to include the presence of bonding layers, which provide adhesion to the constituents. The effects of these bonding layers are subsequently studied. In Chapter 4, the influence of the applied external loads on the actuation mechanism is modeled and investigated. In Chapter 5, a new actuator configuration is proposed for the purpose of alleviating the intensity of interfacial shear and peeling stresses. The significance of the present research is finally summarized in the concluding chapter along with recommendations for further study.

1.5 Reference

Bailey, T. and Hubbard Jr., J. E., 1985, "Distributed Piezoelectric-Polymer Active Vibration Control of a Cantilever Beam," Journal of Guidance and Control, Vol. 8, No. 5, pp. 605-611.

Crawley, E. F. and de Luis, J., 1987, "Use of Piezoelectric Actuators as Elements of Intelligent Structures," AIAA Journal, Vol. 25, No. 10, pp. 1373-1385.

Dimitriadis, E. K., Fuller, C. R., and Rogers, C. A., 1991, "Piezoelectric Actuators for Distributed Vibration Excitation of Thin Plates," Journal of Vibration and Acoustics, Vol. 113, pp. 100-107.

Fanson, J. L. and Chen, J. C., 1986, "Structural Control by the Use of Piezoelectric Active Members," Proceedings of NASA/DOD Control/Structures Interaction Conference, NASA CP-2447, Part II.

Garcia, E. and Inman, D., 1990, "Advantages of Slewing an Active Structure," Journal of Intelligent Material Systems and Structures, Vol. 1, No. 3, pp. 261-272.

Ha, S. K., Keillers, C., and Chang, F.-K., 1991, "Analysis of Laminated Composites Containing Distributed Piezoelectric Ceramics," Journal of Intelligent Material Systems and Structures, Vol. 2, No. 1, pp. 59-71.

Haftka, R. T. and Adelman, H. M., 1985, "An Analytical Investigation of Shape Control of Large Space Structures by Applied Temperatures," AIAA Journal, Vol. 23, No. 3, pp. 450-457.

Lazarus, K. B. and Crawley, E. F., 1989, "Induced Strain Actuation of Composite Plates," GTL Report No. 197, Gas Turbine Laboratory, Massachusetts Institute of Technology, Cambridge, Massachusetts, March 1989.

Lee, C. K., 1987, "Piezoelectric Laminates for Torsional and Bending Modal Control: Theory and Experiment," Ph. D. Dissertation, Cornell University.

Liang, C., Rogers, C. A. and Fuller, C. R., 1991, "Acoustic Transmission and Radiation Analysis of Adaptive Shape Memory Alloy Reinforced Laminated Plates," Journal of Sound and Vibration, Vol. 144, No. 3.

Librescu, L., Rogers, C. A., and Song, O., 1992, "Adaptive Response Control of Wing Structures Carrying Heavy Tip Weights," Proceedings of the AIAA/ASME/ASCE/AHS/ASC 33rd SDM Conference, Dallas, TX, April 13-15, 1992.

Reddy, J. N., 1987, "A Generalization of Two-Dimensional Theories of Laminated Composite Plates," Communications in Applied Numerical Methods, Vol. 3, p. 173.

Robbins, D. H. and Reddy, J. N., 1990, "Finite Element Analysis of Piezoelectrically Actuated Beams," Report, Department of Engineering Science and Mechanics, Virginia Polytechnic Institute and State University, Blacksburg, Virginia, May 1990.

Rogers, C. A., 1990, "An Introduction to Intelligent Material Systems and Structures," in *Intelligent Structures* (Proceedings of the International Workshop on Intelligent Structures, Taipei, Taiwan, 23-26 July 1990), K. P. Chong, S. C. Liu and J. C. Li, Eds., Elsevier, London, pp. 3-41.

Rogers, C. A., Liang, C. and Li S., 1991, "Active Damage Control of Hybrid Material Systems Using Induced Strain Actuators," Proceedings of the AIAA/ASME/ASCE/AHS/ASC 32nd SDM Conference, Baltimore, MD, April 8-10, 1991,

Rogers, C. A., 1993, "Intelligent Material Systems - The Dawn of a New Materials Age," Editorial, Journal of Intelligent Material Systems and Structures, Vol. 4, No. 1, pp. 4-12.

Sato, T., Ishida, H. and Ikeda, O., 1980, "Adaptive PVDF Piezoelectric Deformable Mirror System," Applied Optics, Vol. 19, No. 9, pp. 1430-1434.

Scott, R. C. and Weisshaar, T. A., 1991, "Controlling Panel Flutter Using Adaptive Materials," Proceedings of the AIAA/ASME/ASCE/AHS/ASC 32nd SDM Conference, Baltimore, MD, April 8-10, 1991.

Sensharma, P. K., Palantera, M. J., and Haftka, R. T., 1992, "Stress Reduction in an Isotropic Plate with a Hole," Proceedings of the AIAA/ASME/ASCE/AHS/ASC 33rd SDM Conference, Dallas, TX, April 13-15, 1992.

Shah, D. K., Chan, W. S., and Joshi, S. P., 1993, "Finite Element Analysis of Plates with Piezoelectric Layers," Proceedings of the AIAA/ASME/ASCE/AHS/ASC 34th SDM Conference, La Jolla, CA, April 19-22, 1993.

Sung, C.-C., Varadan, V. V., Bao, X. Q. and Varadan, V. K., 1990, "Active Control of Torsional Vibration Using Piezoceramic Sensors and Actuators," Proceedings of the AIAA/ASME/ASCE/AHS/ASC 31st SDM Conference, Long Beach, CA, April 2-4, 1990.

Takagi, T., 1990, "A Concept of Intelligent Materials," Journal of Intelligent Material Systems and Structures Vol. 1, No. 2, pp. 149-156.

Tzou, H. S. and Tseng, C. I., 1990a, "Distributed Piezoelectric Sensor/Actuator Design for Dynamic Measurement/Control of Distributed Parameter Systems: A Piezoelectric Finite Element Approach," Journal of Sound and Vibration, Vol. 138, No. 1, pp. 17-34.

Tzou, H. S. and Tseng, C. I., 1990b, "Distributed Dynamic Identification and Control of Flexible Shells: Theory and Finite Element Development," Proceedings of the AIAA/ASME/ASCE/AHS/ASC 31st SDM Conference, Long Beach, CA, April 2-4, 1990.

Tzou, H. S. and Zhong, J. P., 1991, "Adaptive Piezoelectric Shell Structures: Theory and Experiments," Proceedings of the AIAA/ASME/ASCE/AHS/ASC 32nd SDM Conference, Baltimore, MD, April 8-10, 1991.

21

Wada, B. K., Fanson J. L., and Crawley E. F., 1990, "Adaptive Structures," Journal of Intelligent Material Systems and Structures, Vol. 1, No. 2, pp. 157-174.

Wang, B. T. and Rogers, C. A., 1990, "Laminate Plate Theory for Spatially Distributed Induced Strain Actuators," Proceedings, Fifth Japan-U.S. Conference on Composite Materials, Tama City, Japan, June 24-27, 1990.

Wang, B. T. and Rogers, C. A., 1991, "Modeling of Finite-Length Spatially Distributed Induced Strain Actuators for Laminate Beams and Plates," Proceedings of the AIAA/ASME/ASCE/AHS/ASC 32nd SDM Conference, Baltimore, MD, April 8-10, 1991

Chapter 2

Modeling of Actuation Mechanism in a Beam Structure with Induced Strain Actuators

2.1 Introduction

Induced strain actuators have been integrated with conventional structural material to serve as energy input devices or actuating elements in many engineering applications based on the implementation of intelligent material systems and structures. Recent developments in exploring this new technology have produced prominent examples, including active structural vibration control (Bailey and Hubbard, 1985; Fanson and Chen, 1986; Crawley and de Luis, 1987; Barker, 1989), shape control (Sato, 1980; Haftka and Adelman, 1985; Chaudhry and Rogers, 1991), acoustic transmission control (Liang and Rogers, 1991), and damage control (Rogers et al., 1991). Many studies using induced strain actuators, such as piezoelectrics, electrostrictors, and shape memory alloys, have demonstrated how electromechanical and thermomechanical coupling can be incorporated into structures to yield new functional capabilities never before realized (Rogers, 1990; Wada et al., 1990).

One of the most fundamental issues in using integrated induced strain actuators is to determine, *a priori*, the actuation effects being induced in the host substructure and the resulting overall structural response. Another important aspect related to the physical

design of the integrated actuator/substructure system is the determination of interfacial shear and peeling stresses that, coupled with interfacial bonds of low strength, usually result in the failure of structural integrity. To investigate these issues, the whole-field stress distribution in each constituent must be determined.

Analytical modeling of the actuation mechanism is not an easy task. Activation of the actuators causes deformation on the actuators as well as on the substrate due to mechanical interaction of the unmatched free induced strains in each constituent. In other words, the actuators experience a finite induced strain as they are activated, while the substrate has zero induced strain. This mismatch results in a redistribution of the stress state in observance of the self-equilibrium condition. Due to the presence of the geometric and material discontinuity of the integrated structural system, a strong coupling between in-plane and transverse deformation and stresses is induced at the interface near the actuator edges. This, in term, develops a highly complicated three-dimensional stress state difficult to model with simple analytical schemes.

Researchers over the past four decades have investigated similar problems in the study of "free edge effect" in laminated composites and thermally induced stresses in heterogeneous structures (Hess, 1969; Bogy, 1970; Wang and Choi, 1982). Valuable insight regarding interfacial shear/peeling stress state and stress singularity present at the "free edge" has been discussed. The solutions obtained are, however, so complex that additional laborious effort is needed to utilize them in the context of engineering applications.

.The study of this issue has also been undertaken using numerical approaches, mainly finite element methods (Pipes and Pagano, 1970). A new formulation based on generalized laminated plate theory recently proposed by Robbins and Reddy (1991) showed that the model, without a large number of elements, is able to satisfy all the boundary conditions for a piezoelectrically activated beam. Although this method can model the problem without strenuous effort and offers a high degree of flexibility for different geometric configurations, the relatively time-consuming computation hampers it from implementing effective real-time adaptability or control required in most applications of intelligent structures.

Over the past decade, simple mechanical models such as the pin-force model and the Euler-Bernoulli model (Crawley and de Luis, 1987) were frequently used to determine the effective forces/moments being transferred from the actuators to the host substructures. These models were developed based on the framework of the mechanics of material method. Since these formulations consider only axial normal stresses, they are not able to describe the complex stress state near the actuator edges. Therefore, the solutions obtained are valid only in the region away from the edges, and provide no information for the shear and peeling stresses at the interfaces.

In this chapter, a refined model is proposed based on an approximated through-the-thickness second-order axial normal stress field for a beam structure with a pair of surface-mounted induced strain actuator patches. The induced strain actuation problem is first converted to a boundary value problem. The resulting stress fields are then solved in an

approximate manner by the principle of stationary complementary energy. The formulation of the model is presented in detail along with numerical examples to show its capability. The results are compared with those obtained by the pin-force and Euler-Bernoulli models and correlated with finite element analysis. Parametric studies are also performed to provide information for the design of the integrated actuators/substructure system.

2.2 Formulation

Consider a beam-like structure of length $2L$ with a pair of induced strain actuators of length $2l$ symmetrically mounted on the outer surfaces of the beam as shown in Fig. 2.1(a). The thickness of the actuator is a and of the beam is $2b$. The structure's width is relatively larger than it's thickness; thus, the stress field in the width direction is considered to be uniform and a unit width is used.

The problem is analyzed using two-dimensional plane stress formulation, and "perfect bonding" is assumed at the interfaces. The in-plane induced strains of the actuators, λ_t and λ_b, are the only impetuses considered, where subscript t and b refer to the top and bottom actuator, respectively. The induced strains can be exerted by any type of non-mechanical

$$\sigma^{I}_{x(at)} = -E_a \lambda_t$$
$$\tau^{I}_{xz(at)} = \sigma^{I}_{z(at)} = 0$$

z

$-E_a \lambda_t$ a *Activated with* λ_t $-E_a \lambda_t$

$2b$

x

$$\sigma^{I}_{x(s)} = \tau^{I}_{xz(s)} = \sigma^{I}_{z(s)} = 0$$

$-E_a \lambda_b$ a *Activated with* λ_b $-E_a \lambda_b$

$$\sigma^{I}_{x(ab)} = -E_a \lambda_b$$
$$\tau^{I}_{xz(ab)} = \sigma^{I}_{z(ab)} = 0$$

$2l$

$2L$

(a)

$$\sigma^{II}_{x(at)} = ? \; ; \quad \tau^{II}_{xz(at)} = ? \; ; \quad \sigma^{II}_{z(at)} = ?$$

$E_a \lambda_t$ $E_a \lambda_t$

$$\sigma^{II}_{x(s)} = ?$$
$$\tau^{II}_{xz(s)} = ?$$
$$\sigma^{II}_{z(s)} = ?$$

$E_a \lambda_b$ $E_a \lambda_b$

$$\sigma^{II}_{x(ab)} = ? \; ; \quad \tau^{II}_{xz(ab)} = ? \; ; \quad \sigma^{II}_{z(ab)} = ?$$

(b)
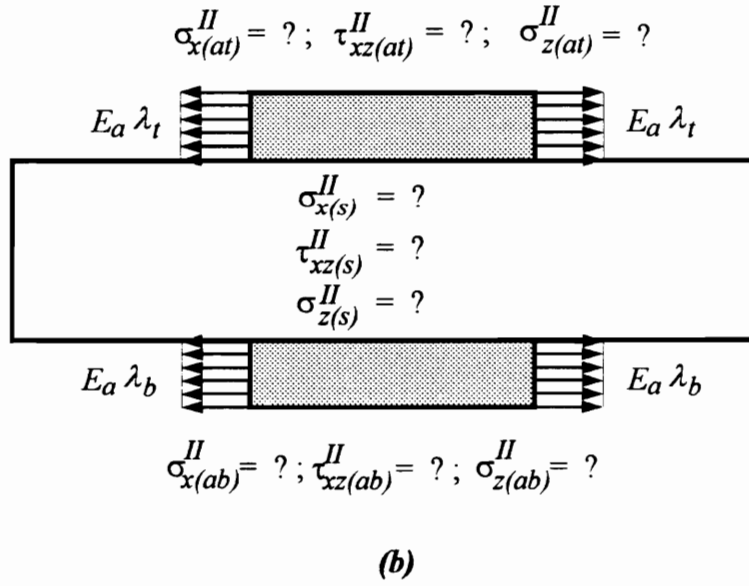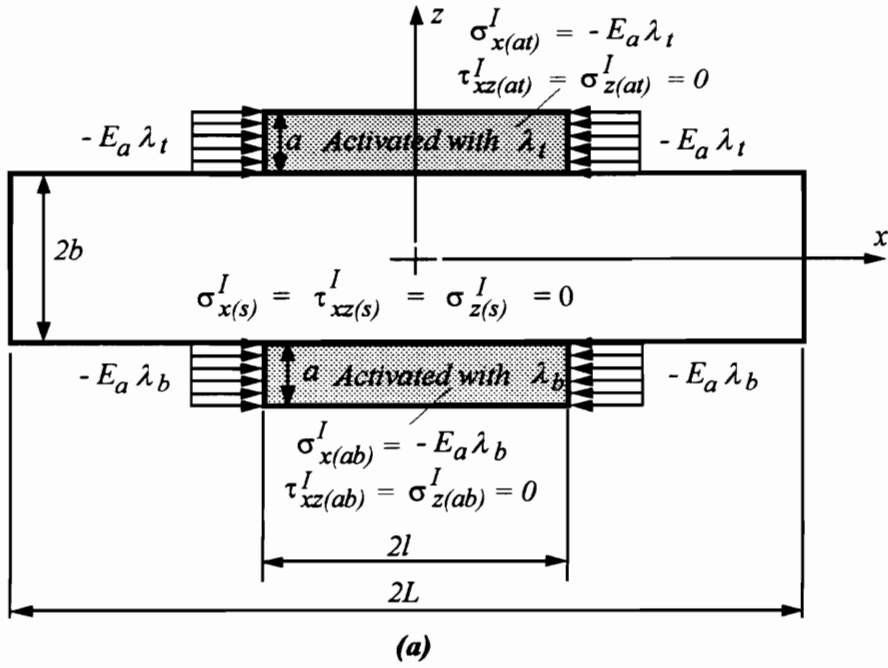
Figure 2.1. Model geometry and *(a)* application of the blocking forces as the actuators are activated; *(b)* application of the end traction.

excitation, depending on the coupling characteristics of the actuators. For instance, $\lambda = d_{31}V$ in the case of piezo-actuators and $\lambda = \alpha\Delta T$ for thermo-actuators, where d_{31} is the piezoelectric constant, V the applied electric field, α the coefficient of thermal expansion, and ΔT is the applied temperature difference. The beam structure is considered to be insensitive to any type of activation; therefore, no induced strain is present in the beam structure.

Activation of the actuators causes deformation on the actuators as well as the beam substrate due to mechanical interaction of the unmatched free induced strains in each constituent. In other words, the actuators experience an induced strain λ_t and λ_b, while the beam substrate has zero induced strain. This mismatch results in a redistribution of the stress state because of the presence of the bond at the interfaces. The new state of stress must satisfy equilibrium in each constituent and overall self-equilibrium of the whole integrated structure system. Generally, the apparent strain, at which the state of equilibrium occurs is lower than the applied free induced strain λ_t and λ_b of the actuators.

Under the condition that both actuators are activated with the same level of induced strain in the same direction, i.e., $\lambda_b = \lambda_t$, the structure will deform in a pure extension or contraction. On the other hand, when the two actuators are activated with opposing direction but with equal induced strain level, i.e., $\lambda_b = -\lambda_t$, the structure will deform in a pure bending mode. If the activated induced strains on each actuator are unequal, the structure will experience a coupled extension (or contraction) and bending deformation.

At any actuation condition, the effective forces and/or moments acting on the beam structure or the resulting deformation, and the shear and peeling stresses at the interfaces are the most desirable quantities to be determined. The former quantity provides information on what level of actuation authority the actuators can deliver and the latter gives the stress level that is critical to the structural integrity. In order to obtain this information, the problem of whole-field stress distribution in each constituent must be determined.

The problem is treated by first considering blocking forces $-E_a\lambda_t$ and $-E_a\lambda_b$ applied at the edges of the top and bottom actuator, respectively, as the actuators are activated with induced strain λ_t and λ_b as shown in Fig. 2.1(a). The applied blocking forces prevent the induced strains λ_t and λ_b in the actuators; therefore, the actuators remain at their original length and induce no strains and stresses on the beam substrate. Under this condition, a uniform state of stress is induced:

$$\sigma^I_{x(at)} = -E_a\lambda_t; \quad \tau^I_{xz(at)} = \sigma^I_{z(at)} = 0 \tag{1.1}$$

$$\sigma^I_{x(s)} = \tau^I_{xz(s)} = \sigma^I_{z(s)} = 0 \tag{1.2}$$

$$\sigma^I_{x(ab)} = -E_a\lambda_b; \quad \tau^I_{xz(ab)} = \sigma^I_{z(ab)} = 0, \tag{1.3}$$

where subscript (at), (s), (ab) refer to the quantities of the top actuator, beam substrate, and bottom actuator, respectively, and E_a is the Young's modulus of the actuators.

Since the original induced strain actuation problem does not have blocking forces acting on the actuator edges, this traction has to be removed. This is accomplished by applying

29

boundary traction with magnitude of $E_a\lambda_t$ and $E_a\lambda_b$ on the top and bottom actuator edges as shown in Fig. 2.1(b). The stress field induced by this boundary traction is non-uniform, and needs to be determined by solving the boundary value problem.

Combination of the loading conditions in Figs. 2.1(a) and 2.1(b) represents the original induced strain actuation problem where the prescribed induced strains of the actuators are the only impetus. Consequently, superposition of the stress fields in Figs. 2.1(a) and 2.1(b),

$$\sigma_x = \sigma_x^I + \sigma_x^{II} \tag{2.1}$$

$$\tau_{xz} = \tau_{xz}^I + \tau_{xz}^{II} \tag{2.2}$$

$$\sigma_z = \sigma_z^I + \sigma_z^{II}, \tag{2.3}$$

gives the solution of the original problem. Since the stress field in Fig. 2.1(a) is known, the only effort remained is to solve the boundary value problem of Fig. 2.1(b).

The problem is solved using two-dimensional plane stress formulation in an approximate manner. The axial normal stress distribution in each constituent is approximated with a parabolic profile in the z-direction as:

$$\sigma_{x(at)}^{II}(x,z) = (\frac{a+b-z}{a})^2 \sigma_{ita}(x) - \frac{(b-z)(2a+b-z)}{a^2} \sigma_{ot}(x) \tag{3.1}$$

$$\sigma_{x(s)}^{II}(x,z) = \frac{(b-z)(b+z)}{b^2} \sigma_c(x) + \frac{z(z+b)}{2b^2} \sigma_{its}(x) + \frac{z(z-b)}{2b^2} \sigma_{ibs}(x) \tag{3.2}$$

$$\sigma_{x(ab)}^{II}(x,z) = (\frac{a+b+z}{a})^2 \sigma_{iba}(x) - \frac{(b+z)(2a+b+z)}{a^2} \sigma_{ob}(x), \tag{3.3}$$

where $\sigma_{ot}(x)$, $\sigma_{ob}(x)$, and $\sigma_c(x)$ are the axial normal stresses at the top outer fiber, the bottom outer fiber of the actuators and the center of the beam substrate, respectively, and $\sigma_{its}(x)$, $\sigma_{ibs}(x)$, $\sigma_{ita}(x)$ and $\sigma_{iba}(x)$ are the axial normal stresses of the actuators and beam at the top and bottom interfaces.

Continuity condition due to the "perfect bonding" assumption at the interfaces requires:

$$\varepsilon_{it}(x) = \frac{\sigma_{its}(x)}{E_s} = \frac{\sigma_{ita}(x)}{E_a} \tag{4.1}$$

$$\varepsilon_{ib}(x) = \frac{\sigma_{ibs}(x)}{E_s} = \frac{\sigma_{iba}(x)}{E_a}, \tag{4.2}$$

where $\varepsilon_{it}(x)$ and $\varepsilon_{ib}(x)$ are the axial normal strain at the top and bottom interfaces, and E_s the Young's modulus of the beam. It should be noted that the contribution of transverse normal stresses on the axial normal strain is neglected in the above expressions.

Substituting Eq. (4) into (3), the stress quantities $\sigma_{ita}(x)$ and $\sigma_{iba}(x)$ are eliminated. The axial normal stresses in each constituent then become:

$$\sigma_{x(at)}^{II}(x,z) = (\frac{a+b-z}{a})^2 \frac{E_a}{E_s} \sigma_{its}(x) - \frac{(b-z)(2a+b-z)}{a^2} \sigma_{ot}(x) \tag{5.1}$$

$$\sigma_{x(s)}^{II}(x,z) = \frac{(b-z)(b+z)}{b^2} \sigma_c(x) + \frac{z(z+b)}{2b^2} \sigma_{its}(x) + \frac{z(z-b)}{2b^2} \sigma_{ibs}(x) \tag{5.2}$$

$$\sigma_{x(ab)}^{II}(x,z) = (\frac{a+b+z}{a})^2 \frac{E_a}{E_s} \sigma_{ibs}(x) - \frac{(b+z)(2a+b+z)}{a^2} \sigma_{ob}(x) \tag{5.3}$$

The self-equilibrium condition of the integrated structure requires that the sum of axial force and moment about the neutral axis of the structure in the original induced strain actuation problem must vanish. This condition yields:

$$\begin{aligned}
\Sigma F &= F_{(at)} + F_{(s)} + F_{(ab)} \\
&= \int_b^{a+b} \sigma_{x(at)} dz + \int_{-b}^b \sigma_{x(s)} dz + \int_{-(a+b)}^{-b} \sigma_{x(ab)} dz \\
&= 0
\end{aligned} \tag{6.1}$$

$$\begin{aligned}
\Sigma M &= M_{(at)} + M_{(s)} + M_{(ab)} \\
&= \int_b^{a+b} z\sigma_{x(at)} dz + \int_{-b}^b z\sigma_{x(s)} dz + \int_{-(a+b)}^{-b} z\sigma_{x(ab)} dz \\
&= 0,
\end{aligned} \tag{6.2}$$

Substituting Eq. (2.1) with the expressions of Eq. (1) and Eq. (5) for the axial normal stresses of each constituent into Eq. (6), the stresses $\sigma_{its}(x)$ and $\sigma_{ibs}(x)$ can be expressed in terms of $\sigma_c(x), \sigma_{ot}(x)$ and $\sigma_{ob}(x)$:

$$\sigma_{its}(x) = \frac{1}{2(aE_a + bE_s)[aE_a(a+4b)+4b^2E_s]}\{-3a^2E_aE_s(aE_a+2bE_s)\lambda_b$$

$$+3aE_aE_s[aE_a(3a+8b)+2bE_s(a+4b)]\lambda_t$$

$$-4bE_s[aE_a(a+4b)+4b^2E_s]\sigma_c(x)$$

$$-aE_s[aE_a(7a+16b)+bE_s(5a+16b)]\sigma_{ot}(x)+a^2E_s(3aE_a+5bE_s)\sigma_{ob}(x)\}$$

$$(7.1)$$

$$\sigma_{ibs}(x) = \frac{1}{2(aE_a + bE_s)[aE_a(a+4b)+4b^2E_s]}\{-3a^2E_aE_s(aE_a+2bE_s)\lambda_t$$

$$+3aE_aE_s[aE_a(3a+8b)+2bE_s(a+4b)]\lambda_b$$

$$-4bE_s[aE_a(a+4b)+4b^2E_s]\sigma_c(x)$$

$$-aE_s[aE_a(7a+16b)+bE_s(5a+16b)]\sigma_{ob}(x)+a^2E_s(3aE_a+5bE_s)\sigma_{ot}(x)\}.$$

$$(7.2)$$

Based on the axial normal stress field of Eq. (5), the shear and transverse normal stresses can be derived from equilibrium consideration. The equations of equilibrium are:

$$\frac{\partial \sigma_x}{\partial x} + \frac{\partial \tau_{xz}}{\partial z} = 0 \tag{8.1}$$

$$\frac{\partial \tau_{xz}}{\partial x} + \frac{\partial \sigma_z}{\partial z} = 0. \tag{8.2}$$

Substituting Eq. (5) for σ_x in Eq. (8.1) for each constituent, and integrating with respect to z, the shear stresses are obtained:

33

$$\tau_{xz(at)}^{II}(x,z) = \frac{1}{3a^2} \{ \frac{E_a (a+b-z)^3}{E_s} \sigma_{its}'(x)$$
$$+(a+b-z)[2a^2 - 2ab - b^2 + 2(a+b)z - z^2]\sigma_{ot}'(x) \} \tag{9.1}$$

$$\tau_{xz(s)}^{II}(x,z) = \frac{z(-3b^2 + z^2)}{3b^2} \sigma_c'(x) + \frac{a}{3}[\sigma_{ot}'(x) - \sigma_{ob}'(x)]$$
$$+ \frac{1}{12b^2 E_s} \{ [2ab^2 E_a + E_s (3b^3 - 3bz^2 - 2z^3)]\sigma_{its}'(x) \tag{9.2}$$
$$-[2ab^2 E_a + E_s (3b^3 - 3bz^2 + 2z^3)]\sigma_{ibs}'(x) \}$$

$$\tau_{xz(ab)}^{II}(x,z) = \frac{-1}{3a^2} \{ \frac{E_a (a+b+z)^3}{E_s} \sigma_{ibs}'(x)$$
$$+(a+b+z)[2a^2 - 2ab - b^2 - 2(a+b)z - z^2]\sigma_{ob}'(x) \}. \tag{9.3}$$

In the above expressions, the boundary traction conditions at upper and lower lateral surface and traction continuity at the interfaces,

$$\tau_{xz(at)}^{II}(x,a+b) = \tau_{xz(ab)}^{II}(x,-a-b) = 0 \tag{10.1}$$

$$\tau_{xz(at)}^{II}(x,b) = \tau_{xz(s)}^{II}(x,b) \tag{10.2}$$

$$\tau_{xz(s)}^{II}(x,-b) = \tau_{xz(ab)}^{II}(x,-b), \tag{10.3}$$

have been used to obtain the constants of integration.

Likewise, substituting Eq. (9) for τ_{xz} in Eq. (8.2) for each constituent, and integrating with respect to z, the transverse normal stresses are obtained:

34

$$\sigma_{z(at)}^{II}(x,z) = \frac{1}{12a^2} \{ \frac{E_a(a+b-z)^4}{E_s} \sigma_{its}''(x) + (a+b-z)^2[5a^2 - 2ab$$
$$-b^2 + 2(a+b)z - z^2]\sigma_{ot}''(x)\} \tag{11.1}$$

$$\sigma_{z(s)}^{II}(x,z) = \frac{-(b^2-z^2)(5b^2-z^2)}{12b^2} \sigma_c''(x) + \frac{a}{24}[(5a-8z)\sigma_{ot}''(x) + (5a+8z)\sigma_{ob}''(x)]$$
$$+ \frac{1}{24b^2 E_s} \{[ab^2 E_a(a-4z) + E_s(b^4 + 6b^3 z - 2bz^3 - z^4)]\sigma_{its}''(x)$$
$$+ [ab^2 E_a(a+4z) + E_s(b^4 - 6b^3 z + 2bz^3 - z^4)]\sigma_{ibs}''(x)\}$$

$$\tag{11.2}$$

$$\sigma_{z(ab)}^{II}(x,z) = \frac{1}{12a^2} \{ \frac{E_a(a+b+z)^4}{E_s} \sigma_{ibs}''(x) + (a+b$$
$$+z)^2[5a^2 - 2ab - b^2 - 2(a+b)z - z^2]\sigma_{ob}''(x)\}. \tag{11.3}$$

The boundary traction conditions at upper and lower lateral surface and traction continuity
at the interfaces,

$$\sigma_{z(at)}^{II}(x,a+b) = \sigma_{z(ab)}^{II}(x,-a-b) = 0 \tag{12.1}$$

$$\sigma_{z(at)}^{II}(x,b) = \sigma_{z(s)}^{II}(x,b) \tag{12.2}$$

$$\sigma_{z(s)}^{II}(x,-b) = \sigma_{z(ab)}^{II}(x,-b) \tag{12.3}$$

have also been used for the constants of integration.

The stress field of Eqs. (5), (9), and (11) satisfies the equilibrium in each constituent and
the overall self-equilibrium of the integrated structure system. The boundary conditions
involving stresses prescribed at the lateral surfaces as well as the traction continuity at the

35

interfaces are also satisfied. The unknown quantities in the above stress field are $\sigma_c(x), \sigma_{ot}(x)$ and $\sigma_{ob}(x)$. Solution of these stress components must satisfy the end traction condition prescribed at the actuator edges:

$$\sigma_{x(at)}^{II}(\pm l, z) = E_a \lambda_t \qquad (13.1)$$

$$\sigma_{x(s)}^{II}(\pm l, z) = 0 \qquad (13.2)$$

$$\sigma_{x(ab)}^{II}(\pm l, z) = E_a \lambda_b \qquad (13.3)$$

$$\tau_{xz(at)}^{II}(\pm l, z) = \tau_{xz(s)}^{II}(\pm l, z) = \tau_{xz(ab)}^{II}(\pm l, z) = 0. \qquad (13.4)$$

To determine the unknown stress quantities, the principle of stationary complementary energy is used. The principle states that for all states of stress satisfying equilibrium within the body and stress boundary conditions on the surface of the body, the actual state of stress is such that the variation of the complementary energy of the body vanishes.

The complementary energy for the present problem is:

$$
\begin{aligned}
U_{(total)} &= U_{(at)} + U_{(s)} + U_{(ab)} \\
&= \frac{1}{2E_a} \int_b^{a+b} \int_{-l}^{l} [\sigma_{x(at)}^{II}{}^2 + \sigma_{z(at)}^{II}{}^2 + 2(1+\nu_a)\tau_{xz(at)}^{II}{}^2 - 2\nu_a\sigma_{x(at)}^{II}\sigma_{z(at)}^{II}]dxdz \\
&+ \frac{1}{2E_s} \int_{-b}^{b} \int_{-l}^{l} [\sigma_{x(s)}^{II}{}^2 + \sigma_{z(s)}^{II}{}^2 + 2(1+\nu_s)\tau_{xz(s)}^{II}{}^2 - 2\nu_s\sigma_{x(s)}^{II}\sigma_{z(s)}^{II}]dxdz \\
&+ \frac{1}{2E_a} \int_{-a-b}^{-b} \int_{-l}^{l} [\sigma_{x(ab)}^{II}{}^2 + \sigma_{z(ab)}^{II}{}^2 + 2(1+\nu_a)\tau_{xz(ab)}^{II}{}^2 - 2\nu_a\sigma_{x(ab)}^{II}\sigma_{z(ab)}^{II}]dxdz.
\end{aligned}
\qquad (14)
$$

In order to simplify the foregoing derivation, the problem is solved for the case of pure extension/contraction and pure bending actuation separately. These solutions can then be linearly superimposed to yield the solution of a general actuation condition.

2.2.1 Pure Extension

Under the condition of pure extension/contraction, i.e., $\lambda_b = \lambda_t$, the axial normal stresses of Eq. (5) are symmetric about the x-axis, which yields:

$$\sigma_{ibs}(x) = \sigma_{its}(x) \tag{15.1}$$

$$\sigma_{ob}(x) = \sigma_{ot}(x). \tag{15.2}$$

Substituting the stress components of Eqs. (5), (9), and (11) into Eq. (14), with the help of Eq. (7), the complementary energy of the system becomes:

$$
\begin{aligned}
U_{(ext)} = {} & K_1^e \lambda_t^2 + K_2^e \lambda_t \sigma_c(x) + K_3^e \sigma_c^2(x) \\
& + K_4^e \lambda_t \sigma_{ot}(x) + K_5^e \sigma_c(x)\sigma_{ot}(x) + K_6^e \sigma_{ot}^2(x) \\
& + K_7^e \sigma_c'^2(x) + K_8^e \sigma_c'(x)\sigma_{ot}'(x) + K_9^e \sigma_{ot}'^2(x) \\
& + K_{10}^e \lambda_t \sigma_c''(x) + K_{11}^e \sigma_c(x)\sigma_c''(x) + K_{12}^e \sigma_c''(x)\sigma_{ot}(x) \\
& + K_{13}^e \sigma_c''^2(x) + K_{14}^e \lambda_t \sigma_{ot}''(x) + K_{15}^e \sigma_c(x)\sigma_{ot}''(x) \\
& + K_{16}^e \sigma_{ot}(x)\sigma_{ot}''(x) + K_{17}^e \sigma_c''(x)\sigma_{ot}''(x) + K_{18}^e \sigma_{ot}''^2(x),
\end{aligned}
\tag{16}
$$

where K_i^e ($i = 1, 18$) are functions of the material properties, E_a, E_s, v_a, v_s, and the thickness of the actuators and beam, a and b. The prime indicates the derivative with respect to x. The complete expressions of K_i^e are given in the appendix.

Variation of the complementary energy $\delta U_{(ext)} = 0$ with the stresses satisfying the prescribed end traction yields the Euler's equations:

$$\left[A_1^e \frac{d^4}{dx^4} + A_2^e \frac{d^2}{dx^2} + A_3^e \right] \sigma_c(x) + \left[B_1^e \frac{d^4}{dx^4} + B_2^e \frac{d^2}{dx^2} + B_3^e \right] \sigma_{ot}(x) = D_1^e \tag{17.1}$$

$$\left[B_1^e \frac{d^4}{dx^4} + B_2^e \frac{d^2}{dx^2} + B_3^e \right] \sigma_c(x) + \left[C_1^e \frac{d^4}{dx^4} + C_2^e \frac{d^2}{dx^2} + C_3^e \right] \sigma_{ot}(x) = D_2^e , \tag{17.2}$$

where

$$A_1^e = 2K_{13}^e; \quad A_2^e = 2\left(K_{11}^e - K_7^e\right); \quad A_3^e = 2K_3^e$$

$$B_1^e = K_{17}^e; \quad B_2^e = K_{12}^e + K_{15}^e - K_8^e; \quad B_3^e = K_5^e$$

$$C_1^e = 2K_{18}^e; \quad C_2^e = 2\left(K_{16}^e - K_9^e\right); \quad C_3^e = 2K_6^e$$

$$D_1^e = -K_2^e \lambda_t; \quad D_2^e = -K_4^e \lambda_t.$$

The boundary condition of Eqs. (13.1), (13.2), and (13.3) can only be satisfied at the outer fiber of the actuators and at the center of the beam for the present formulation. The end traction condition thus becomes:

$$\sigma_{ot}(\pm l) = E_a \lambda_t; \quad \sigma_c(\pm l) = 0 \tag{18.1}$$

$$\sigma_{ot}'(\pm l) = 0; \quad \sigma_c'(\pm l) = 0. \tag{18.2}$$

The general solution of Eq. (17) has the form:

$$\sigma_{ot}(x) = \frac{(A_3^e D_2^e - B_3^e D_1^e)}{(A_3^e C_3^e - (B_3^e)^2)} + \sum_{i=1}^{8} p_i^e (\exp)^{\alpha_i^e x} \tag{19.1}$$

$$\sigma_c(x) = \frac{(C_3^e D_1^e - B_3^e D_2^e)}{(A_3^e C_3^e - (B_3^e)^2)} + \sum_{i=1}^{8} \gamma_i^e p_i^e (\exp)^{\alpha_i^e x} , \tag{19.2}$$

where

$$\gamma_i^e = -\frac{(A_3^e + A_2^e(\alpha_i^e)^2 + A_1^e(\alpha_i^e)^4)}{(B_3^e + B_2^e(\alpha_i^e)^2 + B_1^e(\alpha_i^e)^4)}, \quad i = 1,8.$$

In the above, $\alpha_i^e (i = 1,8)$ are the roots of the characteristic equation for the homogeneous equations of Eq. (17):

$$\begin{vmatrix} (A_1^e (\alpha^e)^4 + A_2^e (\alpha^e)^2 + A_3^e) & (B_1^e (\alpha^e)^4 + B_2^e (\alpha^e)^2 + B_3^e) \\ (B_1^e (\alpha^e)^4 + B_2^e (\alpha^e)^2 + B_3^e) & (C_1^e (\alpha^e)^4 + C_2^e (\alpha^e)^2 + C_3^e) \end{vmatrix} = 0, \tag{20}$$

and $p_i^e (i = 1, 8)$ are arbitrary constants to be determined by the end condition of Eq. (18).

2.2.2 Pure Bending

In the case of pure bending, i.e., $\lambda_b = -\lambda_t$, the axial normal stresses are antisymmetric about the x-axis, which yields:

$$\sigma_{ibs}(x) = -\sigma_{its}(x) \tag{21.1}$$

$$\sigma_{ob}(x) = -\sigma_{ot}(x) \tag{21.2}$$

$$\sigma_c(x) = 0. \tag{21.3}$$

Substituting stress components of Eqs. (5), (9), and (11) into Eq. (14), with the help of Eq. (7), the complementary energy becomes:

$$\begin{aligned} U_{(bend)} &= K_1^b \lambda_t^2 + K_2^b \lambda_t \sigma_{ot}(x) + K_3^b \sigma_{ot}^2(x) + K_4^b \sigma_{ot}'^2(x) \\ &+ K_5^b \lambda_t \sigma_{ot}''(x) + K_6^b \sigma_{ot}(x) \sigma_{ot}''(x) + K_7^b \sigma_{ot}''^2(x), \end{aligned} \tag{22}$$

where $K_i^b (i = 1, 7)$ are given in the appendix.

39

Variation of the complementary energy $\delta U_{(bend)} = 0$, with the stresses satisfying the prescribed end traction yields the Euler's equation:

$$[A_1^b \frac{d^4}{dx^4} + A_2^b \frac{d^2}{dx^2} + A_3^b]\sigma_{ot}(x) = D_1^b,$$ (23)

where

$$A_1^b = 2K_7^b; \quad A_2^b = 2(K_6^b - K_4^b); \quad A_3^b = 2K_3^b$$

$$D_1^b = -K_2^b \lambda_t.$$

The boundary conditions to be satisfied are:

$$\sigma_{ot}(\pm l) = E_a \lambda_t$$ (24.1)

$$\sigma_{ot}'(\pm l) = 0.$$ (24.2)

The general solution of Eq. (23) has the form:

$$\sigma_{ot}(x) = \frac{D_1^b}{A_3^b} + \sum_{i=1}^{4} p_i^b (\exp)^{\alpha_i^b x},$$ (25)

where $\alpha_i^b (i = 1, 4)$ are the roots of the characteristic equation for the homogenous equation of Eq. (23),

$$A_1^b (\alpha^b)^4 + A_2^b (\alpha^b)^2 + A_3^b = 0,$$ (26)

and $p_i^b (i = 1, 4)$ are arbitrary constants to be determined by the end conditions of Eq. (24).

The roots of α_i^e and α_i^b solved in the above are complex in general, but in conjugate pairs; consequently, the stress quantities are real.

2.3 Finite element analysis

In order to assist in verifying the current analytical results, finite element analyses were performed. A typical finite element model with $b/a=3$ thickness ratio and $l/a=10$, $L/a=20$ aspect ratio is depicted in Fig. 2.2. The model consists of 4 x 10 elements for each actuator and 24 x 20 elements for the beam.

Plane strain linear isoparametric elements were used for the beam and the actuators. Since the characteristic induced strains of the actuator resemble the thermal expansion effects of a structural material, a fictitious thermal expansion coefficient was assigned to the actuators. The desired induced strain level was then obtained by applying a temperature field on the model. The analyses were performed using the ABAQUS® finite element package for solution and IDEAS® for pre- and post-processing.

The desired effective forces transferred from the actuators to the beam were calculated by integrating the normal stress through the thickness where the stress distribution in the z direction was determined by linear interpolation from the stresses of the adjacent nodes. Likewise, the effective moments on the beam were obtained by taking moments about the centroid axis of the beam using the same stress profile. For the purpose of ensuring convergence, the analysis was also carried out on a refined mesh which consists of 8 x 40

41
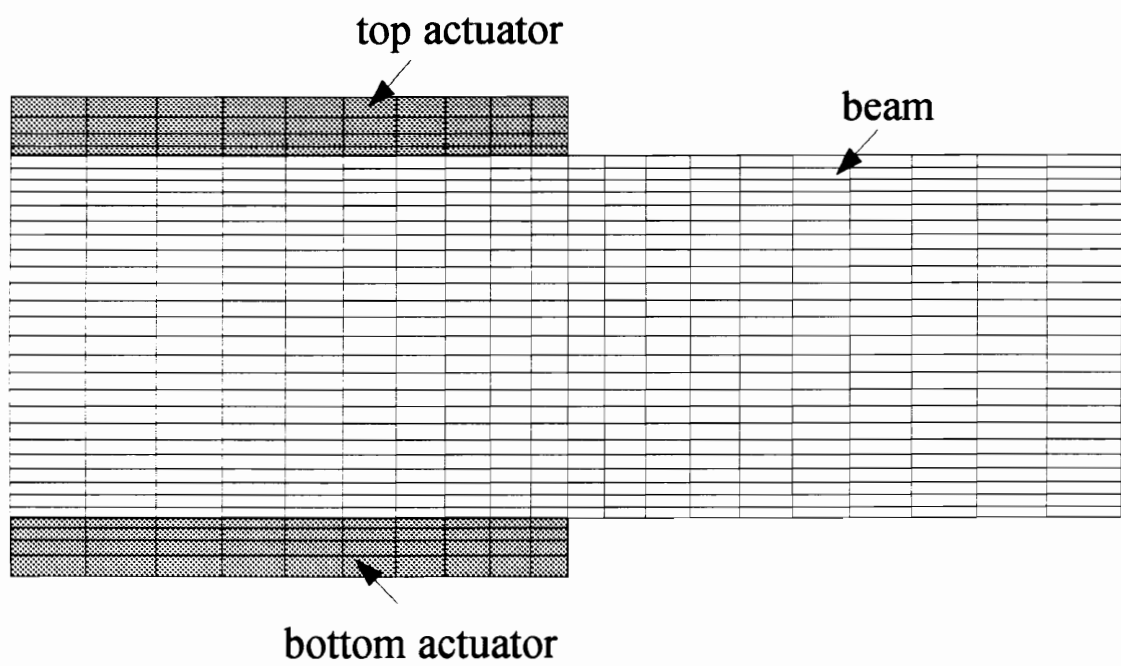
Figure 2.2. Finite element model for surface-mounted actuators/beam structure.

elements for the actuator and 48 x 80 elements for the beam with the same element size bias as that of the Fig. 2.2.

2.4 Case Study

The actuation response of a beam structure with symmetrically surface-bonded actuator patches is investigated using the current analytical model as well as the finite element model (FEM) for a typical 6061 aluminum beam with G-1195 piezoceramic actuators (Piezo Systems, 1987). Table 2.1 gives the configuration and material properties of the constituents. Of particular interest are the actuating force/moment transferred from the actuators to the beam and the resulting interfacial shear and peeling stresses. The former quantity provides information on what level of actuation authority the actuators can deliver and the latter gives the stress level that is critical to structural integrity.

Figure 2.3 shows the effective force induced in the beam as the actuators are activated in pure extension, i.e., $\lambda_b = \lambda_t$. The results obtained from the current model and the finite element analysis, as well as from the pin-force and Euler-Bernoulli model, are included for comparison. The quantity of the effective force is normalized with respect to the total blocking force, $F^* = 2aE_a\lambda_t$, of the actuators, and the x-axis is nondimensionalized with respect to the thickness of the actuator.

43

Table 2.1. Material properties of the constituents

G-1195 piezoceramic	E_a=9.13 (msi)	v_a=0.4	a=0.1 (in)	$\lambda=d_{31}V$=1.3x10^{-4}
6061 aluminum	E_s=10.6 (msi)	v_s=0.3	b=0.3 (in)	
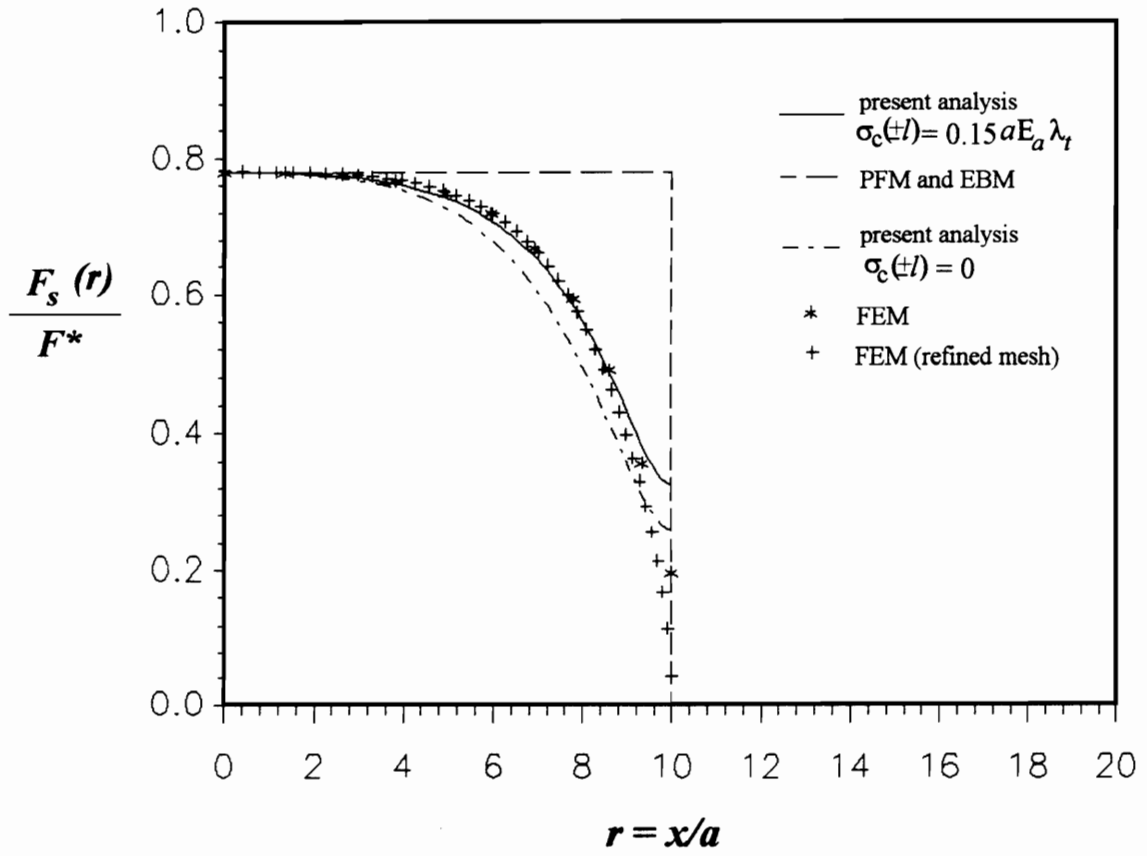
Figure 2.3. Effective force distribution on the beam substrate along the axial direction under pure extension activation.

It is shown that the refinement of the finite element mesh does not affect the distribution of the effective force except on the region close to the very end of the actuators, about one actuator thickness. The force level at the ends of the actuators tend to converge to zero with the mesh refinement as expected. The result of the current model using boundary condition $\sigma_c(\pm l) = 0$ of Eq. (6.1) slightly underestimates the force level near the actuator edges comparing with the finite element analysis. The discrepancy is mainly due to the influence of the adjacent material in the beam uncovered with the actuators not taken into account in the current analytical model. To account for this effect, a traction boundary condition of $\sigma_c(\pm l) = 0.15 E_a \lambda_t$ is used which corresponds to the stress level obtained from the finite element analysis at the same location. This justification yields good agreement between the current analysis and the finite element model except in the region close to the actuator edges within one actuator thickness.

In comparison, the current model captures the trend of attenuation of the effective force transferred to the beam substrate and agrees with finite element analysis, while the pin-force and Euler-Bernoulli models fail to describe this phenomenon. The agreement between the current analysis and the finite element model is good in both the attenuation pattern and the magnitude except in the region within one actuator thickness from the actuator edges. This discrepancy can be attributed to the approximation of axial normal stress field in the current analytical model.

The effective moment transferred to the beam substructure under pure bending actuation, i.e., $\lambda_b = -\lambda_t$, is shown in Fig. 2.4. The results obtained from the current model and the

46
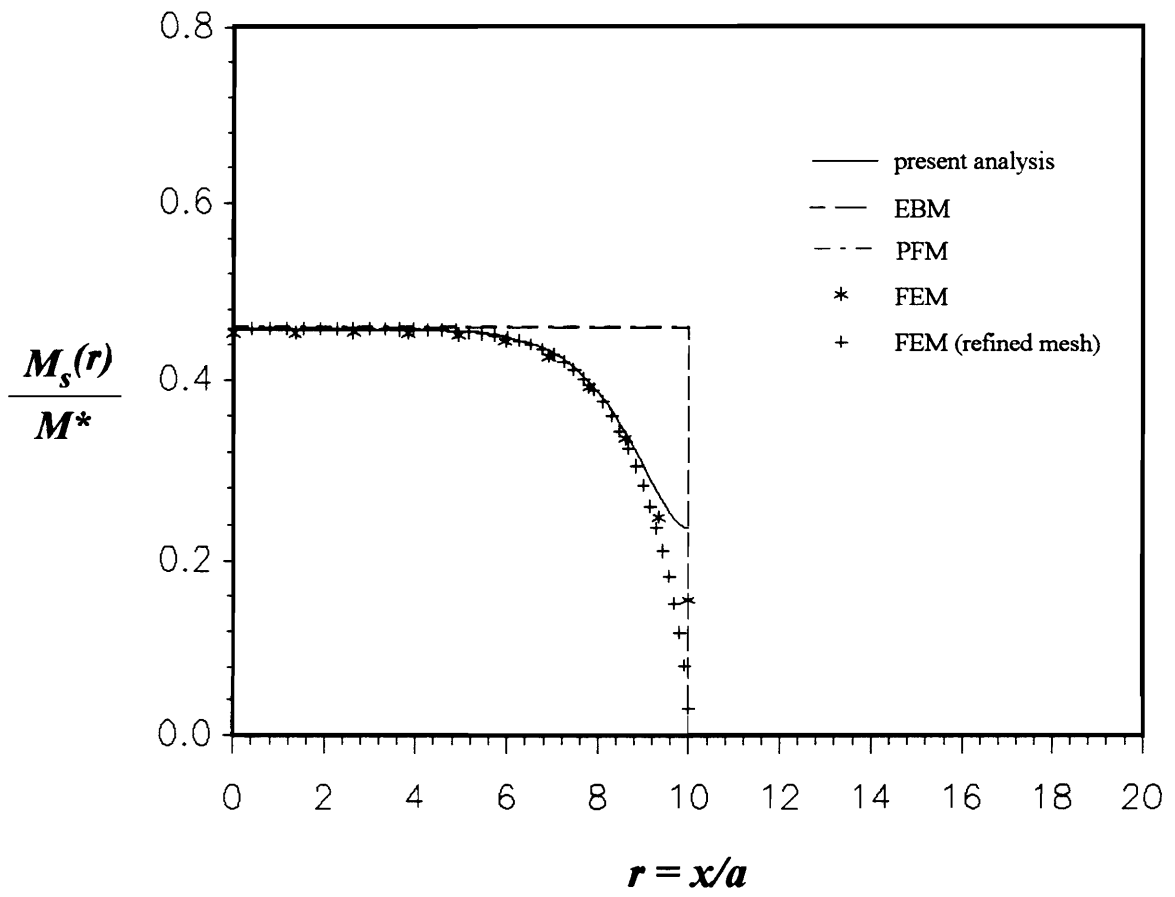
Figure 2.4. Effective moment distribution on the beam substrate along the axial direction under pure bending activation.

finite element analysis, as well as the pin-force and Euler-Bernoulli models, are all depicted for comparison. The magnitude of the moment is normalized with the moment that the blocking force of the actuators produce about the neutral axis, i.e., $M^* = 2aE_a\lambda_t(a/2+b)$.

The refined mesh of the finite element model yields the same resultant moment except in the region close to the very end of the actuator edges. The refinement of the mesh also results in convergence of the moment to zero at $r = 10$, as expected. The current model agrees well with the finite element results. The attenuation of the effective moment due to edge effects is well predicted by the current analysis except in the region within one actuator thickness from the actuator edges due to the approximated parabolic profile made on the axial normal stress field in the current analytical model. The pin-force and Euler-Bernoulli models, on the other hand, fail to describe this phenomenon at all.

Figures 2.5 and 2.6 show the shear and peeling stress distribution at the upper interface, i.e., $z = b$, along the x-axis for the case of pure extension and pure bending, respectively. The stress quantities are normalized with respect to the blocking stress of the actuator $E_a\lambda_t$. It should be noted that the pin-force and Euler-Bernoulli models cannot predict these quantities. It is shown that the distribution patterns are the same for the case of pure extension and pure bending, but the stress level of the pure extension is higher than that of the pure bending.
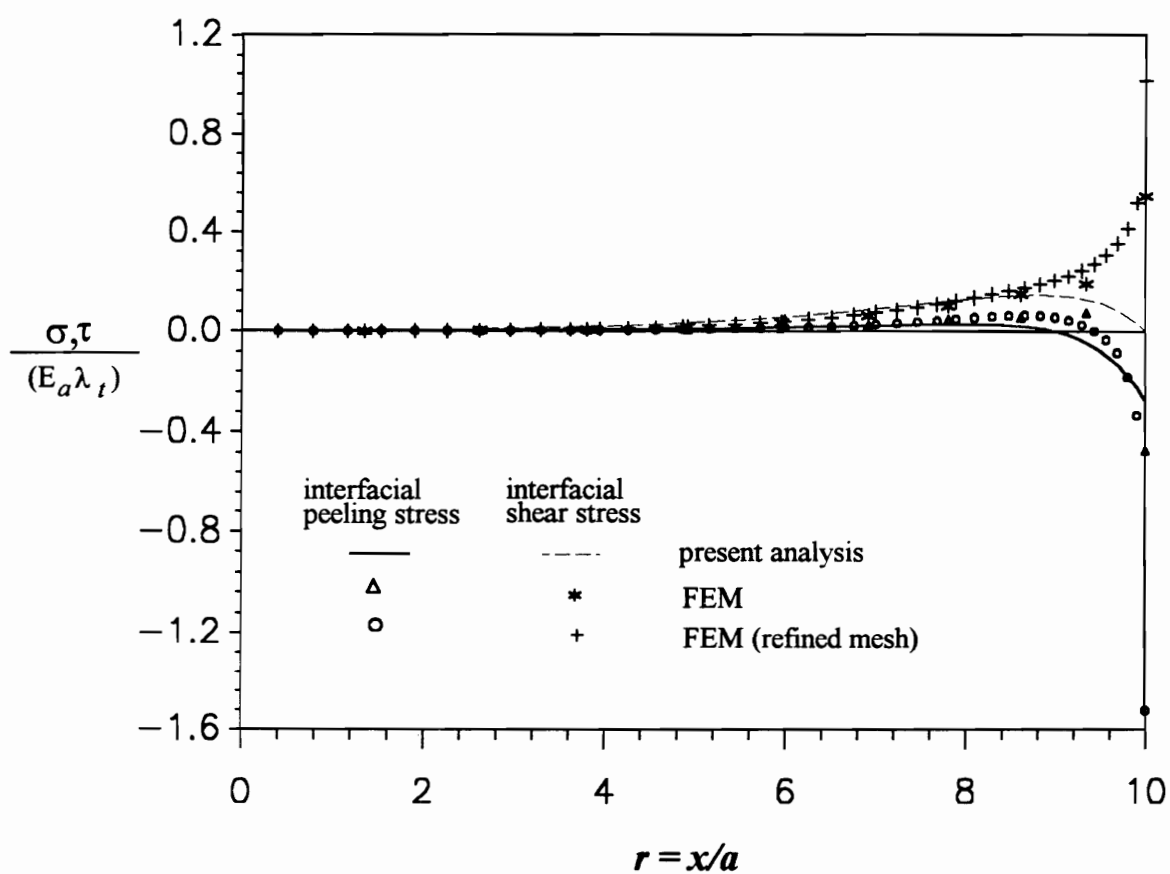
Figure 2.5. Interfacial shear and peeling stress distributions under pure extension activation.

49
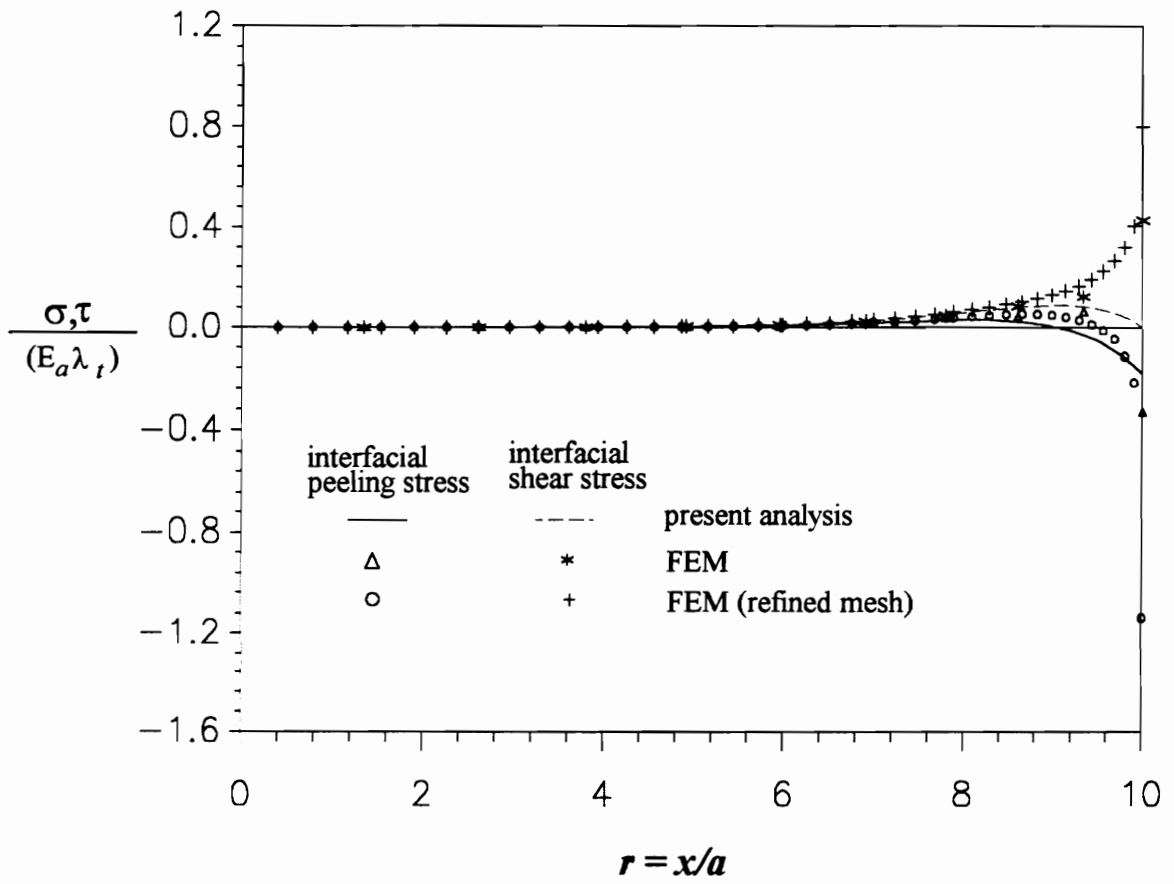
Figure 2.6. Interfacial shear and peeling stress distributions under pure bending activation.

The current model, as well as the finite element analysis, predict a maximum interfacial peeling stress at the ends of the actuators, i.e., $r = 10$. However, the current analysis yields a maximum shear stress at the location about one thickness of the actuator away from the actuator edges, i.e., $r = 9$, while the FEM predicts a maximum shear stress level right at the edges. It is evident that the current model satisfies the shear stress free boundary condition at the actuator edges, but the finite element analysis does not satisfy this condition.

The refined mesh of the finite element model yields the same distribution pattern, but the stress level near the actuator edges is much higher. Apparently, the maximum interfacial shear and peeling stresses tend to increase without bound as the mesh is further refined. It should be noted that the stress state at the interfaces near the actuator edges possesses singular characteristics as discussed in the literature (Wang and Choi, 1982). The actual magnitude of the maximum interfacial shear and peeling stresses cannot be determined without including the singularity. Nevertheless, the current analysis gives a correct distribution pattern of the interfacial shear and peeling stresses that satisfies the boundary conditions. The stress level obtained should be able to serve as a reliable reference to help the design of the integrated actuator/substructure system.

The distribution of each stress component in the z direction obtained by the current analysis is shown in Figs. 2.7 and 2.8 for the cases of pure extension and pure bending, respectively. The stress profile in each constituent is shown at five different locations along the x-axis. The stress components are normalized with respect to the blocking
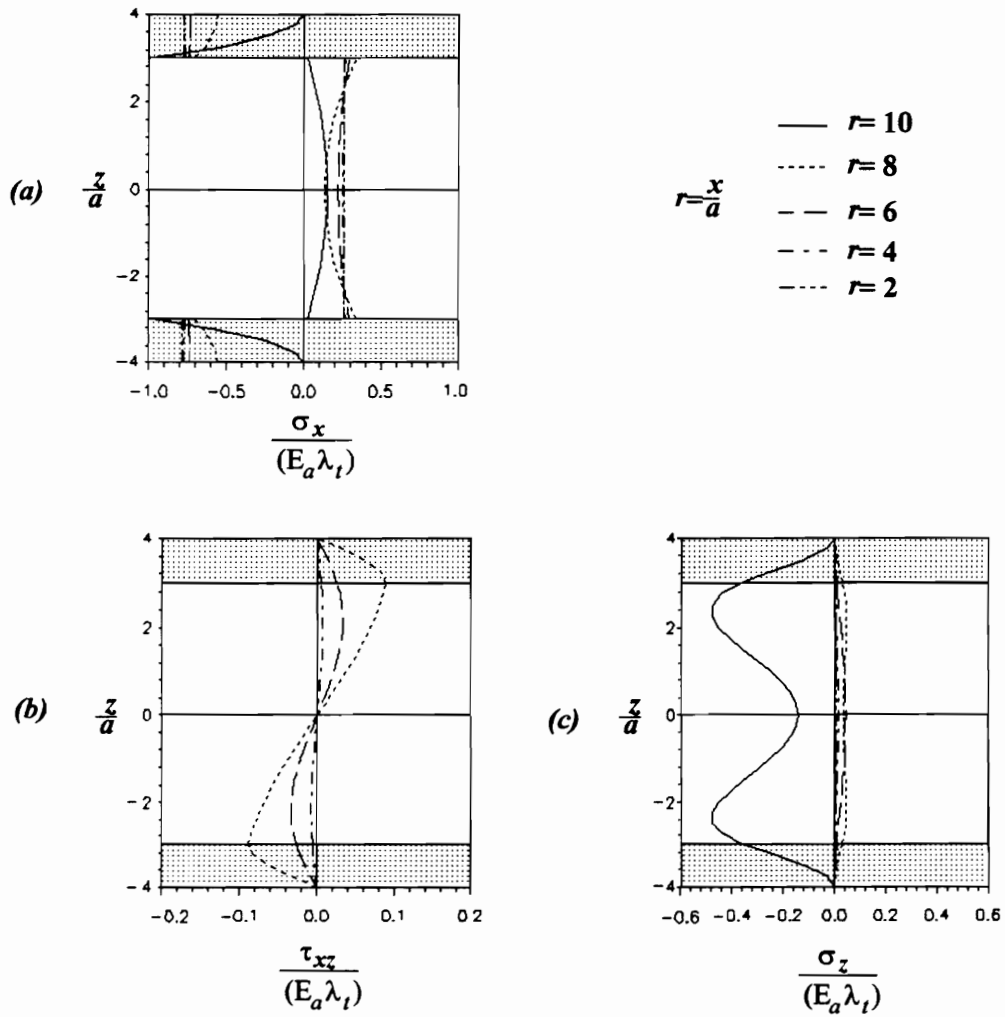
Figure 2.7. Distribution of the stress components under pure extension along the z direction at various x locations: (a) axial normal stress, (b) shear stress, (c) transverse normal stress.
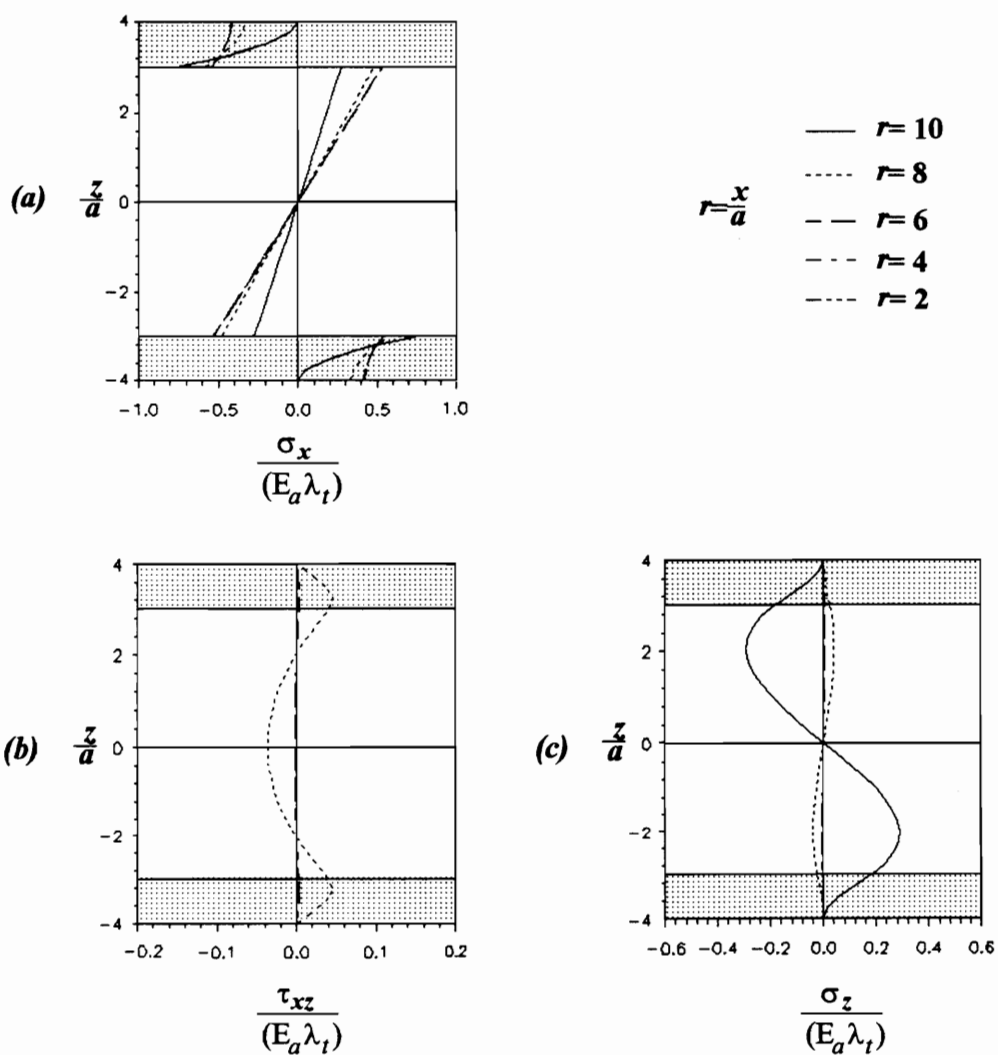
Figure 2.8. Distribution of the stress components under pure bending along the z direction at various x location: (a) axial normal stress, (b) shear stress, (c) transverse normal stress.

stress of the actuator, $E_a \lambda_t$, and the z coordinate is nondimensionalized with respect to the actuator thickness, a.

The stress profile illustrates the approximation made on the axial normal stress, σ_x, in the analysis and how the stress profile changes at each location from the actuator edge to the central location. The resulting shear and transverse normal stress profiles illustrate the variation of these stress components along the z and x directions and the satisfaction of the traction boundary conditions. It is interesting to note that the maximum shear and transverse normal stresses are present not necessarily right at the interfaces. However, the interfaces usually have lowest strength in the structural system; thus, the interfacial shear and peeling stresses are of the most concern.

2.5 Parametric Study

A parametric study is carried out to provide information for the purpose of designing surface-mounted actuator/beam substrate systems. The influence of the beam-to-actuator stiffness ratio, E_s / E_a, and thickness ratios, b/a, are determined. The stiffness ratio indicates the performance of a 'generic' actuator on various beam substrates with different stiffnesses, and the thickness ratio gives the optimum geometric configuration for a typical actuator that delivers maximum actuation authority on a certain beam substrate. The effects of these parameters are illustrated by the deformation of the beam structure induced by the activation of the actuators and the resulting maximum interfacial shear and peeling stresses. The deformation of the beam is presented in an average sense. In the

54

case of pure extension activation, axial normal strain is used which is obtained by dividing the effective force with respect to extensional rigidity, i.e., $\varepsilon_c = F_s / (2bE_s)$. And, in the case of pure bending, curvature is obtained by dividing the effective moment with respect to the flexural rigidity, i.e., $\omega_c = 2M_s / (3b^3 E_s)$.

Figure 2.9 shows the axial normal strain of the beam ε_c, normalized with respect to the input strain λ_t, at the central cross-section of the structure, i.e., $x = 0$, under pure extension activation as a function of the beam-to-actuator stiffness ratio E_s / E_a for the configuration of $b/a = 3$. The variation of unsaturated length, ξ, which indicates the distance from the actuator edges needed for the effective force to reach its constant level is also depicted in the figure. It is shown that the current analysis, the pin-force model, and the Euler-Bernoulli model predict the same level of strain at the central cross-section of the structure and that this value agrees very well with that obtained by finite element analysis.

The deformation of the structure decreases with increasing stiffness of the beam substrate, and this reduction is more evident as $E_s / E_a < 5$. The unsaturated length also decreases with increasing stiffness ratio, as expected. This trend indicates that a compliant beam substrate requires a longer distance from the actuator edges for the effective force to reach its constant level. It is shown that for the stiffness ratio of $E_s / E_a = 0.5$, the length of one beam thickness is needed. The prediction of the current analysis agrees well with that of the finite element analysis. It should be noted that the pin-force and Euler-Bernoulli models cannot provide this quantity.
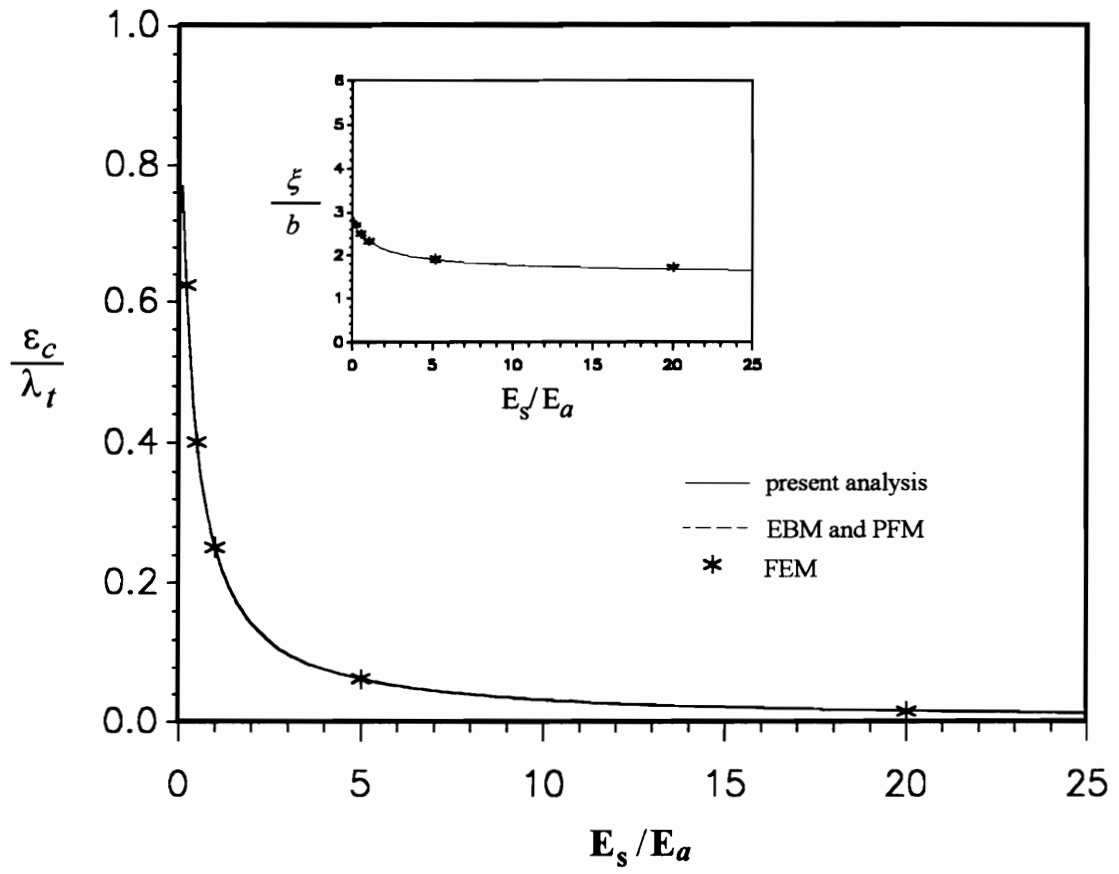
Figure 2.9. Axial normal strain of the beam substrate at the central cross-section as a function of beam-to-actuator stiffness ratio.

The curvature of the structure, ω_c, normalized with respect to λ_t at $x = 0$ under pure bending activation as a function of E_s / E_a is illustrated in Fig. 2.10. It is shown that the results of the current analysis and the Euler-Bernoulli model coincide and agree well with that of the finite element analysis. The variation of the unsaturated length ξ shows no noticeable change as the stiffness ratio increases. It remains almost constant as $\xi / b = 1.5$.

The effects of the stiffness ratio, E_s / E_a, on the maximum interfacial shear and peeling stresses are shown in Fig. 2.11. The results of the current analysis for both pure extension and pure bending actuation are depicted. Apparently, the interfacial stress level induced under the pure extension activation is higher than that under the pure bending. It is shown that both the interfacial shear and the peeling stress increase with increasing E_s / E_a. In general, a stiffer beam results in less deformation, as indicated above, yet higher interfacial shear and peeling stresses.

Figure 2.12 shows the axial normal strain of the structure at $x = 0$, normalized with respect to λ_t, under pure extension activation as a function of the beam-to-actuator thickness ratio b / a for $E_s / E_a = 1.16$, which is comparable to an aluminum beam with piezoceramic actuators. It is shown that the current analysis, the pin-force model and the Euler-Bernoulli model predict the same level of the strain, and that this value agrees very well with that of the finite element analysis. The axial normal strain ε_c increases with decreasing thickness ratio b / a, indicating that the thicker the actuator, the greater the actuation effect.
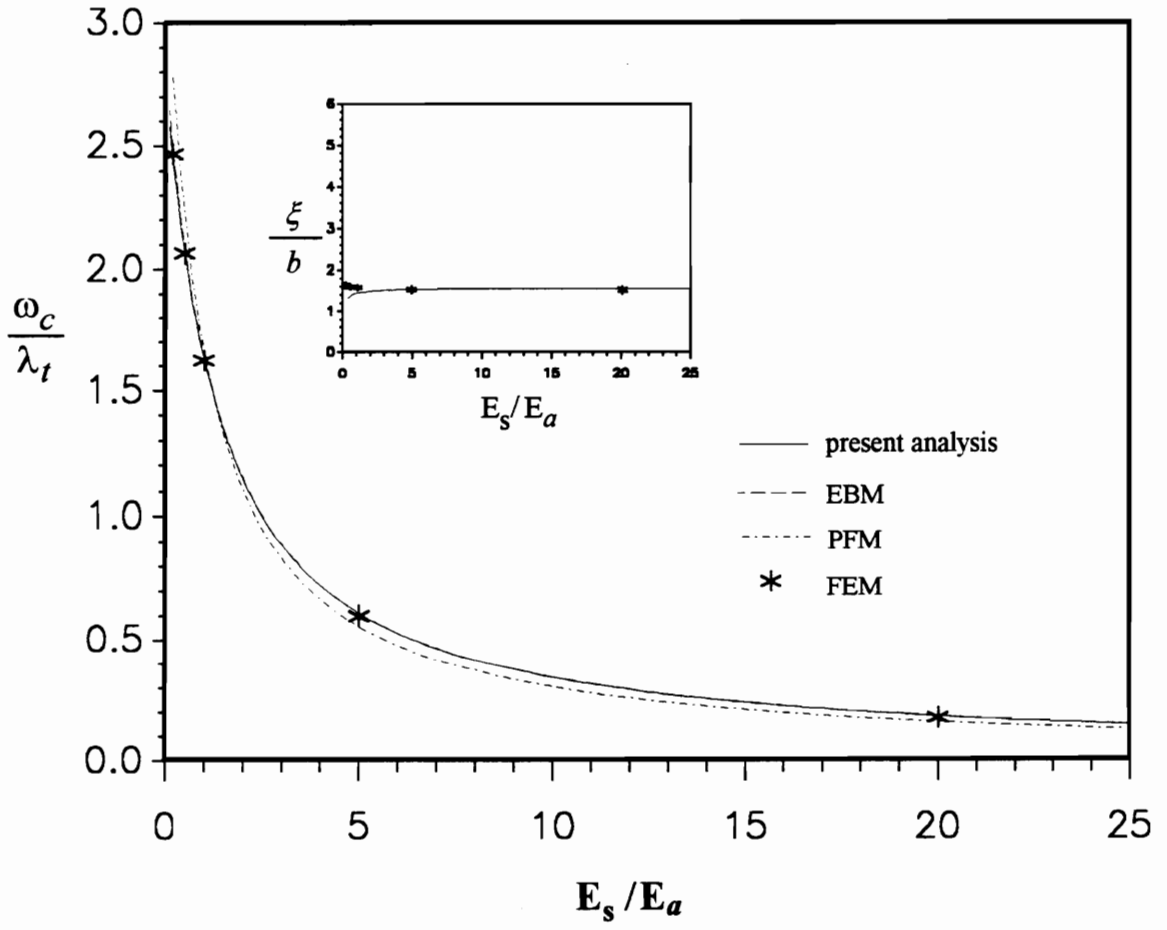
Figure 2.10. Curvature of the beam substrate at the central cross-section as a function of beam-to actuator stiffness ratio.

58
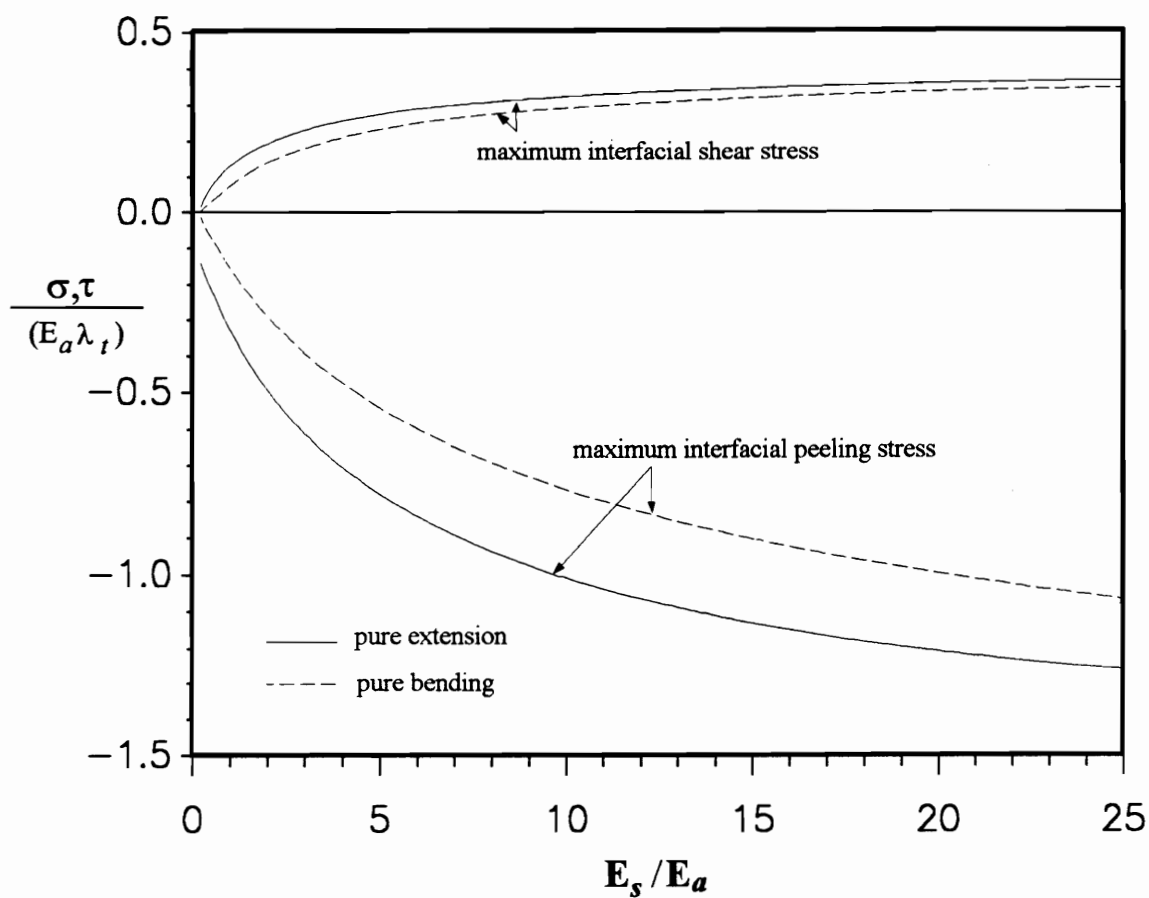
Figure 2.11. Influence of the beam-to-actuator stiffness ratio on the maximum interfacial shear and peeling stresses.
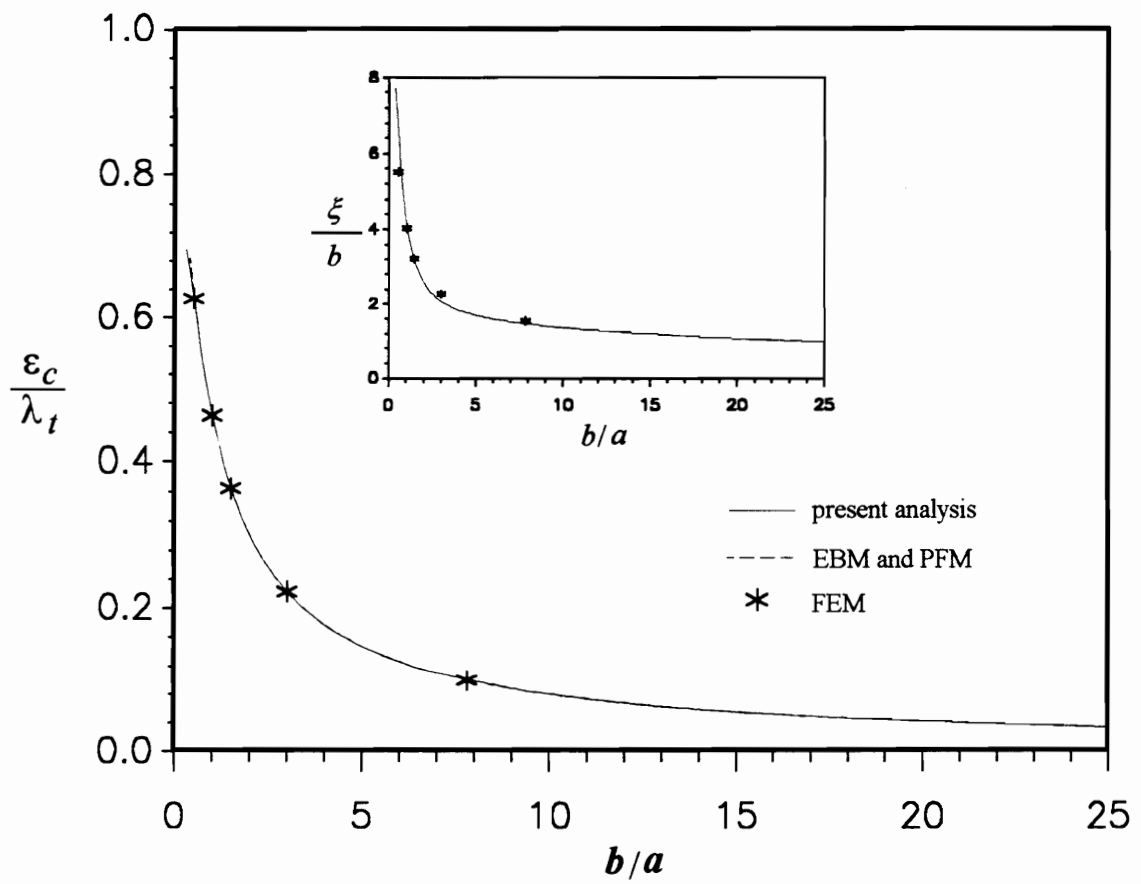
Figure 2.12. Axial normal strain of the beam substrate at the central cross-section as a function of beam-to-actuator thickness ratio.

The unsaturated length, ξ, likewise decreases with increasing thickness ratio b/a, as expected. This trend indicates that a thicker actuator requires more distance from the actuator edge to achieve a constant effective force level. It should be noted that the results of the current analysis agree well with those of the finite element analysis, while the pin-force and Euler-Bernoulli models cannot describe this phenomenon.

The effect of the thickness ratio, b/a, on the curvature, ω_c, at $x=0$, under pure bending activation is shown in Fig. 2.13. The results from the current analysis and the Euler-Bernoulli model agree well with those of the finite element analysis. The pin-force model, on the other hand, overestimates the curvature at low thickness ratios as $b/a<3$. The unsaturated length ξ obtained from the current analysis has the same trend as that of the finite element analysis; however, the magnitude does not agree well at low thickness ratios.

It is evident that an optimum thickness ratio, which yields maximum curvature, exists at $b/a=1.8$. Increasing the thickness of the actuator lower than this ratio results in a smaller curvature. The mechanism of the reduction is well-illustrated in Fig. 2.14. Figure 2.14 shows the axial normal stress distribution in the z direction in the actuator and beam substrate at the central cross-section of the structure with a relatively thick actuator, as $b/a=0.5$. In the outer portion of the actuator, a stress resultant opposite to that of the inner portion is present. This is mainly due to the fact that the outer portions of the actuators are allowed to deform completely to their free induced strain level, λ_t and λ_b, because of the lack of material constraints of the beam substructure. Therefore, this part of the actuator has no

61
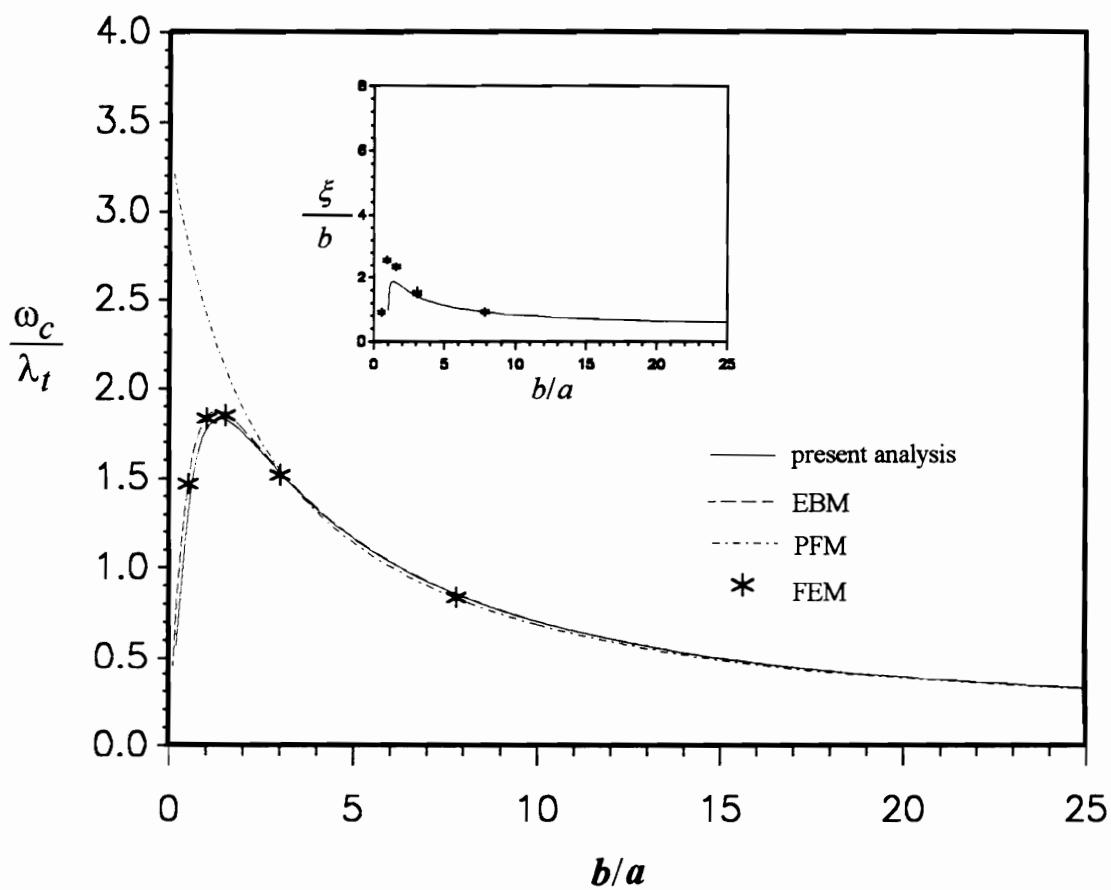
Figure 2.13. Curvature of the beam substrate at the central cross-section as a function of beam-to-actuator thickness ratio.
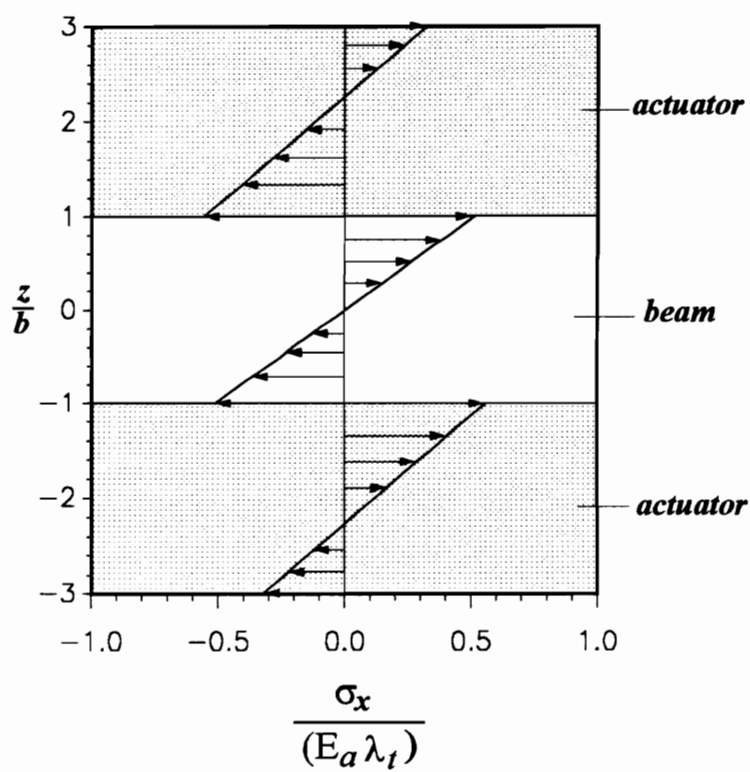
Figure 2.14. Axial normal stress distribution in the *z* direction at *x=0* at the thickness ratio *b/a*=0.5.

contribution for actuating purposes. On the contrary, it adds additional stiffness to the system, resulting in an overall stiffer structure.

Figure 2.15 shows the maximum interfacial shear and peeling stresses under pure extension and pure bending conditions as a function of thickness ratio b/a. It is shown that no significant change in interfacial shear stress as b/a increases for pure extension actuating, while for the case of pure bending, it remains almost unchanged as $b/a > 5$, but decreases with decreasing thickness ratio. The variation in the interfacial peeling stress appears to have a peek stress level at $b/a = 2.1$ for the case of pure extension and $b/a = 2.6$ for pure bending. Since the interfacial shear and peeling stresses are generally responsible for the structural integrity, this factor needs to be taken into account in the selection of the actuator's thickness.

2.5 Conclusion

The actuation mechanism in a beam structure with surface bonded induced strain actuators is modeled. The induced strain actuation problem is converted to a boundary value problem with prescribed end traction conditions and solved by the principle of stationary complementary energy. The stress field obtained satisfies both the equations of equilibrium in each constituent as well as the overall self-equilibrium of the integrated structural system. The solutions of the whole field stress distribution are obtained in closed-form for both pure extension/contraction and pure bending actuation conditions.
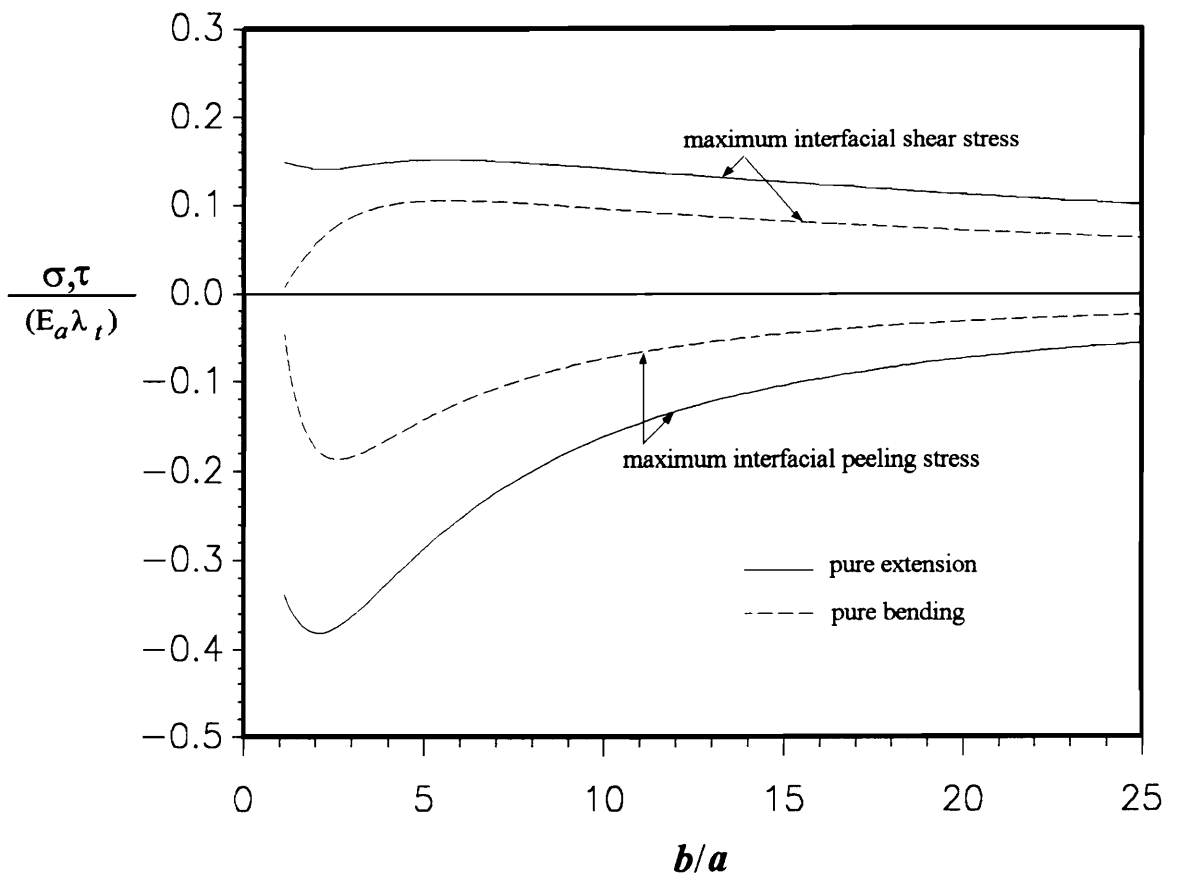
Figure 2.15. Influence of the beam-to-actuator thickness ratio on the maximum interfacial shear and peeling stresses.

The results of the model were presented, along with those of the pin-force and Euler-Bernoulli models, and compared with finite element results. A case study was performed for a typical aluminum beam with piezoceramic actuators and parametric studies on the effect of the stiffness and thickness ratio were also carried out. The results showed that the current analysis captures the attenuation of the effective force/moment near the actuator edges, and is in good agreement with the finite element results except in the region about one actuator thickness from the actuator edges. The pin-force and Euler-Bernoulli models, on the other hand, fail to describe this phenomenon.

The current analytical model is also able to predict the interfacial shear and peeling stress distribution that satisfies the boundary conditions, while the pin-force and Euler-Bernoulli models provide no information for these quantities. The magnitude of the interfacial shear and peeling stress obtained, although an approximation due to the singular nature of the complex stress state near the actuator edges, nevertheless, should be able to serve as a reliable reference for the design of integrated actuator/substructure systems.

2.6 References

Bailey, T. and Hubbard Jr., J. E., 1985, "Distributed Piezoelectric-Polymer Active Vibration Control of a Cantilever Beam, "Journal of Guidance and Control, Vol. 8, No. 5, pp. 605-611.

Barker, D. K., 1989, "Active Dynamic Response Tuning of Adaptive Composites Utilizing Embedded Nitinol Actuators," Thesis, Mechanical Engineering Department, Virginia Polytechnic Institute and State University, August, 1989.

Bogy, D. B., 1970, "On the Problem of Edge-Bonded Elastic Quarter-Planes Loaded at the Boundary," International Journal of Solids and Structures, Vol. 6, pp. 1287-1313.

Chaudhry, Z., and Rogers, C. A., 1991, "Bending and Shape Control of Beams Using SMA Actuators," Journal of Intelligent Material Systems and Structures, Vol. 2, No. 4, pp. 581-602.

Crawley, E. F. and de Luis, J., 1987, "Use of Piezoelectric Actuators as Elements of Intelligent Structures," AIAA Journal, Vol. 25, No. 10, pp. 1373-1385.

Fanson, J. L. and Chen, J. C., 1986, "Structural Control by the Use of Piezoelectric Active Members," Proceedings of NASA/DOD Control/Structures Interaction Conference, NASA CP-2447, Part II.

Haftka, R. T. and Adelman, H. M., 1985, "An Analytical Investigation of Shape Control of Large Space Structures by Applied Temperatures," AIAA Journal, Vol. 23, No. 3, pp. 450-457.

Hess, M. S., 1969, "The End Problem for a Laminated Elastic Strip-I. The General Solution," Journal of Composite Materials, Vol. 3, pp. 262-280.

Liang, C., Rogers, C. A. and Fuller, C. R., 1991, "Acoustic Transmission and Radiation Analysis of Adaptive Shape Memory Alloy Reinforced Laminated Plates," Journal of Sound and Vibration, Vol. 145, No. 1, pp. 23-41.

Piezo Systems, 1987, Piezoelectric Motor Actuation Kit Manual, Piezo Electric Products, Inc., Advanced Technology Group, Cambridge, Massachusetts.

Pipes, R. B. and Pagano, N. J., 1970, "Interlaminar Stresses in Composite Laminates Under Uniform Axial Extension," Journal of Composite Materials, Vol. 4, pp. 538-548.

Robbins, D. H. and Reedy, J. N., 1991, "Finite Element Analysis of Piezoelectrically Activated Beams," Computers and Structures, Vol. 41, No. 2, pp. 265-279.

Rogers, C. A., 1990, "An Introduction to Intelligent Material Systems and Structures," in Intelligent Systems (Proceedings of the International Workshop on Intelligent Structures, Taipei, Taiwan, 23-26 July, 1990), K. P. Chong, S. C. Liu, and J. C. Li, Eds, Elsevier, London, pp. 3-41.

Rogers, C. A., Liang, C. and Li, S., 1991, "Active Damage Control of Hybrid Material Systems Using Induced Strain Actuators," Proceedings of the AIAA/ASME/ASCE/AHS/ASC 32nd SDM Conference, Baltimore, MD, April 8-10, 1991,

Sato, T., Ishida, H. and Ikeda, O., 1980, "Adaptive PVDF Piezoelectric Deformable Mirror System," Applied Optics, Vol. 19, No. 9, pp. 1430-1434.

Wang, S. S., and Choi, I., 1982, "Boundary-Layer Effects in Composite Laminates: Part 1 - Free-Edge Stress Singularities," Journal of Applied Mechanics, Vol. 49, pp. 541-548.

Wada, B. K., Fanson, J. L., and Crawley, E. F., 1990, "Adaptive Structures," Journal of Intelligent Material Systems and Structures, Vol. 1, No. 2, pp. 157-174.

2.7 Appendix

$$K_1^e = 81648a^2E_a^3E_s(aE_a + bE_s) \tag{A.1}$$

$$K_2^e = -72576abE_a^2E_s(aE_a + bE_s) \tag{A.2}$$

$$K_3^e = 12096bE_a(aE_a + bE_s)(2aE_a + 3bE_s) \tag{A.3}$$

$$K_4^e = -72576a^2E_a^2E_s(aE_a + bE_s) \tag{A.4}$$

$$K_5^e = 24192abE_aE_s(aE_a + bE_s) \tag{A.6}$$

$$K_6^e = 12096aE_s(aE_a + bE_s)(3aE_a + 2bE_s) \tag{A.6}$$

$$K_7^e = 1152b^2E_a\{17a^2bE_a^2(1+v_s) \\ +aE_aE_s[5a^2(1+v_a)+18b^2(1+v_s)]+6b^3E_s^2(1+v_s)\} \tag{A.7}$$

$$K_8^e = -2304abE_aE_s\{bE_s[8a^2(1+v_a)+3b^2(1+v_s)] \\ +aE_a[3a^2(1+v_a)+8b^2(1+v_s)]\} \tag{A.8}$$

$$K_9^e = 1152a^2E_s\{6a^3E_a^2(1+v_a)+bE_aE_s[18a^2(1+v_a)+5b^2(1+v_s)] \\ +17ab^2E_s^2(1+v_a)\} \tag{A.9}$$

$$K_{10}^e = 432abE_a^2E_s[12b^3E_sv_s + aE_a(15a^2v_a + 35abv_s + 32b^2v_s)] \tag{A.10}$$

$$K_{11}^e = 288b^2E_a[a^2(35a+68b)E_a^2v_s - 3aE_aE_s(5a^2v_a - 24b^2v_s)+24b^3E_s^2v_s] \tag{A.11}$$

$$K_{12}^e = -288abE_aE_s[-36E_s(a^2v_a - 4b^2v_s)+aE_a(12a^2v_a + 35abv_s + 32b^2v_s)] \tag{A.12}$$

$$K_{13}^e = 4b^2 E_a [a^2 b E_a^2 (315a^2 + 1008ab + 992b^2)$$
$$+ a E_a E_s (35a^4 + 504ab^3 + 1056b^4) + 288b^5 E_s^2]$$

(A.13)

$$K_{14}^e = -216a^2 E_a^2 E_s [3a^2 E_a (27av_a + 35bv_s) + bE_s (111a^2 v_a$$
$$+ 175abv_s + 40b^2 v_s)]$$

(A.14)

$$K_{15}^e = 144ab E_a [-105a^3 E_a^2 v_s + a E_a E_s (81a^2 v_a$$
$$- 175abv_s - 64b^2 v_s) + 3b E_s^2 (37a^2 v_a - 8b^2 v_s)]$$

(A.15)

$$K_{16}^e = 144a^2 E_s [-39ab^2 E_s^2 v_a + b E_a E_s (39a^2 v_a + 175abv_s + 40b^2 v_s)$$
$$+ 3a^2 E_a^2 (16av_a + 35bv_s)]$$

(A.16)

$$K_{17}^e = -4ab E_a [189a^3 b E_a^2 (5a + 8b) + a E_a E_s (165a^4 + 1575a^2 b^2$$
$$+ 3780ab^3 + 928b^4) + 5b E_s^2 (47a^4 + 252ab^3 + 96b^4)]$$

(A.17)

$$K_{18}^e = a^2 [2835a^4 b E_a^3 + 9a^2 E_a^2 E_s (107a^3 + 1050ab^2$$
$$+ 336b^3) + b E_a E_s^2 (2586a^4 + 7875a^2 b^2 + 5040ab^3 + 896b^4) + 1763a^3 b^2 E_s^3]$$

(A.18)

$$K_1^b = 6804a(a + 2b)^2 E_a^2 E_s (3a E_a + 5b E_s)$$

(A.19)

$$K_2^b = -2268a(a + 2b) E_a^2 E_s [a(13a + 16b) E_a + b(25a + 32b) E_s]$$

(A.20)

$$K_3^b = 189 E_s [3a^2 E_a^2 (21a^2 + 64ab + 64b^2)$$
$$+ ab E_a E_s (125a^2 + 384ab + 448b^2) + 128b^4 E_s^2]$$

(A.21)

$$K_4^b = 18a\{1088ab^4 E_s^3 (1 + v_a) + 315a^4 b E_a^3 (1 + v_s)$$
$$+ 3a^3 E_a^2 E_s [a(11a + 16b)(1 + v_a) + 2b^2 (239 + 64v_a + 175v_s)]$$
$$+ 2b^2 E_a E_s^2 [-48a^3 (1 + v_a) + 56b^2 (5a + 4b)(1 + v_s)$$
$$+ 3a^2 b(367 + 192v_a + 175v_s)]\}$$

(A.22)

$$K_5^b = -108a(a+2b)E_a^2 E_s[3a^2 E_a(3a^2\nu_a + 27ab\nu_a + 35b^2\nu_s)$$
$$+ b^2 E_s(111a^2\nu_a + 210ab\nu_s + 56b^2\nu_s)] \tag{A.23}$$

$$K_6^b = 18aE_s\{-312ab^4 E_s^2\nu_a + 3aE_a^2[a(11a^2 + 121ab + 128b^2)\nu_a + 35b^2(5a+8b)\nu_s]$$
$$+ b^2 E_a E_s[39a^2(11a+8b)\nu_a + 14b(15a+4b)(5a+8b)\nu_s]\} \tag{A.24}$$

$$K_7^b = a[945a^4b^3 E_a^3 + 9a^2(2a^5 + 26a^4b + 107a^3b^2 + 420ab^4 + 112b^5)E_a^2 E_s$$
$$+ 3b^2(98a^5 + 862a^4b + 1275a^2b^3 + 720ab^4 + 128b^5)E_a E_s^2 + 1763a^3b^4 E_s^3] \tag{A.25}$$

Chapter 3

Bonding Layer Effects on the Actuation Mechanism of an Induced Strain Actuator/Substructure System

3.1 Introduction

Induced strain actuators have been integrated with conventional structural material to serve as energy input devices or actuating elements in many engineering applications implementing intelligent material system and structure concepts. Recent developments in applying these new technologies have yielded applications in active structural vibration control (Bailey and Hubbard, 1985; Fanson and Chen, 1986; Crawley and de Luis, 1987; Barker, 1989), shape control (Sato, 1980; Haftka and Adelman, 1985; Chaudhry and Rogers, 1991), acoustic transmission control (Liang and Rogers, 1991), and damage control (Rogers et al., 1991). Many induced strain actuators such as piezoelectrics, electrostrictors, and shape memory alloys have demonstrated how electromechanical and thermomechanical coupling can be incorporated into structures to yield new functional capabilities never before realized (Rogers, 1990; Wada et al., 1990).

In the process of fabricating integrated induced strain actuator/substructure systems, a third-phase adhesive bonding layer is necessary to provide bond between the adherends,

71

whether the actuators are embedded or surface-bonded. The bonding layer in general is much thinner than the actuators and substructure, and possesses a lower strength and stiffness. The presence of the bonding layer brings about two primary concerns about the integrated structural system. One is the losses in transferring actuation strain from the actuators to the substructure due to the compliance of the adhesive; the other is the failure of structural integrity caused by intensive shear and peeling stresses present at the bonding layer near the actuator ends. In order to study these issues, an analytical model including bonding layer is needed.

Simple models based on the shear lag assumptions have been used to study these issues (Crawley and de Luis, 1987; Kim and Jones, 1991; Lin and Rogers, 1990). These models, formulated under the framework of the mechanics of materials, include a thin shear layer in which the in-plane shear stress is the only stress component considered. With the presence of the shear layer, the axial normal stress distribution can adjust to satisfy stress-free boundary conditions at each end of the actuators. However, the shear stress-free boundary condition cannot be satisfied, resulting in an overestimation in the maximum interfacial shear stress. As a result, the transverse normal stress (peeling stress) distribution is incorrectly described. These models help explain the transfer of the actuation mechanism; yet lack quantitative accuracy and fail to predict the interfacial shear/peeling stress distribution.

An alternative approach using finite element analysis has been employed to investigate the bonding layer effects. Recent work by Robbins and Reddy (1991) showed that a new

finite element formulation based on the generalized laminated plate theory can model a piezoelectrically activated beam including a bonding layer and is able to satisfy all the boundary conditions without a large number of elements. However, the thickness of the bonding layer employed is of the same order of magnitude as that of the adherends. For a thin adhesive, e.g. with an adhesive-to-actuator thickness ratio on the order of 10^{-2}, a large number of elements will be needed in order to yield reliable results In addition, the relatively time-consuming computation involved with this method cannot fulfill the near real-time adaptability or control required in most applications of intelligent structures.

Similar problems of bonding layer effects have also been investigated in studies of mechanically-loaded lap joints (Goland and Reissner, 1944), and thermal stresses in two-layered composite beams with an adhesive layer (Chen et al., 1982; Williams, 1985). Valuable insight regarding the essential features of the load transfer mechanism and shear/peeling stress state in the adhesive layer were discussed. It is clear from these studies that truly realistic models of a laminate composite structure including adhesive layers must satisfy the stress-free boundary condition in the adhesive at the free edges. This conclusion has also been experimentally verified in measuring thermal stress distribution in a glass-plastic-glass composite plate using the photoelasticity technique (Durelli and Tsao, 1955).

In this chapter, the analytical model by Lin and Rogers (1993) for a beam structure with symmetrically surface-bonded induced strain actuator patches is extended to include an adhesive bonding layer. The bonding adhesive is considered capable of carrying axial

normal, shear, and transverse normal stresses. The solutions of the resulting stress field in each constituent are obtained in an approximate manner by the principle of stationary complementary energy. The results are presented by numerical examples and compared with those obtained by the shear lag theory. Parametric studies are also performed to investigate the stiffness and thickness effects of the bonding layer on the transfer of the actuation mechanism and the interfacial shear/peeling stress distribution.

3.2 Formulation

The analysis considers a beam structure of length $2L$ with a pair of induced strain actuators of length $2l$ symmetrically mounted on the outer surfaces of the beam by a layer of adhesive, as shown in Fig. 3.1 (a). The thicknesses of the actuator, adhesive, and beam are a, h, and $2b$, respectively. The in-plane induced strains of the actuators are the only impetus considered. The input induced strains can be exerted by any type of non-mechanical stimulus, such as electromechanical, thermomechanical, and magnetomechanical excitation, depending on the coupling characteristics of the actuators.

The induced strain actuation problem can be converted to a boundary value problem by first considering the blocking forces, $-E_a\lambda_t$ and $-E_a\lambda_b$, applied at the edges of the top and bottom actuator, respectively, when the actuators are activated with induced strains λ_t and λ_b, as shown in Fig. 3.1 (a). Under this activation and boundary loading condition, the stress field is uniform since the imposed blocking forces prevent the induced strains λ_t and λ_b in the actuators and, consequently, induce no deformation in the bonding

$$z \quad \sigma^I_{x(at)} = -E_a\lambda_t$$
$$\tau^I_{xz(at)} = \sigma^I_{z(at)} = 0$$

$-E_a\lambda_t$ *a Activated with* λ_t $-E_a\lambda_t$

$$\uparrow h$$
$$2b$$
$$\downarrow h$$

$$\sigma^I_{x(ht)} = \tau^I_{xz(ht)} = \sigma^I_{z(ht)} = 0$$
$$\sigma^I_{x(s)} = \tau^I_{xz(s)} = \sigma^I_{z(s)} = 0$$
$$\sigma^I_{x(hb)} = \tau^I_{xz(hb)} = \sigma^I_{z(hb)} = 0$$

x

$-E_a\lambda_b$ *a Activated with* λ_b $-E_a\lambda_b$

$$\sigma^I_{x(ab)} = -E_a\lambda_b$$
$$\tau^I_{xz(ab)} = \sigma^I_{z(ab)} = 0$$

$$2l$$
$$2L$$

(a)

$$\sigma^{II}_{x(at)} = ? \; ; \quad \tau^{II}_{xz(at)} = ? \; ; \quad \sigma^{II}_{z(at)} = ?$$

$E_a\lambda_t$ $E_a\lambda_t$

$$\sigma^{II}_{x(ht)} = ? \quad \sigma^{II}_{x(s)} = ? \quad \sigma^{II}_{x(hb)} = ?$$
$$\tau^{II}_{xz(ht)} = ? \quad \tau^{II}_{xz(s)} = ? \quad \tau^{II}_{xz(hb)} = ?$$
$$\sigma^{II}_{z(ht)} = ? \quad \sigma^{II}_{z(s)} = ? \quad \sigma^{II}_{z(hb)} = ?$$

$E_a\lambda_b$ $E_a\lambda_b$

$$\sigma^{II}_{x(ab)} = ? \; ; \quad \tau^{II}_{xz(ab)} = ? \; ; \quad \sigma^{II}_{z(ab)} = ?$$

(b)
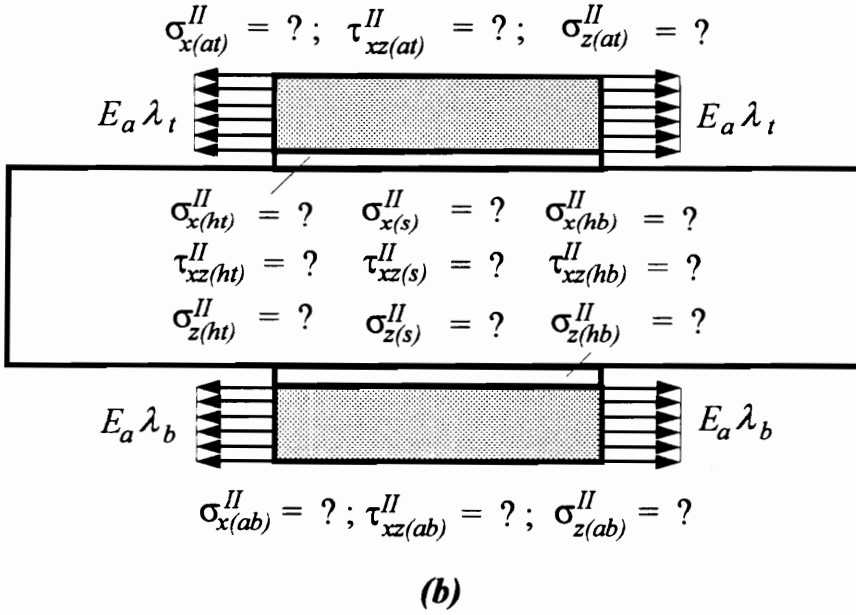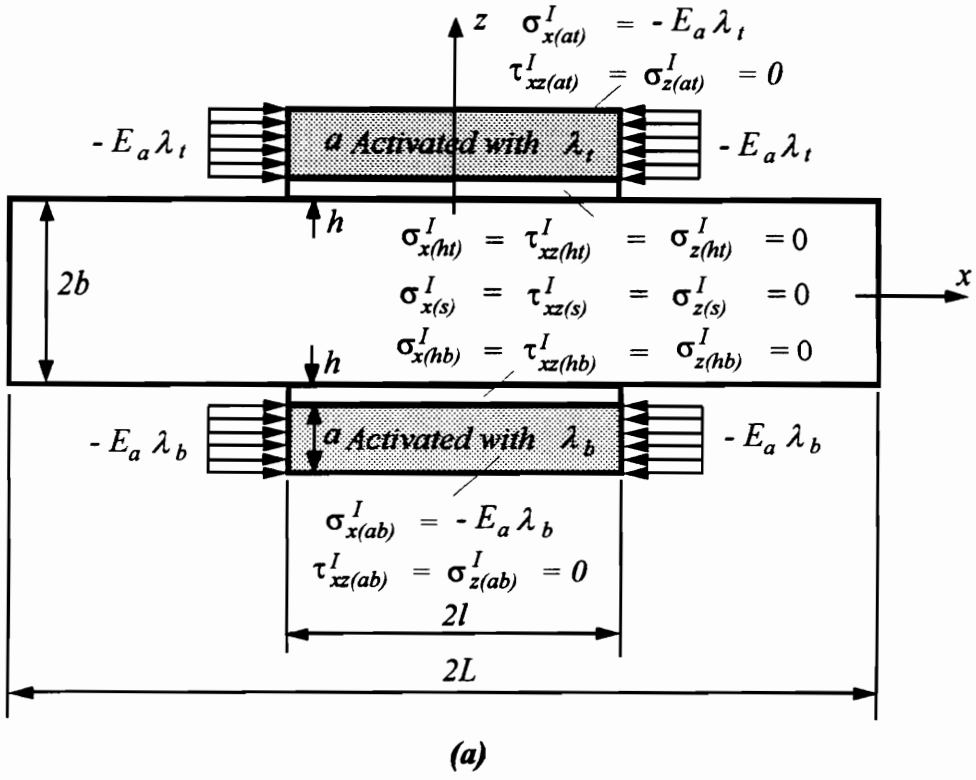
Figure 3.1. Model geometry and (*a*) application of the blocking forces as the actuators are activated; (*b*) application of the end traction.

layer and beam substrate. The stress components in each constituent are therefore known quantities, as indicated in the figure.

Since there are no blocking forces acting on the actuator edges in the original induced strain actuation problem, this traction has to be removed. This is accomplished by applying boundary traction with magnitudes of $E_a\lambda_t$ and $E_a\lambda_b$ on the top and bottom actuator edges as the actuators are not activated, as shown in Fig. 3.1(b). The stress field under this loading condition is non-uniform, and needs to be determined by solving the boundary value problem.

Combination of the loading conditions in Fig. 3.1(a) and 3.1(b) represents the original induced strain actuation problem where the prescribed induced strains of the actuators are the only impetus. Consequently, superposition of the stress fields in Fig. 3.1(a) and 3.1(b),

$$\sigma_x = \sigma_x^I + \sigma_x^{II} \tag{1.1}$$

$$\tau_{xz} = \tau_{xz}^I + \tau_{xz}^{II} \tag{1.2}$$

$$\sigma_z = \sigma_z^I + \sigma_z^{II}, \tag{1.3}$$

gives the solution of the original problem. Since the stress field in Fig 3.1(a) is known and has the expressions:

$$\sigma_{x(at)}^I = -E_a\lambda_t; \quad \tau_{xz(at)}^I = \sigma_{z(at)}^I = 0 \tag{2.1}$$

$$\sigma_{x(ht)}^I = \tau_{xz(ht)}^I = \sigma_{z(ht)}^I = 0 \tag{2.2}$$

76

$$\sigma^I_{x(s)} = \tau^I_{xz(s)} = \sigma^I_{z(s)} = 0 \tag{2.3}$$

$$\sigma^I_{x(hb)} = \tau^I_{xz(hb)} = \sigma^I_{z(hb)} = 0 \tag{2.4}$$

$$\sigma^I_{x(ab)} = -E_a \lambda_b; \quad \tau^I_{xz(ab)} = \sigma^I_{z(ab)} = 0, \tag{2.5}$$

the only effort remaining is to solve the boundary value problem of Fig. 3.1(*b*). In the above, the subscript (*at*), (*ht*), (*s*), (*hb*), and (*ab*) refer to the quantities of the top actuator, top adhesive, beam substrate, bottom adhesive, and bottom actuator, respectively, and E_a is the Young's modulus of the actuators.

The boundary value problem of Fig. 3.1(*b*) is solved using plane stress formulation based on an approximated axial normal stress field with parabolic profile in the *z*-direction. The axial normal stress field in each constituent of Fig. 3.1 (*b*) is expressed in terms of the axial normal stress of the actuators at the top and bottom outer fiber, $\sigma_{ot}(x)$ and $\sigma_{ob}(x)$, and at the actuator/adhesive interfaces, $\sigma_{ita}(x)$ and $\sigma_{iba}(x)$, and of the beam substrate at the central axis, $\sigma_c(x)$, as:

$$\sigma^{II}_{x(at)}(x,z) = \frac{(a+b+h-z)^2}{a^2}\sigma_{ita}(x) - \frac{(b+h-z)(2a+b+h-z)}{a^2}\sigma_{ot}(x) \tag{3.1}$$

$$\sigma^{II}_{x(ht)}(x,z) = \frac{E_h(b+h-z)(b+h+z)}{E_s(b+h)^2}\sigma_c(x)$$
$$+\frac{E_h z(-b-h+z)}{2E_a(b+h)^2}\sigma_{iba}(x) + \frac{E_h z(b+h+z)}{2E_a(b+h)^2}\sigma_{ita}(x) \tag{3.2}$$

$$\sigma_{x(s)}^{II}(x,z) = \frac{(b+h-z)(b+h+z)}{(b+h)^2}\sigma_c(x)$$
$$+\frac{E_s z(-b-h+z)}{2E_a(b+h)^2}\sigma_{iba}(x) + \frac{E_s z(b+h+z)}{2E_a(b+h)^2}\sigma_{ita}(x) \tag{3.3}$$

$$\sigma_{x(bh)}^{II}(x,z) = \frac{E_h(b+h-z)(b+h+z)}{E_s(b+h)^2}\sigma_c(x)$$
$$+\frac{E_h z(-b-h+z)}{2E_a(b+h)^2}\sigma_{iba}(x) + \frac{E_h z(b+h+z)}{2E_a(b+h)^2}\sigma_{ita}(x) \tag{3.4}$$

$$\sigma_{x(ab)}^{II}(x,z) = \frac{(a+b+h+z)^2}{a^2}\sigma_{iba}(x) - \frac{(b+h+z)(2a+b+h+z)}{a^2}\sigma_{ob}(x). \tag{3.5}$$

In the above expressions, continuity conditions are used at each interface,

$$\varepsilon_x(x, b+h) = \frac{\sigma_{ita}(x)}{E_a} = \frac{\sigma_{x(ht)}(x, b+h)}{E_h} \tag{4.1}$$

$$\varepsilon_x(x, b) = \frac{\sigma_{x(ht)}(x, b)}{E_h} = \frac{\sigma_{x(s)}(x, b)}{E_s} \tag{4.2}$$

$$\varepsilon_x(x, -b) = \frac{\sigma_{x(s)}(x, -b)}{E_s} = \frac{\sigma_{x(hb)}(x, -b)}{E_h} \tag{4.3}$$

$$\varepsilon_x(x, -b-h) = \frac{\sigma_{x(hb)}(x, -b-h)}{E_h} = \frac{\sigma_{iba}(x)}{E_a}, \tag{4.4}$$

where ε_x is the axial normal strain, and E_h and E_s are the Young's modulus of the adhesive and beam structure, respectively. Note that the contribution of transverse normal stresses on the axial normal strain is neglected in the above relations.

78

The self-equilibrium condition of the integrated actuator/adhesive/substrate system requires that the sum of axial forces and moments about the neutral axis of the structure vanish provided there is no external loading. This condition yields:

$$\Sigma F = F_{(at)} + F_{(ht)} + F_{(s)} + F_{(hb)} + F_{(ab)}$$

$$= \int_{b+h}^{a+b+h} \sigma_{x(at)} dz + \int_{b}^{b+h} \sigma_{x(ht)} dz + \int_{-b}^{b} \sigma_{x(s)} dz + \int_{-b-h}^{-b} \sigma_{x(hb)} dz + \int_{-a-b-h}^{-b-h} \sigma_{x(ab)} dz$$

$$= 0 \tag{5.1}$$

$$\Sigma M = M_{(at)} + M_{(ht)} + M_{(s)} + M_{(hb)} + M_{(ab)}$$

$$= \int_{b+h}^{a+b+h} z\sigma_{x(at)} dz + \int_{b}^{b+h} z\sigma_{x(ht)} dz + \int_{-b}^{b} z\sigma_{x(s)} dz + \int_{-b-h}^{-b} z\sigma_{x(hb)} dz + \int_{-a-b-h}^{-b-h} z\sigma_{x(ab)} dz$$

$$= 0, \tag{5.2}$$

resulting in a relation of the stresses $\sigma_{ita}(x)$ and $\sigma_{iba}(x)$ in terms of $\sigma_c(x)$, $\sigma_{ot}(x)$, and $\sigma_{ob}(x)$ as:

$$\sigma_{ita}(x) = \{3aE_a^2 E_s (b+h)[2b^3 E_s (a+4b+4h) + aE_a (b+h)^2 (3a+8b+8h)$$
$$+2hE_h (a+4b+4h)(3b^2+3bh+h^2)]\lambda_t$$
$$-3a^2 E_a^2 E_s (b+h)[2b^3 E_s + aE_a (b+h)^2 + 2hE_h (3b^2+3bh+h^2)]\lambda_b$$
$$-2E_a [4b^3 E_s + aE_a (b+h)(a+4b+4h)$$
$$+4hE_h (3b^2+3bh+h^2)][h^2 E_h (3b+2h) + bE_s (2b^2+6bh+3h^2)]\sigma_c(x)$$
$$-aE_a E_s (b+h)[b^3 E_s (5a+16b+16h) + aE_a (b+h)^2 (7a+16b+16h)$$
$$+hE_h (5a+16b+16h)(3b^2+3bh+h^2)]\sigma_{ot}(x)$$
$$+a^2 E_a E_s (b+h)[5b^3 E_s + 3aE_a (b+h)^2 + 5hE_h (3b^2+3bh+h^2)]\sigma_{ob}(x)\}$$
$$/\{2E_s [b^3 E_s + aE_a (b+h)^2 + hE_h (3b^2+3bh+h^2)][4b^3 E_s$$
$$+aE_a (b+h)(a+4b+4h) + 4hE_h (3b^2+3bh+h^2)]\}$$

$$\tag{6.1}$$

$$\sigma_{iba}(x) = \{-3a^2 E_a{}^2 E_s(b+h)[2b^3 E_s + aE_a(b+h)^2 + 2hE_h(3b^2 + 3bh + h^2)]\lambda_t$$
$$+3aE_a{}^2 E_s(b+h)[2b^3 E_s(a+4b+4h) + aE_a(b+h)^2(3a+8b+8h)$$
$$+2hE_h(a+4b+4h)(3b^2 + 3bh + h^2)]\lambda_b$$
$$-2E_a[4b^3 E_s + aE_a(b+h)(a+4b+4h)$$
$$+4hE_h(3b^2 + 3bh + h^2)][h^2 E_h(3b+2h) + bE_s(2b^2 + 6bh + 3h^2)]\sigma_c(x)$$
$$+a^2 E_a E_s(b+h)[5b^3 E_s + 3aE_a(b+h)^2 + 5hE_h(3b^2 + 3bh + h^2)]\sigma_{ot}(x)$$
$$-aE_a E_s(b+h)[b^3 E_s(5a+16b+16h) + aE_a(b+h)^2(7a+16b+16h)$$
$$+hE_h(5a+16b+16h)(3b^2 + 3bh + h^2)]\sigma_{ob}(x)\}$$
$$/\{2E_s[b^3 E_s + aE_a(b+h)^2 + hE_h(3b^2 + 3bh + h^2)][4b^3 E_s$$
$$+aE_a(b+h)(a+4b+4h) + 4hE_h(3b^2 + 3bh + h^2)]\}.$$

$$(6.2)$$

Based on the axial normal stress field of Eq. (3), the shear and transverse normal stresses can be derived from equilibrium considerations:

$$\frac{\partial \sigma_x}{\partial x} + \frac{\partial \tau_{xz}}{\partial z} = 0 \tag{7.1}$$

$$\frac{\partial \tau_{xz}}{\partial x} + \frac{\partial \sigma_z}{\partial z} = 0. \tag{7.2}$$

Substituting Eq. (3) for σ_x in Eq. (7.1) for each constituent, and integrating with respect to z, the shear stresses are obtained:

$$\tau^{II}_{xz(at)}(x,z) = \frac{(a+b+h-z)^3}{3a^2}\sigma'_{ita}(x)$$
$$+\frac{[3a^2 - (a+b+h-z)^2](a+b+h-z)}{3a^2}\sigma'_{ot}(x) \tag{8.1}$$

$$\tau^{II}_{xz(ht)}(x,z) = \frac{E_h(b+h-z)^2(2b+2h+z)}{3E_s(b+h)^2}\sigma'_c(x) + \frac{2a}{3}\sigma'_{ot}(x)$$
$$+ \frac{4aE_a(b+h)^2 + E_h(b+h-z)[5(b+h)^2 + 5(b+h)z + 2z^2]}{12E_a(b+h)^2}\sigma'_{ita}(x)$$
$$- \frac{E_h(b+h-z)^2(b+h+2z)}{12E_a(b+h)^2}\sigma'_{iba}(x) \tag{8.2}$$

$$\tau^{II}_{xz(s)}(x,z) = \frac{-z[3(b+h)^2 - z^2]}{3(b+h)^2}\sigma'_c(x) - \frac{a}{3}\sigma'_{ob}(x) + \frac{a}{3}\sigma'_{ot}(x)$$
$$- \frac{2aE_a(b+h)^2 + 3E_hh(b+h)(2b+h) + E_s[3b^2(b+h) - 3(b+h)z^2 + 2z^3)]}{12E_a(b+h)^2}\sigma'_{iba}(x)$$
$$+ \frac{2aE_a(b+h)^2 + 3E_hh(b+h)(2b+h) + E_s[3b^2(b+h) - 3(b+h)z^2 - 2z^3)]}{12E_a(b+h)^2}\sigma'_{ita}(x) \tag{8.3}$$

$$\tau^{II}_{xz(hb)}(x,z) = \frac{-E_h(2b+2h-z)(b+h=z)^2}{3E_s(b+h)^2}\sigma'_c(x) - \frac{2a}{3}\sigma'_{ob}(x)$$
$$- \frac{4aE_a(b+h)^2 + E_h(b+h+z)[5(b+h)^2 - 5(b+h)z + 2z^2]}{12E_a(b+h)^2}\sigma'_{iba}(x)$$
$$+ \frac{E_h(b+h-2z)(b+h+z)^2}{12E_a(b+h)^2}\sigma'_{ita}(x) \tag{8.4}$$

$$\tau^{II}_{xz(ab)}(x,z) = \frac{-(a+b+h+z)^2}{3a^2}\sigma'_{iba}(x)$$
$$- \frac{(a+b+h+z)[3a^2 - (a+b+h+z)^2]}{3a^2}\sigma'_{ob}(x). \tag{8.5}$$

In the above expressions, the boundary traction conditions at upper and lower lateral surfaces and the traction continuity at the interfaces,

$$\tau^{II}_{xz(at)}(x,a+b+h) = \tau^{II}_{xz(ab)}(x,-a-b-h) = 0 \tag{9.1}$$
$$\tau^{II}_{xz(at)}(x,b+h) = \tau^{II}_{xz(ht)}(x,b+h) \tag{9.2}$$

$$\tau_{xz(ab)}^{II}(x,-b-h) = \tau_{xz(hb)}^{II}(x,-b-h) \tag{9.3}$$

$$\tau_{xz(ht)}^{II}(x,b) = \tau_{xz(s)}^{II}(x,b) \tag{9.4}$$

$$\tau_{xz(s)}^{II}(x,-b) = \tau_{xz(hb)}^{II}(x,-b), \tag{9.5}$$

are used to obtain the constants of integration.

Likewise, the transverse normal stresses can be obtained by substituting Eq. (8) for τ_{xz} in Eq. (7.2) for each constituent, and integrating with respect to z:

$$\sigma_{z(at)}^{II}(x,z) = \frac{(a+b+h-z)^4}{12a^2}\sigma_{ita}''(x)$$
$$+ \frac{[6a^2-(a+b+h-z)^2](a+b-h-z)^2}{12a^2}\sigma_{ot}''(x) \tag{10.1}$$

$$\sigma_{z(ht)}^{II}(x,z) = \frac{E_h(b+h-z)^3(3b+3h+z)}{12E_s(b+h)^2}\sigma_c''(x) - \frac{E_h(b+h-z)^3(b+h+z)}{24E_a(b+h)^2}\sigma_{iba}''(x)$$
$$+ \frac{2aE_a(b+h)^2[a+4(b+h-z)]+E_h(b+h-z)^2[7(b+h)^2+4(b+h)z+z^2]}{24E_a(b+h)^2}\sigma_{ita}''(x)$$
$$+ \frac{a(5a+8b+8h-8z)}{12}\sigma_{ot}''(x) \tag{10.2}$$

$$\sigma_{z(s)}^{II}(x,z) = -\frac{-E_h h^3(4b+3h)+E_s(b-z)(b+z)[-b^2+6(b+h)^2-z^2]}{12E_s(b+h)^2}\sigma_c''(x)$$
$$-\{-aE_a(b+h)^2(a+4h+4z)-E_h h[h(6b^2+8bh+3h^2)+6(b+h)(2b+h)z]$$
$$+E_s[b^4-6b^2(b+h)z+2(b+h)z^3-z^4]\}\sigma_{iba}''(x)/24E_a(b+h)^2$$
$$-\{-aE_a(b+h)^2(a+4h-4z)-E_h h[h(6b^2+8bh+3h^2)-6(b+h)(2b+h)z]$$
$$+E_s[b^4+6b^2(b+h)z-2(b+h)z^3-z^4]\}\sigma_{ita}''(x)/24E_a(b+h)^2$$
$$+\frac{a(5a+8h+8z)}{24}\sigma_{ob}''(x)+\frac{a(5a+8h-8z)}{24}\sigma_{ot}''(x) \tag{10.3}$$

$$\sigma^{II}_{z(hb)}(x,z) = \frac{E_h(3b+3h-z)(b+h+z)^3}{12E_s(b+h)^2}\sigma''_c(x)$$

$$+\frac{E_h(b+h+z)^2[7(b+h)^2-4(b+h)z+z^2]+2aE_a(b+h)^2(a+4(b+h+z))}{24E_a(b+h)^2}\sigma''_{iba}(x)$$

$$-\frac{E_h(b+h-z)(b+h+z)^3}{24E_a(b+h)^2}\sigma''_{ita}(x)+\frac{a(5a+8b+8h+8z)}{12}\sigma''ob(x)$$

$$(10.4)$$

$$\sigma^{II}_{z(ab)}(x,z) = \frac{(a+b+h+z)^4}{12a^2}\sigma''_{iba}(x)$$

$$+\frac{(a+b+h+z)^2[6a^2-(a+b+h+z)^2]}{12a^2}\sigma''_{ob}(x).$$

$$(10.5)$$

The boundary traction conditions at the upper and lower lateral surfaces and the traction continuity at the interfaces,

$$\sigma^{II}_{z(at)}(x,a+b+h) = \sigma^{II}_{z(ab)}(x,-a-b-h) = 0 \qquad (11.1)$$

$$\sigma^{II}_{z(at)}(x,b+h) = \sigma^{II}_{z(ht)}(x,b+h) \qquad (11.2)$$

$$\sigma^{II}_{z(ab)}(x,-b-h) = \sigma^{II}_{z(hb)}(x,-b-h) \qquad (11.3)$$

$$\sigma^{II}_{z(ht)}(x,b) = \sigma^{II}_{z(s)}(x,b) \qquad (11.4)$$

$$\sigma^{II}_{z(s)}(x,-b) = \sigma^{II}_{z(hb)}(x,-b), \qquad (11.5)$$

are used for the constants of integration.

The stress fields of Eqs. (3), (8), and (10) satisfy the equilibrium in each constituent as well as the overall self-equilibrium of the integrated structural system. The boundary conditions involving stresses at the lateral surfaces, along with the traction continuity at the interfaces, are also satisfied. The unknowns to be determined in this stress field are

83

$\sigma_{ot}(x)$, $\sigma_{ob}(x)$, and $\sigma_c(x)$, which are independent of the z-coordinate and subject to boundary constraint of the end traction condition, as indicated in Fig. 3.1(b).

To solve these unknown stress components, the principle of stationary complementary energy is used. The complementary energy for the present problem is:

$$
\begin{aligned}
U_{(total)} &= U_{(at)} + U_{(ht)} + U_{(s)} + U_{(hb)} + U_{(ab)} \\
&= \frac{1}{2E_a} \int_{b+h}^{a+b+h} \int_{-l}^{l} [\sigma_{x(at)}^{II}{}^2 + \sigma_{z(at)}^{II}{}^2 + 2(1+v_a)\tau_{xz(at)}^{II}{}^2 - 2v_a\sigma_{x(at)}^{II}\sigma_{z(at)}^{II}]dxdz \\
&\quad + \frac{1}{2E_h} \int_{b}^{b+h} \int_{-l}^{l} [\sigma_{x(ht)}^{II}{}^2 + \sigma_{z(ht)}^{II}{}^2 + 2(1+v_h)\tau_{xz(ht)}^{II}{}^2 - 2v_h\sigma_{x(ht)}^{II}\sigma_{z(ht)}^{II}]dxdz \\
&\quad + \frac{1}{2E_s} \int_{-b}^{b} \int_{-l}^{l} [\sigma_{x(s)}^{II}{}^2 + \sigma_{z(s)}^{II}{}^2 + 2(1+v_s)\tau_{xz(s)}^{II}{}^2 - 2v_s\sigma_{x(s)}^{II}\sigma_{z(s)}^{II}]dxdz \\
&\quad + \frac{1}{2E_h} \int_{-b-h}^{-b} \int_{-l}^{l} [\sigma_{x(hb)}^{II}{}^2 + \sigma_{z(hb)}^{II}{}^2 + 2(1+v_h)\tau_{xz(hb)}^{II}{}^2 - 2v_h\sigma_{x(hb)}^{II}\sigma_{z(hb)}^{II}]dxdz \\
&\quad + \frac{1}{2E_a} \int_{-a-b-h}^{-b-h} \int_{-l}^{l} [\sigma_{x(ab)}^{II}{}^2 + \sigma_{z(ab)}^{II}{}^2 + 2(1+v_a)\tau_{xz(ab)}^{II}{}^2 - 2v_a\sigma_{x(ab)}^{II}\sigma_{z(ab)}^{II}]dxdz,
\end{aligned}
$$

(12)

where v_a, v_h, and v_s are the Poisson's ratio of the actuator, adhesive, and beam structure, respectively. In order to simplify the foregoing derivation, the problem is solved for the case of pure extension/contraction and pure bending separately.

In the case of pure extension/contraction, the imposed induced strains of the actuators are equal and in the same direction, i.e., $\lambda_b = \lambda_t$. This actuation condition yields a symmetric axial normal stress field about the x-axis, i.e., $\sigma_{ob}(x) = \sigma_{ot}(x)$. The unknowns remaining to be determined are then $\sigma_{ot}(x)$ and $\sigma_c(x)$. Variation of the

complementary energy, $\delta U = 0$, with the stresses satisfying the prescribed end traction yields the Euler's equations:

$$\left[A_1^e \frac{d^4}{dx^4} + A_2^e \frac{d^2}{dx^2} + A_3^e \right] \sigma_c(x) + \left[B_1^e \frac{d^4}{dx^4} + B_2^e \frac{d^2}{dx^2} + B_3^e \right] \sigma_{ot}(x) = D_1^e$$

(13.1)

$$\left[B_1^e \frac{d^4}{dx^4} + B_2^e \frac{d^2}{dx^2} + B_3^e \right] \sigma_c(x) + \left[C_1^e \frac{d^4}{dx^4} + C_2^e \frac{d^2}{dx^2} + C_3^e \right] \sigma_{ot}(x) = D_2^e.$$

(13.2)

This leads to a general solution for $\sigma_{ot}(x)$ and $\sigma_c(x)$:

$$\sigma_{ot}(x) = \frac{(A_3^e D_2^e - B_3^e D_1^e)}{(A_3^e C_3^e - (B_3^e)^2)} + \sum_{i=1}^{8} p_i^e (\exp)^{\alpha_i^e x}$$

(14.1)

$$\sigma_c(x) = \frac{(C_3^e D_1^e - B_3^e D_2^e)}{(A_3^e C_3^e - (B_3^e)^2)} + \sum_{i=1}^{8} \gamma_i^e p_i^e (\exp)^{\alpha_i^e x},$$

(14.2)

where

$$\gamma_i^e = -\frac{(A_3^e + A_2^e (\alpha_i^e)^2 + A_1^e (\alpha_i^e)^4)}{(B_3^e + B_2^e (\alpha_i^e)^2 + B_1^e (\alpha_i^e)^4)}, \quad i = 1,8,$$

in which A_i^e, B_i^e, C_i^e, (i=1,3) and $D_i^e (i = 1,2)$ are functions of the material properties and the geometries of the actuators, adhesive, and beam. The complete expressions are given in the Appendix. In the above, $\alpha_i^e (i = 1,8)$ are the roots of the characteristic equation:

$$\begin{vmatrix} (A_1^e (\alpha^e)^4 + A_2^e (\alpha^e)^2 + A_3^e) & (B_1^e (\alpha^e)^4 + B_2^e (\alpha^e)^2 + B_3^e) \\ (B_1^e (\alpha^e)^4 + B_2^e (\alpha^e)^2 + B_3^e) & (C_1^e (\alpha^e)^4 + C_2^e (\alpha^e)^2 + C_3^e) \end{vmatrix} = 0,$$

(15)

and $p_i^e (i = 1,8)$ are arbitrary constants to be determined by the end traction conditions:

85

$$\sigma_{ot}(\pm l) = E_a \lambda_t; \quad \sigma_c(\pm l) = 0 \tag{16.1}$$

$$\sigma'_{ot}(\pm l) = 0; \quad \sigma'_c(\pm l) = 0. \tag{16.2}$$

In the case of pure bending, the input induced strains of the actuators are equal yet in the opposite direction, i.e., $\lambda_b = -\lambda_t$. This condition yields an antisymmetric axial normal stress field about the x-axis, i.e., $\sigma_{ob}(x) = -\sigma_{ot}(x)$ and $\sigma_c(x) = 0$. The only unknown stress component to be determined in this case is then $\sigma_{ot}(x)$. Variation of the complementary energy, $\delta U = 0$, with the stresses satisfying the prescribed end traction yields the Euler's equation:

$$[A_1^b \frac{d^4}{dx^4} + A_2^b \frac{d^2}{dx^2} + A_3^b] \sigma_{ot}(x) = D_1^b. \tag{17}$$

This leads to a general solution for $\sigma_{ot}(x)$:

$$\sigma_{ot}(x) = \frac{D_1^b}{A_3^b} + \sum_{i=1}^4 p_i^b (\exp)^{\alpha_i^b x}. \tag{18}$$

The expressions of the constants A_i^b ($i = 1, 3$) and D_1^b are given in the Appendix. In the above, $\alpha_i^b (i = 1,4)$ are the roots of the characteristic equation:

$$A_1^b (\alpha^b)^4 + A_2^b (\alpha^b)^2 + A_3^b = 0, \tag{19}$$

and $p_i^b (i = 1,4)$ are arbitrary constants to be determined by the end traction conditions:

$$\sigma_{ot}(\pm l) = E_a \lambda_t \tag{20.1}$$

$$\sigma'_{ot}(\pm l) = 0. \tag{20.2}$$

86

The roots of α_i^e and α_i^b solved in the above are complex in general, but in conjugate pairs. Consequently, the stress quantities are real. Although the solutions were obtained for two separate cases, pure extension/contraction and pure bending, they can be linearly superimposed to yield the solution for a general actuation condition. It is noted that the solutions are in closed form which is of importance for the requirement of near real-time adaptability or control in most applications of intelligent material systems and structures.

3.3 Results

The results of the analysis are presented by numerical examples for an aluminum beam with surface-bonded piezoelectric actuators. Table 3.1 gives the configuration and material properties of the actuator and beam structure. Since the adhesive layer is a third-phase material and the effects of its presence are the primary interest in this study, the material properties and geometry of the adhesive are therefore treated as independent parameters.

Figure 3.2 shows the effective force distribution induced in the beam substrate for different adhesive thicknesses as the actuators are activated in pure extension, i.e., $\lambda_b = \lambda_t$. The length of the actuators is chosen to be $l = 2in$, and the stiffness of the adhesive is $E_h = 0.28 msi$, which is comparable to an epoxy bond. The quantity of the effective force is normalized with respect to the total blocking force, $F^* = 2aE_a\lambda_t$, of the actuator, and the x-axis is nondimensionalized with respect to the thickness of the

Table 3.1. Material properties and geometries of the constituents

G-1195 piezoceramic	E_a=9.13 (msi)	v_a=0.4	a=0.1 (in)	$\lambda=d_{31}V$=1.3x10^{-4}
6061 aluminum	E_s=10.6 (msi)	v_s=0.3	b=0.3 (in)	
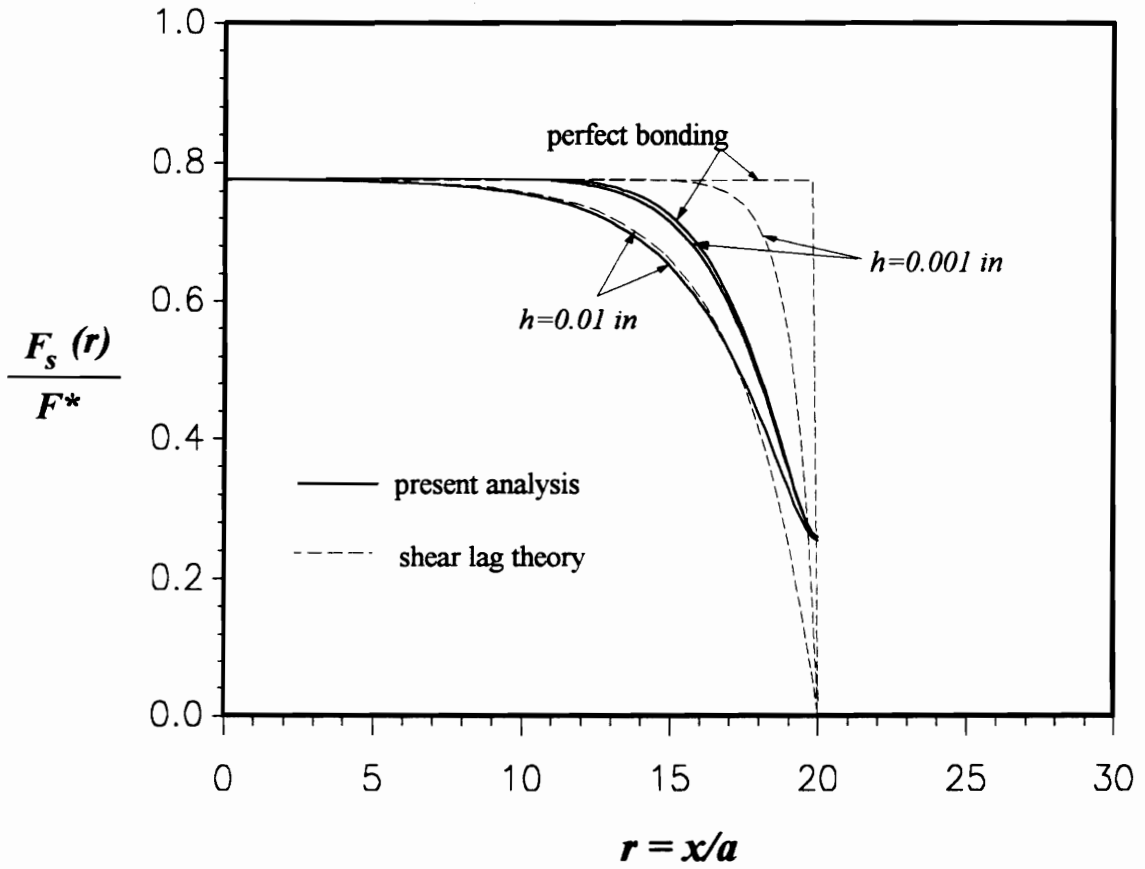
Figure 3.2. Effective force distribution in the beam substrate along the x-axis under pure extension actuation for different adhesive thicknesses with $E_h = 0.28\ msi$ and $\nu_h = 0.3$.

actuators. For comparison, the results obtained from the shear lag theory (Crawley and de Luis, 1987) are included.

It is shown that for the case of perfect bonding, i.e., $h = 0$, the shear lag theory cannot describe the edge effect of the effective force transferring, while the current analysis captures this phenomenon. In the case of a thin bonding layer, $h = 0.001$ in, the shear lag theory overpredicts the effective force level near the actuator edges, although it can adjust to satisfy axial normal stress free boundary condition. Comparable results are obtained from both analyses for relatively thick adhesive, $h = 0.01$ in. It is noted that for compliant adhesives such as epoxy, the force level at locations away from the edges remains unchanged, since compliant adhesives bear little structural loads.

The interfacial shear and peeling stress distribution along the x-direction under pure extension activation for different adhesive thicknesses is shown in Fig. 3.3. The stress quantity is normalized with respect to the blocking stress of the actuators, i.e., $E_a \lambda_t$. The results of the present analysis and those obtained by shear lag theory are depicted for comparison. Note that the location of the shear stress shown is at the actuator/adhesive interface, i.e., $z = b + h$, and the location of the peeling stress is at the adhesive/beam interface, i.e., $z = b$, where a higher level of stress is present.

It is shown that the shear lag theory does not satisfy shear stress free boundary condition. The decrease in adhesive thickness results in a drastic increase in shear, which tends to

Figure 3.3. Interfacial shear and peeling stress distributions along the x-axis under pure extension actuation for different adhesive thicknesses with $E_h = 0.28\ msi$ and $\nu_h = 0.3$.

increase without bond. On the contrary, the present analysis satisfies the shear stress free boundary condition, and the maximum shear stress occurs at a short distance of about one actuator thickness from the ends. It also predicts an increase in shear stress with decreasing adhesive thickness.

The present analysis predicts a maximum peeling stress right at the edges. The sign of the maximum peeling stress is opposite to that of the shear stress. This result agrees with those shown in the analysis of mechanically-loaded lap joints (Goland and Reissner, 1944) and thermal stresses in laminate structures (Chen et al., 1982), as well as with experimental observation of thermal stresses in laminate structures (Durelli and Tsao, 1955). It is shown that the maximum peeling stress level decreases with increasing adhesive stiffness. The shear lag theory, on the other hand, predicts a much lower peeling stress level which does not agree with those shown in the literature.

Figure 3.4 shows the effective moment distribution induced in the beam substrate for different adhesive stiffnesses as the actuators are activated in pure bending, i.e., $\lambda_b = -\lambda_t$. The length of the actuator is chosen to be $l = 2in$, and the thickness of the adhesive is $h = 0.005in$. The results for the case of perfect bonding and the case of adhesive layer with $E_h = 0.28msi$ and $E_h = 10.6msi$ are shown, which are comparable to epoxy bonds and aluminum (close to perfect bonds). The magnitude of the effective moment is normalized with the moment that the blocking force of the actuators produce about the neutral axis of the structure, i.e., $M^* = 2aE_a\lambda_t(a/2+b)$. For comparison, the results of the present analysis and the shear lag theory are depicted.
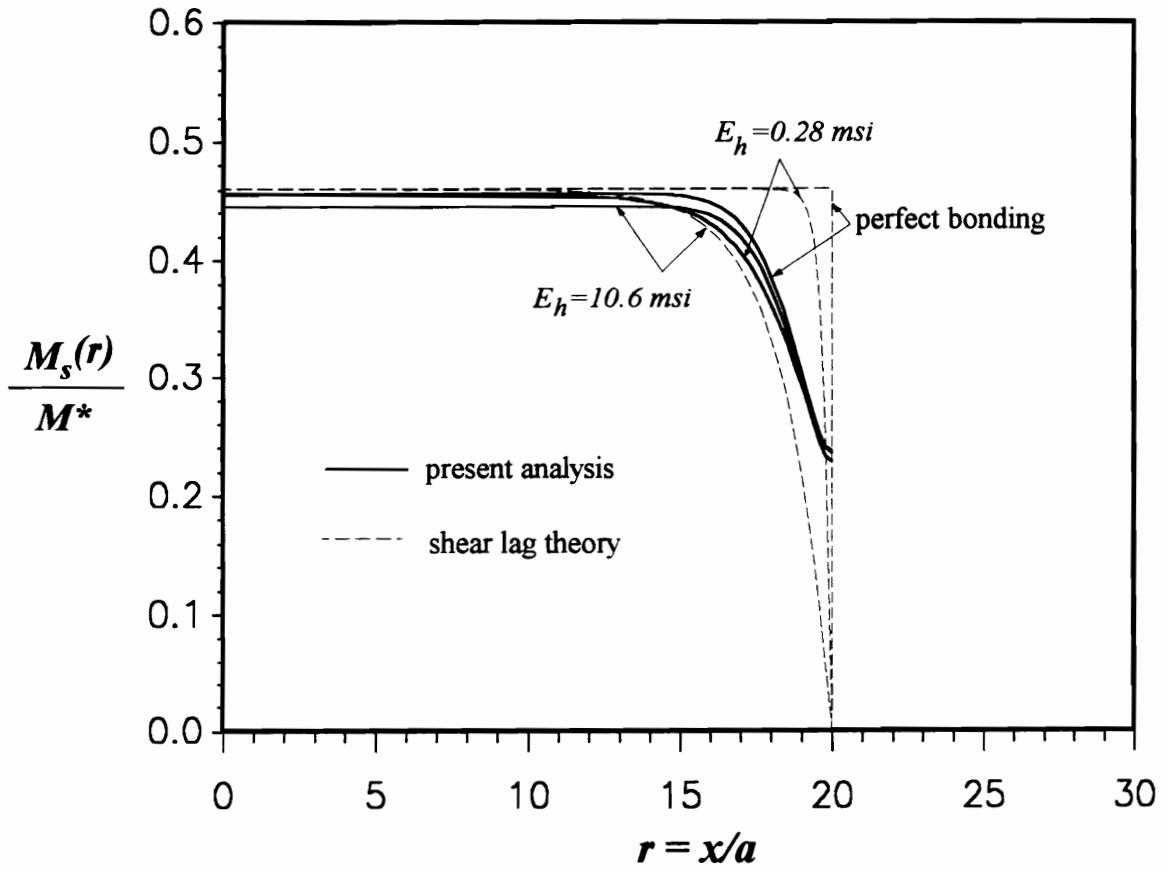
Figure 3.4. Effective moment distributions in the beam substrate along the x-axis under pure bending actuation for different adhesive stiffnesses with $h = 0.005\, in.$

It is shown that more compliant adhesive requires a longer distance from the actuator ends to reach the constant moment level. This trend is shown on both analyses, yet the shear lag theory cannot describe the edge effects for the case of perfect bonding. It is noted that the adhesive layer carries no axial normal stresses in the shear lag assumption, thus the magnitude of the effective moment away from the edges remains unchanged. The current analysis, on the other hand, shows the adhesive layer being capable of bearing both normal and shear stresses. Therefore, the adhesive carries part of the structural loads, resulting in a lower effective moment level on the beam substrate. This result is more evident in the case of adhesives of high stiffness.

The interfacial shear and peeling stress distributions in the x-direction under pure bending activation for different adhesive stiffnesses is shown in Fig. 3.5. The results of the present analysis and those obtained by shear lag theory are included for comparison. The location of the shear stress shown is at the actuator/adhesive interface, i.e., $z = b + h$, and the location of the peeling stress is at the adhesive/beam interface, i.e., $z = b$, where a higher level of stress is obtained.

It is shown that the interfacial shear and peeling stresses increase with increasing adhesive stiffness. The shear lag theory does not satisfy the shear stress free boundary condition and overestimates the maximum shear stress level. In addition, the interfacial peeling stress is underestimated in magnitude and incorrect in sign as predicted by the shear lag theory.
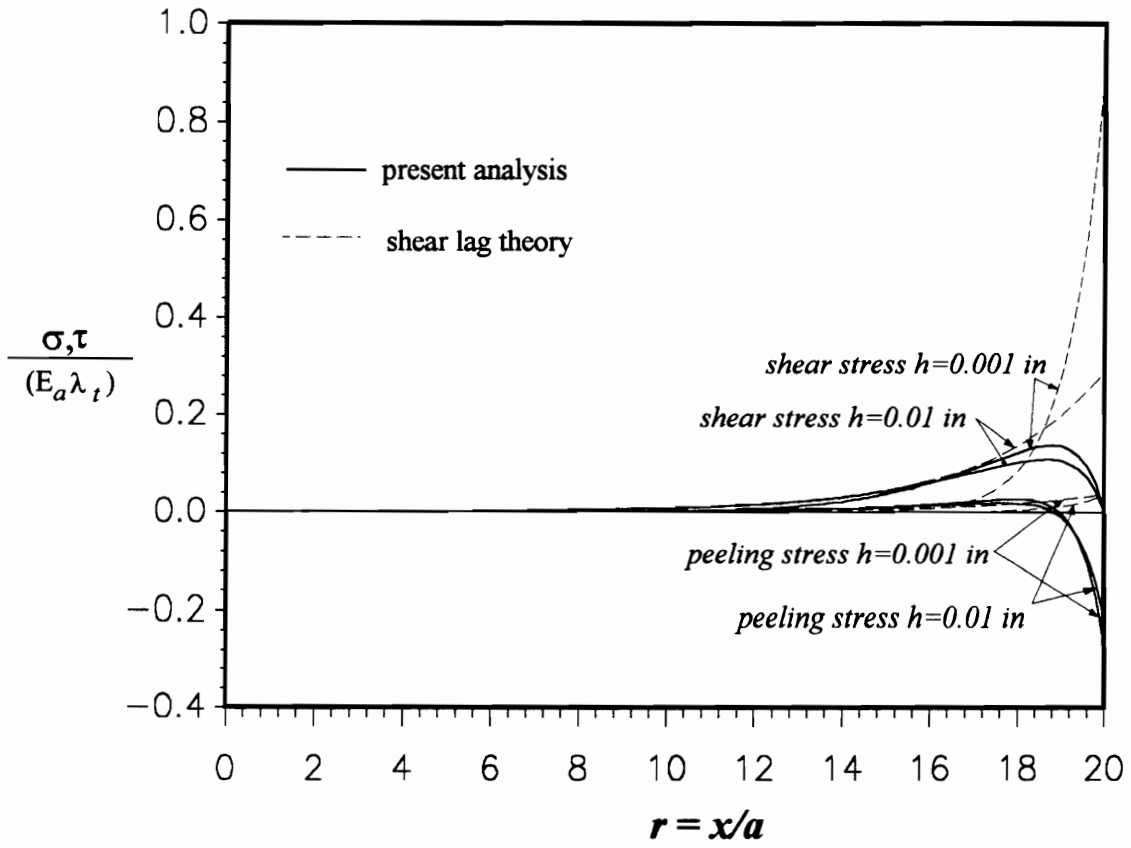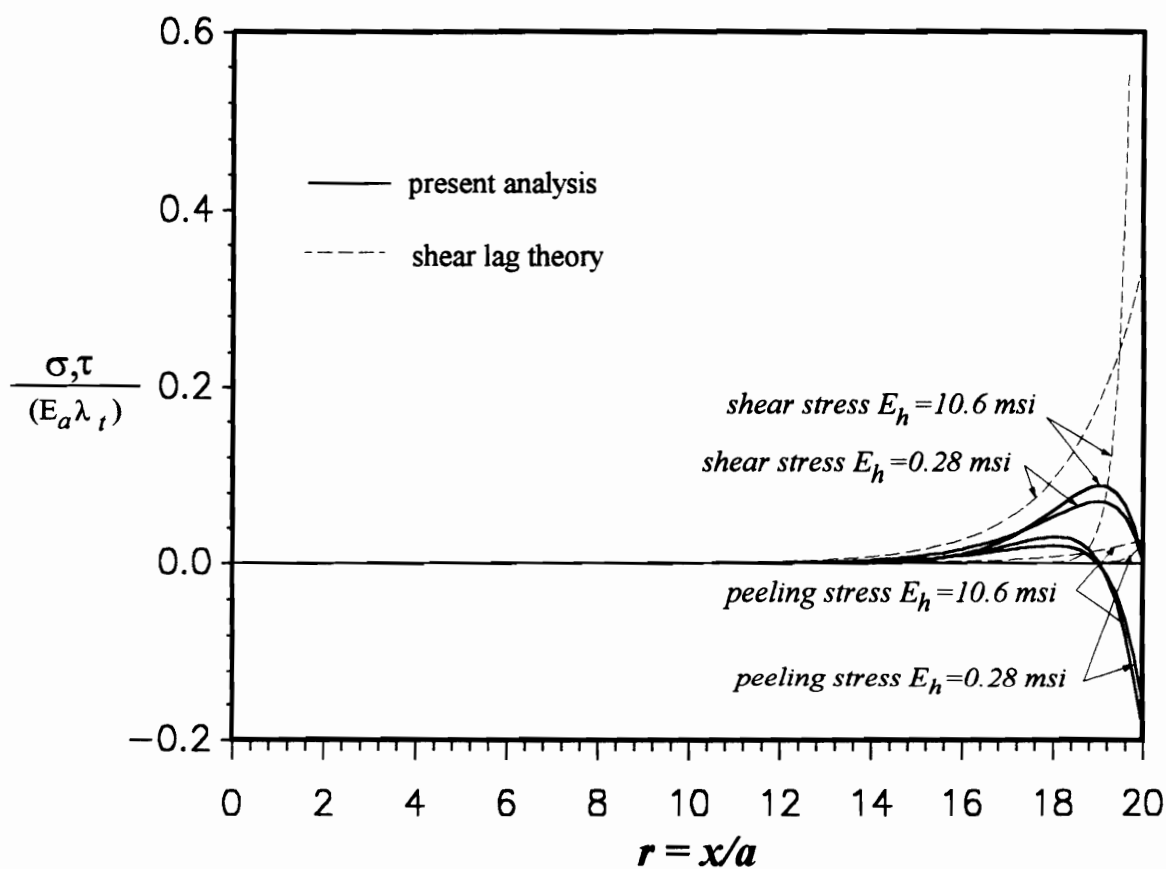
Figure 3.5. Interfacial shear and peeling stress distribution along the x-axis under pure bending actuation for different adhesive stiffness with $h = 0.005\,in$.

A parametric study has been performed to investigate the influence of the adhesive stiffness and thickness on the transfer of the actuation mechanism and the induced interfacial shear and peeling stresses. Figure 3.6 shows the effects of the adhesive stiffness on the effective force transferred from the actuators to the beam substructure as the actuators are activated in pure extension. The results for three different adhesive thicknesses are illustrated, where F_d is the effective force on the beam at $x = 0$ and ξ is the unsaturated length which indicates the distance from the actuator edges needed for the effective force to reach its constant level. The adhesive stiffness is normalized with that of an epoxy bond, i.e., $E_h^* = 0.28\,msi$, and the effective force is normalized with that obtained as $\overline{E}_h = 1$. The length of the actuator is chosen to be $l = 8\,in$. This ensures that the actuator length is long enough for the effective force to reach its constant level.

It is shown that the effective force level at $x = 0$ is not significantly affected. The reduction of the magnitude is within 10% even with $\overline{E}_h = 25$ and $h = 0.05\,in$. Nevertheless, the unsaturated length ξ increases with decreasing adhesive stiffness, and this trend is more apparent as $\overline{E}_h < 5$. This indicates that a more compliant adhesive requires a longer distance from the actuator ends to achieve its full actuation level. Note that for $\overline{E}_h = 0.5$ (or $E_h = 0.14\,msi$), and $h = 0.005\,in$, the required distance can be as long as $\overline{\xi} = 0.15$ (or $\xi = 1.2\,in$).

The influence of the adhesive thickness on the effective moment transferred from the actuators to the beam substructure as the actuators are activated in pure bending is shown in Fig. 3.7. The results for three different adhesive stiffnesses are illustrated, where M_d is
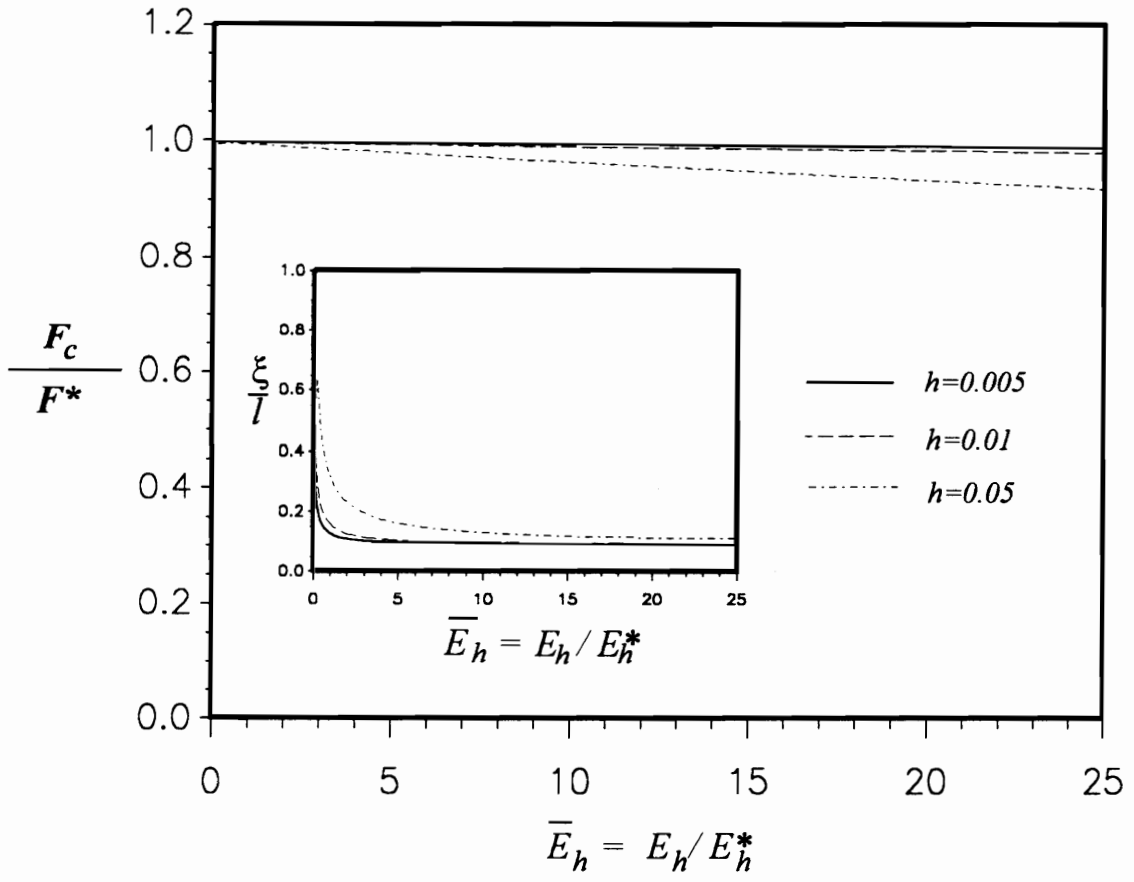
Figure 3.6. Effective forces and unsaturated lengths in the beam substrate under pure extension actuation as a function of the stiffness of the adhesive bond.
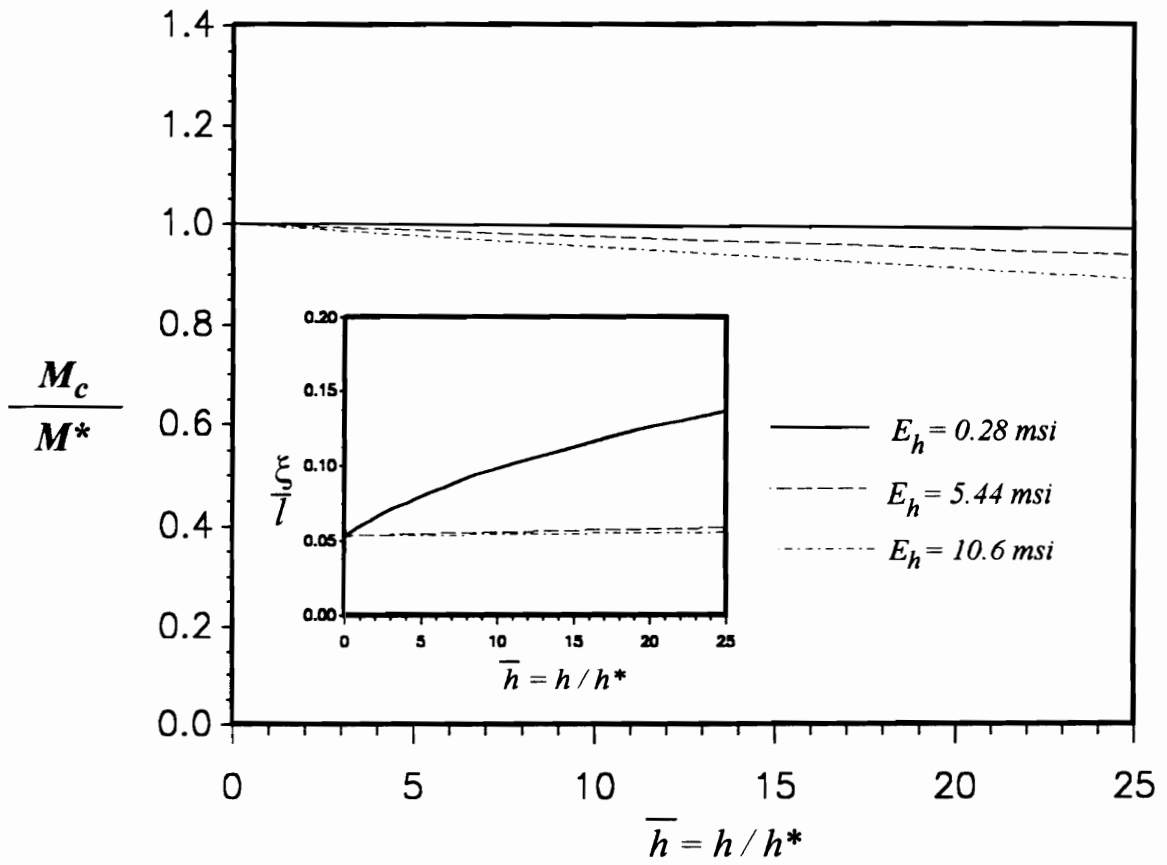
Figure 3.7. Effective moments and unsaturated lengths in the beam substrate under pure bending actuation as a function of the thickness of the adhesive bond.

98

the effective moment on the beam at $x = 0$. The adhesive thickness is normalized with $h^* = 0.001in$, and the effective moment is normalized with that obtained as $h = 0$, i.e., the case of perfect bonding.

It is shown that the effective moment level at $x = 0$ is not significantly affected. With $\bar{h} = 25$ and $E_h = 10.6msi$, the reduction of the magnitude is within 10%. However, the unsaturated length ξ increases with increasing adhesive thickness, and this trend is more evident for the case of a compliant adhesive.

Figure 3.8 illustrates the adhesive stiffness effects on the maximum interfacial shear and peeling stresses for both pure extension and pure bending actuation with adhesive thickness $h = 0.005in$. The stress quantity is normalized with the blocking stress of the actuator, $E_a \lambda_t$, and the adhesive stiffness is normalized with that of an epoxy bond, $E_h^* = 0.28msi$. It is shown that both the maximum interfacial shear and peeling stresses increase with increasing adhesive stiffness, and this trend is more apparent for $\overline{E}_h < 5$.

The influence of the adhesive thickness on the maximum interfacial shear and peeling stresses is shown in Fig. 3.9 for both pure extension and pure bending cases, where the adhesive stiffness of an epoxy bond is used, i.e., $E_h = 0.28msi$. The thickness of the adhesive is normalized with $h^* = 0.001in$. It is shown that the interfacial shear and peeling stresses decrease with increasing adhesive thickness. A thick adhesive will relax the interfacial shear and peeling stress. However, as indicated in Figs. 3.6 and 3.7, a

99
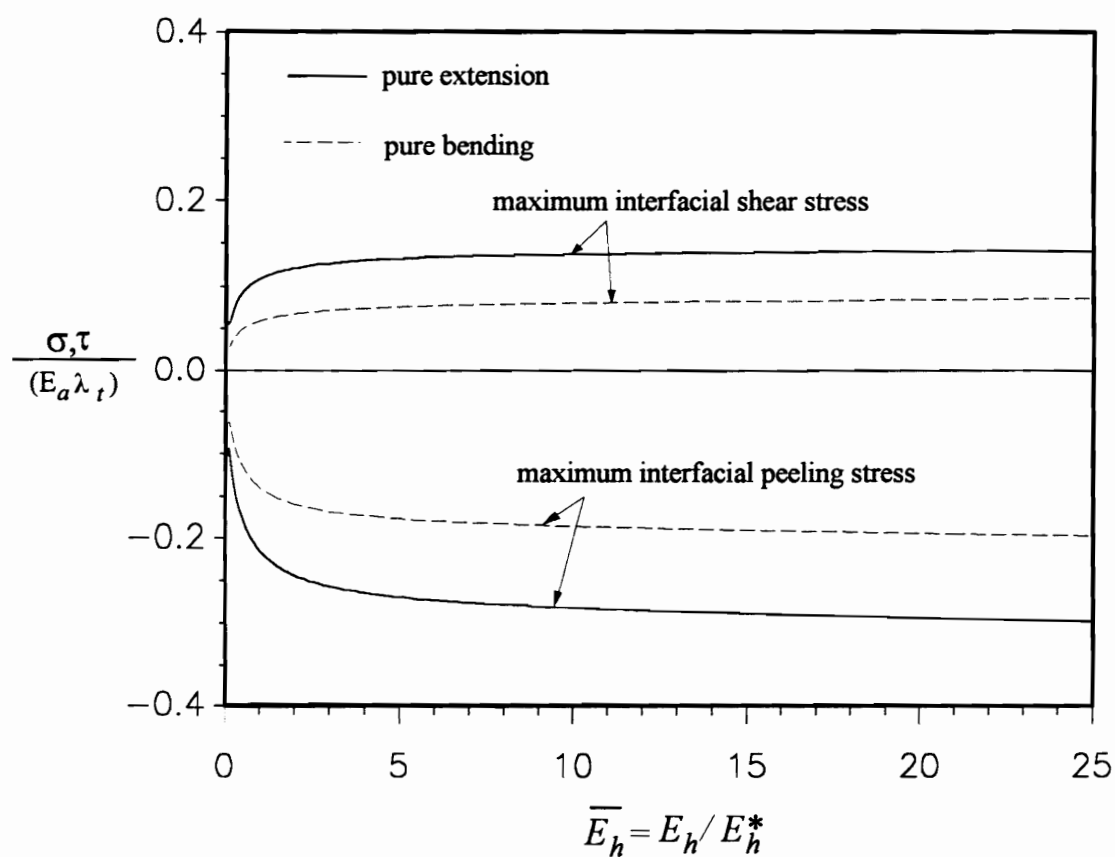
Figure 3.8. Influence of the adhesive stiffness on the maximum interfacial shear and peeling stresses.
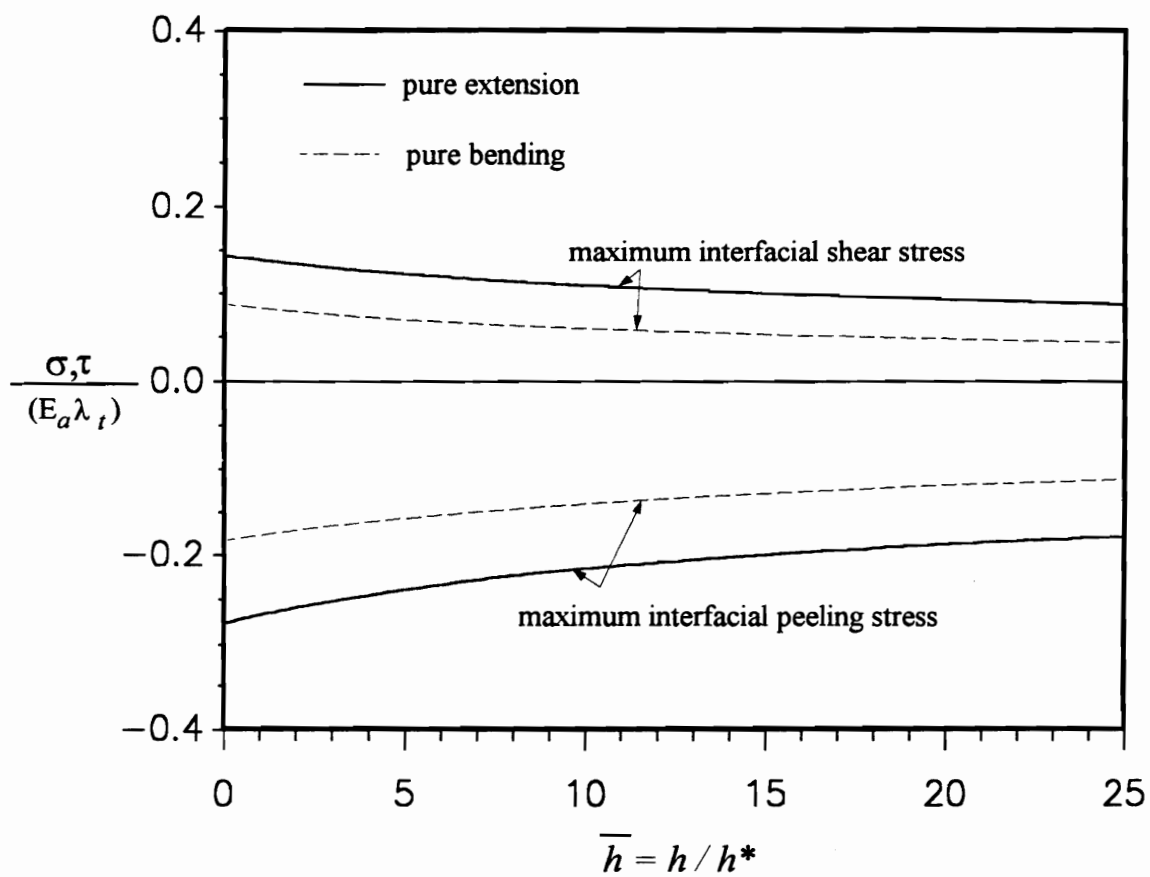
Figure 3.9. Influence of the adhesive thickness on the maximum interfacial shear and peeling stresses.

longer distance from the actuator edges is needed for effective force/moment to achieve its constant level in the case of a thick adhesive.

3.4 Conclusion

An analytical model is developed to study bonding layer effects in integrated induced strain actuator/substructure systems. The problem is modeled by plane stress formulation on the basis of the theory of elasticity and solved by the principle of stationary complementary energy. The solution obtained is in an approximate manner, in closed form. The effects of the adhesive layer on the transfer of the actuation mechanism from the actuators to the substructure, as well as on the interfacial shear and peeling stresses, are investigated.

The results show that a relatively thick and compliant adhesive layer requires a longer distance from the actuator edges to achieve its constant effective force/moment level. In other words, a lower actuation mechanism can be transferred from the actuators to the substructure. Nevertheless, thicker and more compliant adhesives will result in a lower interfacial shear and peeling stress level, which is beneficial to the structural integrity.

3.5 References

Bailey, T. and Hubbard Jr., J. E., 1985, "Distributed Piezoelectric-Polymer Active Vibration Control of a Cantilever Beam, "Journal of Guidance and Control, Vol. 8, No. 5, pp. 605-611.

Barker, D. K., 1989, "Active Dynamic Response Tuning of Adaptive Composites Utilizing Embedded Nitinol Actuators," Thesis, Mechanical Engineering Department, Virginia Polytechnic Institute and State University, August, 1989.

Chaudhry, Z., and Rogers, C. A., 1991, "Bending and Shape Control of Beams Using SMA Actuators," Journal of Intelligent Material Systems and Structures, Vol. 2, No. 4, pp. 581-602.

Chen, D., Cheng, S., and Gerhardt, T. D., 1982, "Thermal Stresses in Laminated Beams," Journal of Thermal Stresses, Vol. 5, pp. 67-84.

Crawley, E. F. and de Luis, J., 1987, "Use of Piezoelectric Actuators as Elements of Intelligent Structures," AIAA Journal, Vol. 25, No. 10, pp. 1373-1385.
Crawley, E. F. and Lazarus, K. B., 1991, "Induced Strain Actuation of Isotropic and Anisotropic Plates," AIAA Journal, Vol. 29, No. 6, pp. 944-951.

Durelli, A. J., and Tsao, C. H., 1955, "Determination of Thermal Stresses in Three-Ply Laminates," Journal of Applied Mechanics, Vol. 12, pp. 190-192.

Fanson, J. L. and Chen, J. C., 1986, "Structural Control by the Use of Piezoelectric Active Members," Proceedings of NASA/DOD Control/Structures Interaction Conference, NASA CP-2447, Part II.

Goland, M., and Reissner, E., 1944, "The Stresses in Cemented Joints," Journal of Applied Mechanics, Vol. 1, No. 1, A.17-A.27.

Haftka, R. T. and Adelman, H. M., 1985, "An Analytical Investigation of Shape Control of Large Space Structures by Applied Temperatures," AIAA Journal, Vol. 23, No. 3, pp. 450-457.

Kim, S. J., and Jones, J. D., 1991, "Optimal Design of Piezoactuators for Active Noise and Vibration Control," AIAA Journal, Vol. 29, No. 12, pp. 2047-2053.

Liang, C., Rogers, C. A. and Fuller, C. R., 1991, "Acoustic Transmission and Radiation Analysis of Adaptive Shape Memory Alloy Reinforced Laminated Plates," Journal of Sound and Vibration, Vol. 145, No. 1, pp. 23-41.

Lin, M. W., and Rogers, C. A., 1993, "Modeling of the Actuation Mechanism in a Beam Structure with Induced Strain Actuators," Proceedings of the AIAA/ASME/AHS/ASC 34th SDM Conference, La Jolla, CA, April 19-22, 1993.

Lin, M. W., and Rogers, C. A., 1991, "Analysis of Stress Distribution in a Shape Memory Alloy Composite Beam," Proceedings of the AIAA/ASME/AHS/ASC 32nd SDM Conference, Baltimore, MD, April 13-15, 1991.

Robbins, D. H. and Reedy, J. N., 1991, "Finite Element Analysis of Piezoelectrically Activated Beams," Computers and Structures, Vol. 41, No. 2, pp. 265-279.

Rogers, C. A., 1990, "An Introduction to Intelligent Material Systems and Structures," in Intelligent Systems (Proceedings of the International Workshop on Intelligent Structures, Taipei, Taiwan, 23-26 July, 1990), K. P. Chong, S. C. Liu, and J. C. Li, Eds, Elsevier, London, pp. 3-41.

Rogers, C. A., Liang, C. and Li S., 1991, "Active Damage Control of Hybrid Material Systems Using Induced Strain Actuators," Proceedings of the AIAA/ASME/ASCE/AHS/ASC 32nd SDM Conference, Baltimore, MD, April 8-10, 1991,

Sato, T., Ishida, H. and Ikeda, O., 1980, "Adaptive PVDF Piezoelectric Deformable Mirror System," Applied Optics, Vol. 19, No. 9, pp. 1430-1434.

Wada, B. K., Fanson, J. L., and Crawley, E. F., 1990, "Adaptive Structures," Journal of Intelligent Material Systems and Structures, Vol. 1, No. 2, pp. 157-174.

Williams, H. E., 1985, "Asymptotic Analysis of the Thermal Stresses in a Two-Layer Composite with an Adhesive Layer," Journal of Thermal Stresses, Vol. 8, pp. 183-203.

3.6 Appendix

$$A_1^e = 2K_{13}^e; \quad A_2^e = 2\left(K_{11}^e - K_7^e\right); \quad A_3^e = 2K_3^e$$

$$B_1^e = K_{17}^e; \quad B_2^e = K_{12}^e + K_{15}^e - K_8^e; \quad B_3^e = K_5^e$$

$$C_1^e = 2K_{18}^e; \quad C_2^e = 2\left(K_{16}^e - K_9^e\right); \quad C_3^e = 2K_6^e$$

$$D_1^e = -K_2^e \lambda_t; \quad D_2^e = -K_4^e \lambda_t. \tag{A.1}$$

$$A_1^b = 2K_7^b; \quad A_2^b = 2\left(K_6^b - K_4^b\right); \quad A_3^b = 2K_3^b$$

$$D_1^b = -K_2^b \lambda_t. \tag{A.2}$$

where

$$K_2^e = -18144 a E_a^2 E_h E_s^2 [4b^6 E_s^2 + h^4 E_h^2 (15b^2 + 15bh + 4h^2)$$
$$-ah^2 E_a E_h (6b^3 - 4b^2 h - 11bh^2 - 4h^3) + abE_a E_s (4b^4 + 20b^3 h + 46b^2 h^2 + 36bh^3 + 9h^4)$$
$$+bh E_h E_s (24b^4 + 60b^3 h + 80b^2 h^2 + 45bh^3 + 9h^4)]$$

$$K_3^e = 3024 E_a E_h E_s [12b^7 E_s^3 + 3h^5 E_h^3 (15b^2 + 15bh + 4h^2) + a^2 h^3 E_a^2 E_h (20b^2 + 25bh + 8h^2)$$
$$+ah^4 E_a E_h^2 (57b^2 + 66bh + 20h^2) + 3b^2 h E_h E_s^2 (28b^4 + 60b^3 h + 80b^2 h^2 + 45bh^3 + 9h^4)$$
$$+3bh^2 E_h^2 E_s (24b^4 + 60b^3 h + 95b^2 h^2 + 60bh^3 + 13h^4)$$
$$+a^2 b E_a^2 E_s (8b^4 + 40b^3 h + 80b^2 h^2 + 60bh^3 + 15h^4)$$
$$+ab^2 E_a E_s^2 (20b^4 + 72b^3 h + 144b^2 h^2 + 108bh^3 + 27h^4)$$
$$+2abh E_a E_h E_s (24b^4 + 78b^3 h + 144b^2 h^2 + 108bh^3 + 27h^4)]$$

$$K_4^e = -36288 a^2 E_a^2 E_h E_s^3 [2a E_a (b + h)^4 + b^3 E_s (2b^2 - 2bh - h^2)$$
$$+h E_h (12b^4 + 21b^3 h + 20b^2 h^2 + 10bh^3 + 2h^4)]$$

$$K_5^e = 12096aE_aE_hE_s^2[b^6E_s^2(2b^2 - 6bh - 3h^2) - h^3E_h^2(9b^3 - 6bh^2 - 2h^3)$$
$$-ah^2E_aE_h(9b^3 + 4b^2h - 4bh^2 - 2h^3) + abE_aE_s(2b^4 + 10b^3h + 29b^2h^2 + 24bh^3 + 6h^4)$$
$$+bhE_hE_s(18b^4 + 33b^3h + 49b^2h^2 + 30bh^3 + 6h^4)]$$

$$K_6^e = 12096aE_hE_s^3[2b^6E_s^2 + 3a^2E_a^2(b+h)^4 + 4b^3hE_hE_s(3b^2 + 3bh + h^2) + 2h^2E_h^2(3b^2 + 3bh + h^2)^2$$
$$+ab^3E_aE_s(5b^2 + 4bh + 2h^2) + ahE_aE_h(21b^4 + 48b^3h + 50b^2h^2 + 25bh^3 + 5h^4)]$$

$$K_7^e = 144E_aE_s\{10a^3E_aE_h[h^2E_a(3b+2h) + bE_s(2b^2 + 6bh + 3h^2)]^2(1 + v_a)$$
$$+h[9ah^5E_aE_h^3(7b+4h)^2 + 105ab^2hE_aE_hE_s^2(2b+h)(2b+3h)(2b^2 + 6bh + 3h^2)$$
$$+35a^2bh^2E_a^2E_hE_s(8b+5h)(2b^2 + 6bh + 3h^2) + 70a^2b^2E_a^2E_s^2(2b^2 + 6bh + 3h^2)^2$$
$$+3h^6E_h^4(63b^2 + 63bh + 16h^2) + a^2h^4E_a^2E_h^2(336b^2 + 427bh + 136h^2)$$
$$+3bh^4E_h^3E_s(210b^3 + 539b^2h + 378bh^2 + 81h^3)$$
$$+6abh^3E_aE_h^2E_s(175b^3 + 539b^2h + 441bh^2 + 108h^3)$$
$$+3b^2h^2E_h^2E_s^2(280b^4 + 1050b^3h + 1386b^2h^2 + 735bh^3 + 135h^4)](1 + v_h)$$
$$+2b^3E_hE_s[24b^6E_s^2 + 12ab^3E_aE_s(6b^2 + 14bh + 7h^2) + 12b^3hE_hE_s(18b^2 + 21bh + 7h^2)$$
$$+6ahE_aE_h(68b^4 + 252b^3h + 322b^2h^2 + 175bh^3 + 35h^4)$$
$$+3h^2E_h^2(204b^4 + 504b^3h + 483b^2h^2 + 210bh^3 + 35h^4)$$
$$+a^2E_a^2(68b^4 + 336b^3h + 588b^2h^2 + 420bh^3 + 105h^4)](1 + v_s)\}$$

$$K_8^e = -288aE_aE_s^2\{4a^2E_h[8b^3E_s + 3aE_a(b+h)^2$$
$$+8hE_h(3b^2 + 3bh + h^2)][h^2E_h(3b+2h) + bE_s(2b^2 + 6bh + 3h^2)](1 + v_a)$$
$$+h[105b^4hE_hE_s^2(2b+h)(2b+3h) + 140ab^4E_aE_s^2(2b^2 + 6bh + 3h^2)$$
$$+3h^4E_h^3(105b^3 + 119b^2h + 49bh^2 + 8h^3) + ah^3E_aE_h^2(525b^3 + 714b^2h + 343bh^2 + 64b^3)$$
$$+35abhE_aE_hE_s(12b^4 + 52b^3h + 49b^2h^2 + 18bh^3 + 3h^4)$$
$$+3bh^2E_h^2E_s(140b^4 + 455b^3h + 343b^2h^2 + 105bh^3 + 15h^4)](1 + v_h)$$
$$+4b^5E_hE_s[6b^3E_s + 3hE_h(16b^2 + 21bh + 7h^2) + aE_a(16b^2 + 42bh + 21h^2)](1 + v_s)\}$$

$$K_9^e = 576a^2 E_s^3 \{2aE_h[17b^6 E_s^2 + 18ab^3 E_a E_s (b+h)^2 + 6a^2 E_a^2 (b+h)^4$$
$$+34b^3 hE_h E_s (3b^2 + 3bh + h^2) + 18ah E_a E_h (b+h)^2 (3b^2 + 3bh + h^2)$$
$$+17h^2 E_h^2 (3b^2 + 3bh + h^2)^2](1 + v_a)$$
$$+5hE_a[14b^6 E_s^2 + 7b^3 hE_h E_s (6b^2 + 4bh + h^2)$$
$$+h^2 E_h^2 (42b^4 + 63b^3 h + 42b^2 h^2 + 14bh^3 + 2h^4)](1 + v_h) + 10b^7 E_a E_h E_s (1 + v_s)\}$$

$$K_{11}^e = 72 E_a E_h E_s \{-15a^3 E_a[2b^3 E_s + 6b^2 hE_s + 3bh^2 (E_h + E_s) + 2h^3 E_h]^2 v_a$$
$$+h\{18ah^5 E_a E_h^2 (7b + 4h)^2 - 105ab^2 E_a E_s^2 (2b + h)(ab + ah + 2bh + h^2)(2b^2 + 6bh + 3h^2)$$
$$+35a^2 bhE_a^2 E_s (2b^2 + 6bh + 3h^2)[3ab + 2(a + 4b)h + 5h^2] + 6h^6 E_h^3 (63b^2 + 63bh + 16h^2)$$
$$+3bh^5 E_h^2 E_s (238b^2 + 231bh + 57h^2) + a^2 h^3 E_a^2 E_h[315ab^2 + 84b(5a + 8b)h$$
$$+14(10a + 61b)h^2 + 272h^3] - 3b^2 h^2 E_h E_s^2 (280b^4 + 840b^3 h + 798b^2 h^2 + 315bh^3 + 45h^4)$$
$$+3abh^2 E_a E_h E_s[-210ab^3 - 455ab^2 h - 7(45a - 68b)bh^2 - 7(10a - 77b)h^3 + 152h^4]\}v_h$$
$$+b\{96b^8 E_s^3 + 315h^5 E_h^3 (b + h)(2b + h)^2$$
$$+35a^2 h^2 E_a^2 E_h (2b^2 + 6bh + 3h^2)[3ab + 2(a + 4b)h + 5h^2]$$
$$+48ab^5 E_a E_s^2 (6b^2 + 14bh + 7h^2) + 48b^5 hE_h E_s^2 (18b^2 + 21bh + 7h^2)$$
$$+105ah^3 E_a E_h^2 (2b + h)[3ab^2 + 5b(a + 2b)h + (2a + 19b)h^2 + 8h^3]$$
$$+3bh^2 E_h^2 E_s (816b^5 + 2856b^4 h + 4872b^3 h^2 + 4410b^2 h^3 + 1925bh^4 + 315h^5)$$
$$+3abhE_a E_h E_s[4b^4 (35a + 136b) + 42b^3 (15a + 68b)h + 14b^2 (65a + 464b)h^2$$
$$+525b(a + 14b)h^3 + 35(3a + 110b)h^4 + 735h^5]$$
$$+a^2 bE_a^2 E_s[4b^4 (35a + 68b) + 56b^3 (15a + 34b)h + 336b^2 (5a + 17b)h^2$$
$$+420b(3a + 20b)h^3 + 105(3a + 52b)h^4 + 1260h^5]\}v_s\}$$

$$K_{12}^e = -144aE_aE_hE_s^2\{-3a^2[b^3E_s - 4aE_a(b+h)^2$$
$$+hE_h(3b^2 + 3bh + h^2)][h^2E_h(3b + 2h) + bE_s(2b^2 + 6bh + 3h^2)]\nu_a$$
$$+h\{35abE_aE_s(2b^2 + 6bh + 3h^2)[3ab^2 + 3b(a + 2b)h + (a + 4b)h^2 + h^3]$$
$$+3h^4E_h^2(105b^3 + 119b^2h + 49bh^2 + 8h^3)$$
$$+3bh^2E_hE_s(140b^4 + 385b^3h + 308b^2h^2 + 105bh^3 + 15h^4)$$
$$+ah^2E_aE_h[315ab^3 + 525b^2(a + b)h + 21b(15a + 34b)h^2 + 7(10a + 49b)h^3 + 64h^4]\}\nu_h$$
$$+b^3\{24b^5E_s^2 + 105h^4E_h^2(2b + h) + 35ah^2E_aE_h[3ab + 2(a + 4b)h + 5h^2]$$
$$+3bhE_hE_s(64b^3 + 224b^2h + 308bh^2 + 105h^3) + abE_aE_s[2b^2(35a + 32b)$$
$$+14b(15a + 32b)h + 21(5a + 44b)h^2 + 420h^3]\}\nu_s\}$$

$$K_{13}^e = E_s\{1152b^{11}E_hE_s^4 + 2835bh^8E_h^5(2b + h)^2$$
$$+1890abh^6E_aE_h^4(2b + h)(3ab + 2ah + 8bh + 5h^2)$$
$$+315a^2bh^4E_a^2E_h^3(3ab + 2ah + 8bh + 5h^2)^2$$
$$+105a^2b^2hE_a^2E_s^3(2b^2 + 6bh + 3h^2)^2(3a^2 + 12ah + 16h^2)$$
$$+a^2h^2E_a^2E_h^2E_s[756ab^5(5a + 8b) + 252b^4(55a^2 + 176ab + 64b^2)h$$
$$+1890b^3(7a^2 + 58ab + 48b^2)h^2 + 315b^2(21a^2 + 292ab + 608b^2)h^3$$
$$+1260b(3a^2 + 27ab + 118b^2)h^4 + 36(35a^2 + 343ab + 1322b^2)h^5$$
$$+9(448a + 1385b)h^6 + 3968h^7]$$
$$+ah^3E_aE_h^3E_s[18144ab^6 + 63b^2(5a^4 + 1032ab^3 + 960b^4)h$$
$$+84b(5a^4 + 1305ab^3 + 2592b^4)h^2 + 70(2a^4 + 1071ab^3 + 5040b^4)h^3$$
$$+2520b^2(9a + 92b)h^4 + 486b(14a + 131b)h^5 + 18(112a + 815b)h^6 + 4224h^2]$$
$$+2abhE_aE_h^2E_s^2[96b^7(63a + 124b) + 6b^3(35a^4 + 5796ab^3 + 13392b^4)h$$
$$+2b^2(385a^4 + 36540ab^3 + 123696b^4)h^2 + 105b(7a^4 + 774ab^3 + 3864b^4)h^3$$
$$+42(5a^4 + 1170ab^3 + 9144b^4)h^4 + 252b^2(104a + 791b)h^5 + 9b(1659a + 8644b)h^6$$
$$+27(104a + 1347b)h^7 + 9060h^8] + a^2bE_a^2E_hE_s^2[4b^6(315a^2 + 1008ab + 992b^2)$$
$$+72b^5(105a^2 + 448ab + 496b^2)h + 144b^4(105a^2 + 707ab + 992b^2)h^2$$
$$+1008b^3(15a^2 + 150ab + 308b^2)h^3 + 63b^2(265a^2 + 1780ab + 5856b^2)h^4$$
$$+126b(105a^2 + 582ab + 1808b^2)h^5 + 42(90a^2 + 1143ab + 2476b^2)h^6$$
$$+504(27a + 109b)h^7 + 15372h^8]$$

$$+ ab^2 E_a E_h E_s^3 [4b^4 (35a^4 + 504ab^3 + 1056b^4)$$

$$+ 24b^3 (35a^4 + 252ab^3 + 768b^4)h + 48b^2 (35a^4 + 63ab^3 + 612b^4)h^2$$

$$+ 252b(5a^4 + 20ab^3 + 48b^4)h^3 + 315(a^4 + 84ab^3 + 48b^4)h^4$$

$$+ 756b^2 (61a + 104b)h^5 + 126b(243a + 1076b)h^6$$

$$+ 756h^7 (9a + 118b + 26h)] + 9h^5 E_h^4 E_s [h^4 (2358b^2 + 489bh + 128h^2)$$

$$+ 84b^3 (48b^3 + 144b^2 h + 200bh^2 + 115h^3)]$$

$$+ 9b^2 h E_h^2 E_s^3 [6456b^2 h^6 + 7h^5 (624b^3 + 531bh^2 + 104h^3)$$

$$+ 16b^4 (88b^4 + 192b^3 h + 204b^2 h^2 + 63bh^3 + 63h^4)]$$

$$+ 9bh^2 E_h^3 E_s^2 [6483b^2 h^6 + 2h^5 (9492b^3 + 1347bh^2 + 302h^3)$$

$$+ 16b^4 (248b^4 + 1116b^3 h + 2577b^2 h^2 + 3381bh^3 + 2667h^4)]\}$$

$$K_{15}^e = -72a E_a E_h E_s^2 \{-3a^2 [37b^3 E_s + 27a E_a (b + h)^2 + 37h E_h (3b^2 + 3bh + h^2)][h^2 E_a (3b + 2h)$$

$$+ bE_s (2b^2 + 6bh + 3h^2)]v_a$$

$$+ h\{105a^3 h E_a^2 (b + h)^2 (3b + 2h) - 105b^4 E_s^2 (2b + h)[5ab + (5a + 4b)h + 2h^2]$$

$$+ 6h^4 E_h^2 (105b^3 + 119b^2 h + 49bh^2 + 8h^3)$$

$$+ ah^2 E_a E_h [1575ab^3 + 525b^2 (5a + 2b)h + 21b(75a + 68b)h^2 + 14(25a + 49b)h^3 + 128h^4]$$

$$- 35ab E_a E_s [18ab^4 + 48ab^3 h + (71a - 16b)b^2 h^2 + 5(9a - 2b)bh^3 + 9ah^4]$$

$$- 3bh E_h E_s [1050ab^4 + 35b^3 (75a + 16b)h + 70b^2 (35a + 13b)h^2 + 42b(25a + 17b)h^3$$

$$+ 35(5a + 8b)h^4 + 40h^5]\}v_h$$

$$+ b\{48b^7 E_s^2 + 105a^3 E_a^2 (b + h)^2 (2b^2 + 6bh + 3h^2)$$

$$+ 105h^2 E_h^2 (b + h)(2b + h)[15ab^2 + 3b(5a + 4b)h + (5a + 8b)h^2 + 2h^3]$$

$$+ 3b^3 h E_h E_s [2b^2 (175a + 64b) + 7b(75a + 104b)h + 7(25a + 128b)h^2 + 280h^3]$$

$$+ ab^3 E_a E_s [2b^2 (175a + 64b) + 14b(75a + 64b)h + 21(25a + 88b)h^2 + 840h^3]$$

$$+ 35ah E_a E_h [48ab^4 + 3b^3 (61a + 8b)h + 2b^2 (113a + 44b)h^2 + 8b(15a + 11b)h^3$$

$$+ 12(2a + 3b)h^4 + 6h^5]\}v_s\}$$

$$K_{16}^e = 144a^2 E_h E_s^3 \{ -3a\{13b^6 E_s^2 - 13ab^3 E_a E_s (b+h)^2 - 16a^2 E_a^2 (b+h)^4$$

$$+26b^3 h E_h E_s (3b^2 + 3bh + h^2) - 13ah E_a E_h (b+h)^2 (3b^2 + 3bh + h^2)$$

$$+13h^2 E_h^2 (3b^2 + 3bh + h^2)^2 \} \nu_a$$

$$+5h E_a \{ 21a^2 E_a (b+h)^2 (3b^2 + 3bh + h^2)$$

$$+7b^3 E_s [15ab^2 + 3b(5a + 4b)h + (5a + 8b)h^2 + 2h^3]$$

$$+h E_h [315ab^4 + 42b^3 (15a + 4b)h$$

$$+21b^2 (25a + 12b)h^2 + 42b(5a + 4b)h^3 + 7(5a + 8b)h^4 + 8h^5] \} \nu_h$$

$$+5b^3 E_a \{ 21a^2 E_a (b+h)^2 + b^3 E_s (35a + 8b + 56h)$$

$$+7h E_h [15ab^2 + 3b(5a + 4b)h + (5a + 8b)h^2 + 2h^3] \} \nu_s \}$$

$$K_{17}^e = -2a E_a E_s \{ 945a^3 bh E_a^2 E_s^2 (b+h)^2 (a + 2h)(2b^2 + 6bh + 3h^2)$$

$$+945a^3 bh^2 E_a^2 E_h^2 (b+h)^2 (3ab + 2ah + 8bh + 5h^2)$$

$$+105ab^4 h E_a E_s^3 (2b^2 + 6bh + 3h^2)(15a^2 + 42ah + 32h^2)$$

$$+315abh^3 E_a E_h^3 [45a^2 b^3 + 3ab^2 (25a + 58b)h + 3b(15a^2 + 96ab + 32b^2)h^2$$

$$+(10a^2 + 173ab + 124b^2)h^3 + 2(19a + 28b)h^4 + 10h^5]$$

$$+189a^3 E_a^2 E_h E_s (b+h)^2 [2b^4 (5a + 8b) + 10b^3 (3a + 8b)h$$

$$+5b^2 (3a + 28b)h^2 + 15b(a + 4b)h^3 + 5(2a + 5b)h^4 + 16h^5]$$

$$+h^2 E_h^3 E_s [45360ab^7 + 9b^3 (235a^4 + 17640ab^3 + 4032b^4)h$$

$$+3b^2 (1175a^4 + 90090ab^3 + 39312b^4)h^2 + 45b(47a^4 + 4830ab^3 + 4200b^4)h^3$$

$$+10(47a^4 + 10080ab^3 + 12726b^4)h^4 + 126b^2 (285a + 398b)h^5$$

$$+27b(455a + 662b)h^6 + 18(140a + 307b)h^7 + 960h^8]$$

$$+ah E_a E_h^2 E_s (378ab^6 (25a + 64b) + 9b^3 (55a^4 + 4725a^2 b^2 + 15624ab^3 + 1344b^4)h$$

$$+3b^2 (440a^4 + 16275a^2 b^2 + 114240ab^3 + 24192b^4)h^2$$

$$+21b(55a^4 + 1800a^2 b^2 + 16140ab^3 + 8136b^4)h^3$$

$$+30(11a^4 + 945a^2 b^2 + 6321ab^3 + 4620b^4)h^4 + 63b(225a^2 + 1364ab + 1004b^2)h^5$$

$$+18(175a^2 + 1897ab + 1584b^2)h^6 + 18(420a + 557b)h^7 + 1856h^8]$$

$$+ bhE_h^2E_s^2[6b^4(235a^4 + 3780ab^3 + 928b^4) + 135b^3(47a^4 + 336ab^3 + 320b^4)h$$

$$+ b^2(7285a^4 + 46620ab^3 + 78912b^4)h^2 + 3b(1175a^4 + 11025ab^3 + 25368b^4)h^3$$

$$+ 3(235a^4 + 22050ab^3 + 12096b^4)h^4 + 63b^2(1085a + 716b)h^5$$

$$+ 9b(3465a + 4288b)h^6 + 378(15a + 37b)h^7 + 2184h^8]$$

$$+ abE_aE_hE_s^2[2b^4(165a^4 + 1575a^2b^2 + 3780ab^3 + 928b^4)$$

$$+ 6b^3(275a^4 + 1575a^2b^2 + 6048ab^3 + 2784b^4)h$$

$$+ 3b^2(935a^4 + 4725a^2b^2 + 20748ab^3 + 18240b^4)h^2$$

$$+ 9b(220a^4 + 4725a^2b^2 + 6020ab^3 + 8512b^4)h^3$$

$$+ 45(11a^4 + 1085a^2b^2 + 2716ab^3 + 952b^4)h^4$$

$$+ 63b(375a^2 + 2270ab + 872b^2)h^5 + 21(225a^2 + 3393ab + 2552b^2)h^6$$

$$+ 252(57a + 82b))h^7 + 3528h^8] + b^4E_hE_s^3[10b^2(47a^4 + 252ab^3 + 96b^4)$$

$$+ 6b(235a^4 + 672b^4)h + 705a^4h^2 + 6300ab^2h^3$$

$$+ 945b(15a + 8b)h^4 + 378(15a + 44b)h^5 + 6552h^6]$$

$$+ 945bh^5E_h^4(2b + h)[5a(3b^2 + 3bh + h^2) + 2h(6b^2 + 4bh + h^2)]\}$$

$$K_{18}^e = a^2 E_s^2 \{1763 a^3 b^6 E_h E_s^3 + 2835 a^4 b E_a^3 E_h (b + h)^4 + 2835 a^4 h E_a^3 E_s (b + h)^4$$

$$+1890 a^2 b^3 h E_a^2 E_s^2 (b + h)^2 (5a + 4h) + 3526 a^3 b^3 h E_h^2 E_s^2 (3b^2 + 3bh + h^2)$$

$$+1763 a^3 h^2 E_h^3 E_s (3b^2 + 3bh + h^2)^2 + 105 b^6 h E_a E_s^3 (75a^2 + 120 ah + 64 h^2)$$

$$+315 bh^2 E_a E_h^3 (15 ab^2 + 15 abh + 12 b^2 h + 5 ah^2 + 8 bh^2 + 2h^3)^2$$

$$+9 a^2 E_a^2 E_h E_s (b + h)^2 [b^2 (107 a^3 + 1050 ab^2 + 336 b^3) + 2b(107 a^3 + 840 b^3)h$$

$$+a(107 a^2 + 3150 b^2)h^2 + 210 b(15a + 8b)h^3 + 210(5a + 6b)h^4 + 336 h^5]$$

$$+b^3 E_a E_h E_s^2 [b^2 (2586 a^4 + 7875 a^2 b^2 + 5040 ab^3 + 896 b^4)$$

$$+12 b(431 a^4 + 2100 ab^3 + 672 b^4)h + 6(431 a^4 + 7875 a^2 b^2 + 3360 b^4)h^2$$

$$+15750 ab(3a + 4b)h^3 + 3150(5a^2 + 18 ab + 8b^2)h^4 + 504(35a + 36b)h^5$$

$$+4704 h^6] + h E_a E_h^2 E_s [18 ab^4 (431 a^3 + 2625 ab^2 + 840 b^3)$$

$$+54 b^3 (431 a^4 + 875 a^2 b^2 + 2380 ab^3 + 224 b^4)h$$

$$+3b^2 (8620 a^4 + 28875 a^2 b^2 + 35280 ab^3 + 22848 b^4)h^2$$

$$+6b(2155 a^4 + 23625 a^2 b^2 + 17850 ab^3 + 7056 b^4)h^3$$

$$+3(862 a^4 + 39375 a^2 b^2 + 44100 ab^3 + 11424 b^4)h^4$$

$$+630 b(75a^2 + 154 ab + 56b^2)h^5 + 63(5a + 4b)(25a + 88b)h^6$$

$$+252(20a + 27b)h^7 + 896 h^8]$$

$$+1890 a^2 bh E_a^2 E_h^2 (b + h)^2 [5a(3b^2 + 3bh + h^2) + 2h(6b^2 + 4bh + h^2)]\}$$

$$K_2^b = -9072 a E_a^2 E_h E_s (a + 2b + 2h)[a E_a (b + h)^2 (13a + 16b + 16h)$$

$$+b^3 E_s (25a + 32b + 32h) + h E_h (25a + 32b + 32h)(3b^2 + 3bh + h^2)]$$

$$K_3^b = 756 E_h E_s \{128 b^6 E_s^2 + 256 b^3 h E_h E_s (3b^2 + 3bh + h^2)$$

$$+128 h^2 E_h^2 (3b^2 + 3bh + h^2)^2 + 3a^2 E_a^2 (b + h)^2 [21 a^2 + 64(b + h)(a + b + h)]$$

$$+ab^3 E_a E_s [125 a^2 + 64(b + h)(6a + 7b + 7h)] + ah E_a E_h (3b^2 + 3bh + h^2)[125 a^2$$

$$+64(b + h)(6a + 7b + 7h)]\}$$

$$K_4^b = 18a\{4aE_hE_s\{1088b^6E_s^2 - 96ab^3E_aE_s(a - 12b - 12h)(b + h)$$

$$+2176b^3hE_hE_s(3b^2 + 3bh + h^2) - 96ahE_aE_h(a - 12b$$

$$-12h)(b + h)(3b^2 + 3bh + h^2) + 1088h^2E_h^2(3b^2 + 3bh + h^2)^2$$

$$+3a^2E_a^2(b + h)^2[11a^2 + 16ab + 128b^2 + 16(a + 16b)h + 128h^2]\}(1 + \nu_a)$$

$$+7hE_aE_s\{-160b^3hE_hE_s[3(5a - 8b)b + 2(5a - 4b)h]$$

$$+60a^2hE_aE_h(b + h)[3(5a - 8b)b + 2(5a - 4b)h]$$

$$+h^2E_h^2[60h^2(25a^2 - 40ab + 64b^2) + 75b(25a^2 - 16ab + 64b^2)h$$

$$+24(25a^2 + 30ab + 144b^2)h^2 + 64(5a + 23b)h^3 + 256h^4]$$

$$+20[8b^3E_s - 3a^2E_a(b + h)]^2\}(1 + \nu_h)$$

$$+7bE_aE_h\{180a^4E_a^2(b + h)^2 + 120a^2b^2E_aE_s(b + h)(5a + 8h)$$

$$+60a^2hE_aE_h(b + h)[30ab + 3(5a + 8b)h + 8h^2]$$

$$+20b^2hE_hE_s(5a + 8b)[30ab + 3(5a + 8b)h + 8h^2]$$

$$+5h^2E_h^2[30ab + 3(5a + 8b)h + 8h^2]^2 + 8b^4E_s^2[75a^2 + 40ab + 32b^2$$

$$+16(15a + 4b)h + 192h^2]\}(1 + \nu_s)\}$$

$$K_6^b = 36aE_hE_s\{-6a\{104b^6E_s^2 - 13ab^3E_aE_s(b + h)(11a + 8b + 8h)$$

$$+208b^3hE_hE_s(3b^2 + 3bh + h^2) - 13ahE_aE_h(b + h)(11a$$

$$+8b + 8h)(3b^2 + 3bh + h^2) + 104h^2E_h^2(3b^2 + 3bh + h^2)^2$$

$$-a^2E_a^2(b + h)^2[11a^2 + 121ab + 128b^2 + (121a + 256b)h + 128h^2]\}\nu_a$$

$$+7hE_a(5a + 8b + 8h)\{30a^2E_a(b + h)(3b^2 + 3bh + h^2)$$

$$+5b^3E_s[30ab + 3(5a + 8b)h + 8h^2] + 2hE_h[225ab^3 + 60b^2(5a + 2b)h$$

$$+30b(5a + 4b)h^2 + 6(5a + 8b)h^3 + 8h^4]\}\nu_h$$

$$+7b^3E_a(5a + 8b + 8h)\{30a^2E_a(b + h) + 4b^2E_s(15a + 4b + 24h)$$

$$+5hE_h[30ab + 3(5a + 8b)h + 8h^2]\}\nu_s\}$$

$$K_7^b = a\{7052a^3b^6E_hE_s^3 + 3780a^4b^3E_a^3E_h(b+h)^2 + 14104a^3b^3hE_h^2E_s^2(3b^2 + 3bh + h^2)$$

$$+3780a^4hE_a^3E_s(b+h)^2(3b^2 + 3bh + h^2) + 7052a^3h^2E_h^3E_s(3b^2 + 3bh + h^2)^2$$

$$+1260a^2b^3hE_a^2(E_h^2 + E_s^2)(b+h)(30ab + 15ah + 24bh + 8h^2)$$

$$+105b^3h^2E_aE_h^3(30ab + 15ah + 24bh + 8h^2)^2$$

$$+420b^6hE_aE_s^3(75a^2 + 120ah + 64h^2) + 36a^2E_a^2E_hE_s(b+h)[b(2a^5 + 25a^4b$$

$$+107a^3b^2 + 420ab^4 + 112b^5) + (2a^5 + 52a^4b + 321a^3b^2 + 672b^5)h$$

$$+a(26a^3 + 321a^2b + 3150b^3)h^2 + (107a^3 + 4200ab^2 + 1680b^3)h^3$$

$$+420b(5a + 4b)h^4 + 84(5a + 8b)h^5 + 112h^6]$$

$$+3b^3E_aE_hE_s^2[4b(98a^5 + 862a^4b + 1275a^2b^3 + 720ab^4 + 128b^5)$$

$$+8(49a^5 + 862a^4b + 2040ab^4 + 576b^5)h + 8(431a^4 + 7875a^2b^2 + 1632b^4)h^2$$

$$+10500ab(5a + 8b)h^3 + 525(25a^2 + 112ab + 64b^2)h^4$$

$$+2352(5a + 8b)h^5 + 3136h^6] + 12hE_aE_h^2E_s[6ab^3(49a^4 + 431a^3b$$

$$+1050ab^3 + 280b^4) + 6b^2(98a^5 + 1293a^4b + 525a^2b^3 + 2660ab^4 + 224b^5)h$$

$$+b(392a^5 + 8620a^4b + 23625a^2b^3 + 6720ab^4 + 8512b^5)h^2$$

$$+(98a^5 + 4310a^4b + 39375a^2b^3 + 25200ab^4 + 2688b^5)h^3$$

$$+(862a^4 + 26775a^2b^2 + 35280ab^3 + 8064b^4)h^4 + 21b(5a + 8b)(85a + 56b)h^5$$

$$+3(425a^2 + 1920ab + 1536b^2)h^6 + 144(5a + 8b)h^7 + 128h^8]\}$$

Chapter 4

Induced Strain Actuation on a Beam Structure Subjected to External Loads

4.1 Introduction

Induced strain actuators have been highly integrated, embedded or surface bonded, with conventional structural materials to serve as energy input devices or actuating elements in many engineering applications implementing the intelligent material systems and structure concept. Prominent examples include active structural vibration control (Bailey and Hubbard, 1985; Crawley and de Luis, 1987), shape control (Chaudhry and Rogers, 1991), acoustic transmission control (Liang et. al., 1991), and damage control (Rogers, et. al., 1991). In order to use the actuators more effectively, research in modeling the mechanical interaction between the actuators and host substructure to predict the overall structural response has received great attention. However, most analytical efforts have been limited to the case of no external loads being applied to the structure. In most cases, external loads are usually present on the load bearing structure which is to be controlled by the induced strain actuation of the actuators. The effect of the external loads on the actuator performance, therefore, needs to be taken into account.

Due to the highly integrated fashion of the actuators/substructure system, the actuators become a part of the structure. Application of the external loads, thus, is partially transferred to the actuators resulting a prestrain on the actuators. The combined effect of the external loads and induced strain actuation brings about the concerns of the performance and optimum design issues such as optimum actuator-to-substructure thickness ratio which induces maximum bending curvature on the substructure and the intensity of interfacial stresses which usually causes the failure of structural integrity.

The first comprehensive model to investigate these issues was developed by Crawley and de Luis (1987) using the shear lag assumption from a mechanics of materials approach. External loads of axial forces and bending moments applied to the structure were treated as mechanically induced strains to be prescribed as boundary conditions. However, no case study was performed to include the effect of any external loads to illustrate their significance.

Im and Atluri (1989) presented a refined analysis to include the effect of externally applied transverse shear and axial normal forces. Their model was also based on the shear lag assumption. The influence of the transverse shear and axial forces on the interfacial shear stress, which was regarded as the only actuation strain transfer mechanism, was investigated. It was shown that the external loads have noticeable effects on the magnitude of the interfacial shear stresses. However, the calculated interfacial shear stress distribution does not satisfy the shear stress free boundary condition at the free edges of the actuators due to the assumption made in the shear lag theory. The resulting interfacial

116

peeling stress consequently is incorrect in both the distribution and magnitude. This model helps understand the effect of external loads on the interfacial shear transferring via bonding layer, but it lacks quantitative accuracy.

Recently, Chaudhry and Rogers (1993) investigated the effect of external loads on the optimum actuator/substructure thickness ratio which maximizes the induced bending on the substrate. It was demonstrated that the optimum thickness ratio is not only a function of actuator/substructure stiffness ratio but also of external loads and induced strain level of the actuators. Because of the limitation of employed Euler-Bernoulli mechanical model, the influence of the external loads on the interfacial shear and peeling stress was not studied.

In this chapter, the refined analytical model presented by Lin and Rogers (1993a, 1993b) is extended to include external loads. The model was developed under the plane stress formulation of the theory of elasticity and is capable of describing the edge effect and correctly predicting interfacial stress distribution. The formulation for the external loading is first presented. The coupling effect of the external loads and induced strain actuation on the effective force/moment transferring is investigated and verified with finite element analysis. The influence of the external loads on the interfacial stress distribution is also studied. Finally, the optimum actuator geometry under the action of external loads is presented.

4.2 Formulation

Consider a beam structure of length $2L$ with a pair of induced strain actuators of length $2l$ symmetrically bonded on the outer surfaces of the beam as shown in Fig. 4.1. The thickness of the actuator is a and of the beam is $2b$. The interfaces between the actuators and beam are assumed to have a "perfect bond". The structure is subjected to an external axial normal force F_0 and a bending moment M_0 applied at the end of the beam and induced strain actuation, λ_t and λ_b, exerted on the actuators.

Under the consideration of linear system, the external loads and the induced strain actuation mechanisms can be treated separately. The resulting stress field of each mechanism can then be superimposed to yield the complete solution of the original combined loading problem. The induced strain actuation mechanism has been solved by converting the actuation mechanism to a boundary value problem under the framework of plane stress formulation of the theory of elasticity (Lin and Rogers, 1993a). Figures 4.2(*a*) and (*b*) show the two stress fields that yield the solution of this mechanism. A detailed formulation and solution scheme have been given in the reference (Lin and Rogers, 1993a).

The stress field caused by the external loads is a typical boundary value problem in the course of the theory of elasticity. Figure 4.2(*c*) illustrates the loading condition and the resulting stress field to be determined. The complete solution of the original problem of
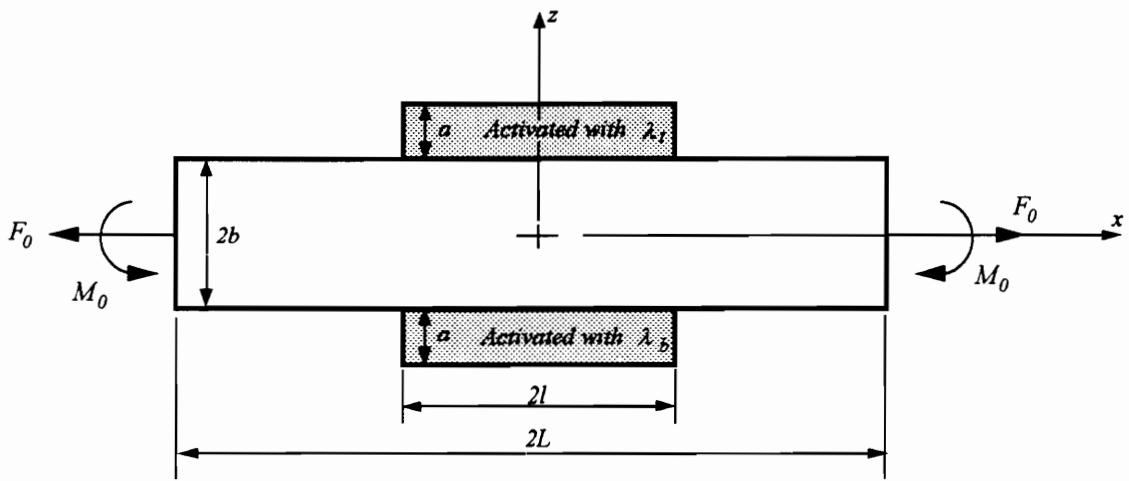
Figure 4.1. Configuration of the analytical model with applied induced strain actuation of the actuators and external loads on the beam substrate.

Fig. 4.1 can be subsequently obtained by superimposing the solutions of Figs. 4.2 (a), (b), and (c):

$$\sigma_x = \sigma_x^I + \sigma_x^{II} + \sigma_x^{III} \qquad (1.1)$$

$$\tau_{xz} = \tau_{xz}^I + \tau_{xz}^{II} + \tau_{xz}^{III} \qquad (1.2)$$

$$\sigma_z = \sigma_z^I + \sigma_z^{II} + \sigma_z^{III}. \qquad (1.3)$$

Since the stress field (I) and (II) have been solved (Lin and Rogers, 1993a), the only effort remaining is to solve the boundary value problem of Fig. 4.2(c).

The boundary value problem of the Fig. 4.2(c) resembles that of the Fig. 4.2(b) with different boundary traction conditions. Thus, the stress field obtained for the problem of Fig. 4.2(b) is also adequate for the Fig. 4.2(c). The stress field in the section where the actuators are present, i.e., $|x| \le l$, can be represented by (Lin and Rogers, 1993a):

$$\sigma_{x(at)}^{III}(x,z) = (\frac{a+b-z}{a})^2 \frac{E_a}{E_s} \sigma_{its}(x) - \frac{(b-z)(2a+b-z)}{a^2} \sigma_{ot}(x) \qquad (2.1)$$

$$\sigma_{x(s)}^{III}(x,z) = \frac{(b-z)(b+z)}{b^2} \sigma_c(x) + \frac{z(z+b)}{2b^2} \sigma_{its}(x) + \frac{z(z-b)}{2b^2} \sigma_{ibs}(x) \qquad (2.2)$$

$$\sigma_{x(ab)}^{III}(x,z) = (\frac{a+b+z}{a})^2 \frac{E_a}{E_s} \sigma_{ibs}(x) - \frac{(b+z)(2a+b+z)}{a^2} \sigma_{ob}(x), \qquad (2.3)$$

$$\sigma^I_{x(at)} = -E_a \lambda_t$$
$$\tau^I_{xz(at)} = \sigma^I_{z(at)} = 0$$

$-E_a \lambda_t$ Activated with λ_t $-E_a \lambda_t$

$$\sigma^I_{x(s)} = \tau^I_{xz(s)} = \sigma^I_{z(s)} = 0$$

$-E_a \lambda_b$ Activated with λ_b $-E_a \lambda_b$

$$\sigma^I_{x(ab)} = -E_a \lambda_b$$
$$\tau^I_{xz(ab)} = \sigma^I_{z(ab)}$$

(a)

$$\sigma^{II}_{x(at)} ; \quad \tau^{II}_{xz(at)} ; \quad \sigma^{II}_{z(at)}$$

$E_a \lambda_t$ $E_a \lambda_t$

$$\sigma^{II}_{x(s)}$$
$$\tau^{II}_{xz(s)}$$
$$\sigma^{II}_{z(s)}$$

$E_a \lambda_b$ $E_a \lambda_b$

$$\sigma^{II}_{x(ab)} ; \quad \tau^{II}_{xz(ab)} ; \quad \sigma^{II}_{z(ab)}$$

(b)

$$\sigma^{III}_{x(at)} = ? ; \quad \tau^{III}_{xz(at)} = ? ; \quad \sigma^{III}_{z(at)} = ?$$

F_0
$$\sigma^{III}_{x(s)} = ?$$
$$\tau^{III}_{xz(s)} = ?$$
$$\sigma^{III}_{z(s)} = ?$$
       F_0

M_0 M_0

$$\sigma^{III}_{x(ab)} = ? ; \quad \tau^{III}_{xz(ab)} = ? ; \quad \sigma^{III}_{z(ab)} = ?$$
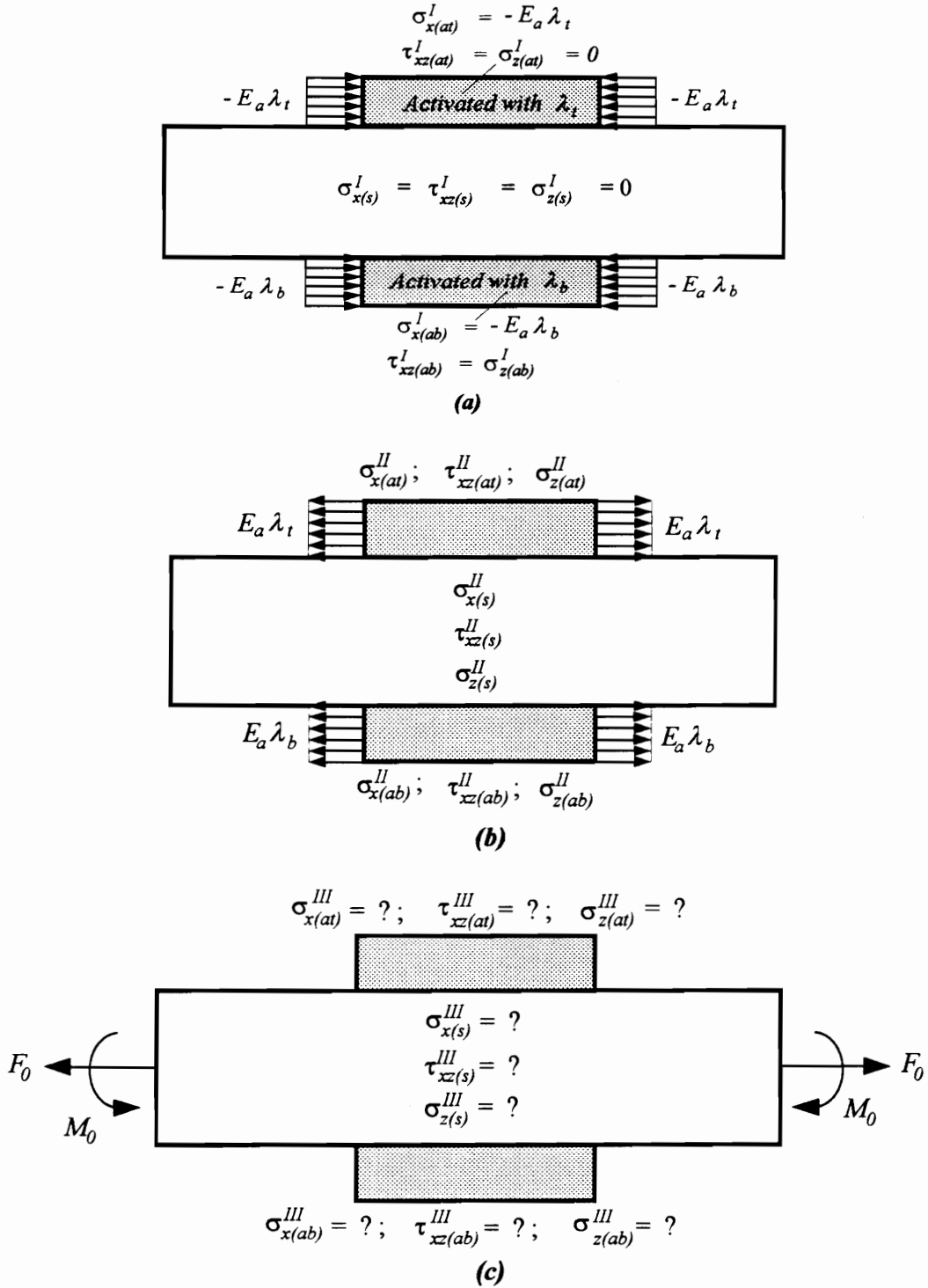
(c)

Figure 4.2. Decomposed loading condition: (*a*) blocking forces on the actuator edges as the actuators are activated; (*b*) end traction on the actuator edges; (*c*) external loads on the ends of the beam substrate.

121

$$\tau_{xz(at)}^{III}(x,z) = \frac{1}{3a^2} \{ \frac{E_a(a+b-z)^3}{E_s} \sigma_{its}'(x)$$
$$+(a+b-z)[2a^2 - 2ab - b^2 + 2(a+b)z - z^2]\sigma_{ot}'(x)\} \tag{3.1}$$

$$\tau_{xz(s)}^{III}(x,z) = \frac{z(-3b^2 + z^2)}{3b^2} \sigma_c'(x) + \frac{a}{3} [\sigma_{ot}'(x) - \sigma_{ob}'(x)]$$
$$+\frac{1}{12b^2 E_s} \{ [2ab^2 E_a + E_s(3b^3 - 3bz^2 - 2z^3)]\sigma_{its}'(x)$$
$$-[2ab^2 E_a + E_s(3b^3 - 3bz^2 + 2z^3)]\sigma_{ibs}'(x)\} \tag{3.2}$$

$$\tau_{xz(ab)}^{III}(x,z) = \frac{-1}{3a^2} \{ \frac{E_a(a+b+z)^3}{E_s} \sigma_{ibs}'(x)$$
$$+(a+b+z)[2a^2 - 2ab - b^2 - 2(a+b)z - z^2]\sigma_{ob}'(x)\}, \tag{3.3}$$

$$\sigma_{z(at)}^{III}(x,z) = \frac{1}{12a^2} \{ \frac{E_a(a+b-z)^4}{E_s} \sigma_{its}''(x) + (a+b$$
$$-z)^2[5a^2 - 2ab - b^2 + 2(a+b)z - z^2]\sigma_{ot}''(x)\} \tag{4.1}$$

$$\sigma_{z(s)}^{III}(x,z) = \frac{-(b^2 - z^2)(5b^2 - z^2)}{12b^2} \sigma_c''(x) + \frac{a}{24} [(5a - 8z)\sigma_{ot}''(x) + (5a + 8z)\sigma_{ob}''(x)]$$
$$+\frac{1}{24b^2 E_s} \{ [ab^2 E_a(a - 4z) + E_s(b^4 + 6b^3 z - 2bz^3 - z^4)]\sigma_{its}''(x)$$
$$+[ab^2 E_a(a + 4z) + E_s(b^4 - 6b^3 z + 2bz^3 - z^4)]\sigma_{ibs}''(x)\} \tag{4.2}$$

$$\sigma_{z(ab)}^{III}(x,z) = \frac{1}{12a^2} \{ \frac{E_a(a+b+z)^4}{E_s} \sigma_{ibs}''(x) + (a+b$$
$$+z)^2[5a^2 - 2ab - b^2 - 2(a+b)z - z^2]\sigma_{ob}''(x)\}, \tag{4.3}$$

where E_a and E_s are the Young's modulus of the actuator and beam substructure, and the

subscript (at), (s), and (ab) indicate the quantities of the top actuator, beam and bottom

actuator, respectively. The quantities $\sigma_{ot}(x)$, $\sigma_{ob}(x)$, and $\sigma_c(x)$ are the axial normal stress at the outer fiber of the top and bottom actuator and at the center of the beam, $\sigma_{its}(x)$ and $\sigma_{ibs}(x)$ are the axial normal stresses of the beam at the top and bottom interfaces, respectively, and the prime indicates the derivative with respect to x.

The stress field in the beam section where the actuators are absent, i.e., $l \langle |x| \langle L - l$, is assumed to be undisturbed by the geometric discontinuity of the bonded actuators and end effects of the applied loads. Accordingly, the axial normal stress is the only nonvanishing stress component and is uniform through the thickness under the axial normal force and linear under the bending moment loads.

The overall equilibrium of the structure requires:

$$\Sigma F = F_{(at)} + F_{(s)} + F_{(ab)}$$
$$= \int_b^{a+b} \sigma_{x(at)}^{III} dz + \int_{-b}^b \sigma_{x(s)}^{III} dz + \int_{-(a+b)}^{-b} \sigma_{x(ab)}^{III} dz$$
$$= F_0 \tag{5.1}$$
$$\Sigma M = M_{(at)} + M_{(s)} + M_{(ab)}$$
$$= \int_b^{a+b} z\,\sigma_{x(at)}^{III} dz + \int_{-b}^b z\,\sigma_{x(s)}^{III} dz + \int_{-(a+b)}^{-b} z\,\sigma_{x(ab)}^{III} dz$$
$$= M_0. \tag{5.2}$$

The stress components at the interfaces $\sigma_{its}(x)$ and $\sigma_{ibs}(x)$ can then be expressed in terms of $\sigma_{ot}(x)$, $\sigma_{ob}(x)$, and $\sigma_c(x)$:

$$\sigma_{its}(x) = \frac{1}{2(aE_a+bE_s)[aE_a(a+4b)+4b^2E_s]} \{6E_s(aE_a+bE_s)M_0$$
$$+3E_s[aE_a(a+4b)+4b^2E_s]F_0$$
$$-4bE_s[aE_a(a+4b)+4b^2E_s]\sigma_c(x)$$
$$-aE_s[aE_a(7a+16b)+bE_s(5a+16b)]\sigma_{ot}(x)+a^2E_s(3aE_a+5bE_s)\sigma_{ob}(x)\}$$

$$(6.1)$$

$$\sigma_{its}(x) = \frac{1}{2(aE_a+bE_s)[aE_a(a+4b)+4b^2E_s]} \{-6E_s(aE_a+bE_s)M_0$$
$$+3E_s[aE_a(a+4b)+4b^2E_s]F_0$$
$$-4bE_s[aE_a(a+4b)+4b^2E_s]\sigma_c(x)$$
$$-aE_s[aE_a(7a+16b)+bE_s(5a+16b)]\sigma_{ob}(x)+a^2E_s(3aE_a+5bE_s)\sigma_{ot}(x)\}.$$

$$(6.2)$$

The stress fields of Eqs. (2) (3) and (4) satisfy the equilibrium in each constituent as well as the overall equilibrium of the integrated structural system. The boundary conditions involving stresses at the lateral surfaces along with the traction continuity at the interfaces are also satisfied. The unknowns remained to be determined in this stress field are $\sigma_{ot}(x)$, $\sigma_{ob}(x)$, and $\sigma_c(x)$.

To solve these unknown stress components, the principle of stationary complementary energy is used. The total complementary energy for the present problem is:

124

$$U_{(total)} = U_{(at)} + U_{(s)} + U_{(ab)}$$

$$= \frac{1}{2E_a} \int_b^{a+b} \int_{-l}^{l} [\sigma_{x(at)}^{III}{}^2 + \sigma_{z(at)}^{III}{}^2 + 2(1+v_a)\tau_{xz(at)}^{III}{}^2 - 2v_a\sigma_{x(at)}^{III}\sigma_{z(at)}^{III}] dxdz$$

$$+ \frac{1}{2E_s} \int_{-b}^{b} \int_{-l}^{l} [\sigma_{x(s)}^{III}{}^2 + \sigma_{z(s)}^{III}{}^2 + 2(1+v_s)\tau_{xz(s)}^{III}{}^2 - 2v_s\sigma_{x(s)}^{III}\sigma_{z(s)}^{III}] dxdz$$

$$+ \frac{1}{2E_a} \int_{-a-b}^{-b} \int_{-l}^{l} [\sigma_{x(ab)}^{III}{}^2 + \sigma_{z(ab)}^{III}{}^2 + 2(1+v_a)\tau_{xz(ab)}^{III}{}^2 - 2v_a\sigma_{x(ab)}^{III}\sigma_{z(ab)}^{III}] dxdz. \tag{7}$$

where v_a and v_s are the Poisson's ratio of the actuator and beam substrate, respectively. In order to simplify the foregoing derivation, the problem is solved for the case of axial normal force and bending moment separately. The solutions of these two cases can be thereafter linearly superimposed to yield the solution of a general loading condition.

Under the loading of axial normal force, i.e., $M_o = 0$, the axial normal stress of Eq. (2) are symmetric about the x-axis, which yields:

$$\sigma_{ibs}(x) = \sigma_{its}(x) \tag{8.1}$$

$$\sigma_{ob}(x) = \sigma_{ot}(x). \tag{8.2}$$

Substituting the stress components of Eqs. (2), (3) and (4) into Eq. (7), with the help of Eq. (6), the complementary energy of the system becomes:

$$U_{(f)} = K_1^f F_0^2 + K_2^f F_0\sigma_c(x) + K_3^f \sigma_c^2(x) + K_4^f F_0\sigma_{ot}(x) + K_5^f \sigma_c(x)\sigma_{ot}(x)$$

$$+ K_6^f \sigma_{ot}^2(x) + K_7^f \sigma_c'^2(x) + K_8^f \sigma_c'(x)\sigma_{ot}'(x) + K_9^f \sigma_{ot}'^2(x) + K_{10}^f F_0\sigma_c''(x)$$

$$+ K_{11}^f \sigma_c(x)\sigma_c''(x) + K_{12}^f \sigma_c''(x)\sigma_{ot}(x) + K_{13}^f \sigma_c''^2(x) + K_{14}^f F_0\sigma_{ot}''(x)$$

$$+ K_{15}^f \sigma_c(x)\sigma_{ot}''(x) + K_{16}^f \sigma_{ot}(x)\sigma_{ot}''(x) + K_{17}^f \sigma_c''(x)\sigma_{ot}''(x) + K_{18}^f \sigma_{ot}''^2(x), \tag{9}$$

where K_i^f ($i = 1, 18$) are functions of the material properties, E_a, E_s, v_a, v_s, and the thicknesses of the actuator and beam, a and b. The complete expressions of K_i^f are given in the appendix.

Variation of the complementary energy $\delta U_{(f)} = 0$ with the stresses satisfying the prescribed end traction yields the Euler's equation:

$$\left[A_1^f \frac{d^4}{dx^4} + A_2^f \frac{d^2}{dx^2} + A_3^f \right] \sigma_c(x) + \left[B_1^f \frac{d^4}{dx^4} + B_2^f \frac{d^2}{dx^2} + B_3^f \right] \sigma_{ot}(x) = D_1^f \tag{10.1}$$

$$\left[B_1^f \frac{d^4}{dx^4} + B_2^f \frac{d^2}{dx^2} + B_3^f \right] \sigma_c(x) + \left[C_1^f \frac{d^4}{dx^4} + C_2^f \frac{d^2}{dx^2} + C_3^f \right] \sigma_{ot}(x) = D_2^f , \tag{10.2}$$

where
$$A_1^f = 2K_{13}^f; \quad A_2^f = 2\left(K_{11}^f - K_7^f\right); \quad A_3^f = 2K_3^f$$
$$B_1^f = K_{17}^f; \quad B_2^f = K_{12}^f + K_{15}^f - K_8^f; \quad B_3^f = K_5^f$$
$$C_1^f = 2K_{18}^f; \quad C_2^f = 2\left(K_{16}^f - K_9^f\right); \quad C_3^f = 2K_6^f$$
$$D_1^f = -K_2^f F_0; \quad D_2^f = -K_4^f F_0 .$$

The general solution of Eq. (10) has the form:

$$\sigma_{ot}(x) = \frac{(A_3^f D_2^f - B_3^f D_1^f)}{(A_3^f C_3^f - (B_3^f)^2)} + \sum_{i=1}^{8} p_i^f (\exp)^{\alpha_i^f x} \tag{11.1}$$

$$\sigma_c(x) = \frac{(C_3^f D_1^f - B_3^f D_2^f)}{(A_3^f C_3^f - (B_3^f)^2)} + \sum_{i=1}^{8} \gamma_i^f p_i^f (\exp)^{\alpha_i^f x} , \tag{11.2}$$

where

$$\gamma_i^f = -\frac{(A_3^f + A_2^f (\alpha_i^f)^2 + A_1^f (\alpha_i^f)^4)}{(B_3^f + B_2^f (\alpha_i^f)^2 + B_1^f (\alpha_i^f)^4)}, \quad i = 1,8.$$

In the above, α_i^f $(i = 1,8)$ are the roots of the characteristic equation:

$$\begin{vmatrix} (A_1^f (\alpha^f)^4 + A_2^f (\alpha^f)^2 + A_3^f) & (B_1^f (\alpha^f)^4 + B_2^f (\alpha^f)^2 + B_3^f) \\ (B_1^f (\alpha^f)^4 + B_2^f (\alpha^f)^2 + B_3^f) & (C_1^f (\alpha^f)^4 + C_2^f (\alpha^f)^2 + C_3^f) \end{vmatrix} = 0, \tag{12}$$

and p_i^f $(i = 1,8)$ are arbitrary constants to be determined by the end traction conditions:

$$\sigma_{ot}(\pm l) = 0; \quad \sigma_c(\pm l) = \frac{F_0}{2b} \tag{13.1}$$

$$\sigma'_{ot}(\pm l) = 0; \quad \sigma'_c(\pm l) = 0. \tag{13.2}$$

Under the loading of an external bending moment, i.e., $F_o = 0$, the axial normal stresses of Eq. (2) are, on the other hand, antisymmetric about the x-axis, which yields:

$$\sigma_{ibs}(x) = -\sigma_{its}(x) \tag{14.1}$$

$$\sigma_{ob}(x) = -\sigma_{ot}(x) \tag{14.2}$$

$$\sigma_c(x) = 0 \tag{14.3}$$

The complementary energy of the system becomes

$$U_{(m)} = K_1^m M_0^2 + K_2^m M_0 \sigma_{ot}(x) + K_3^m \sigma_{ot}^2(x) + K_4^m \sigma'_{ot}^2(x) + K_5^m M_0 \sigma''_{ot}(x)$$
$$+ K_6^m \sigma_{ot}(x) \sigma''_{ot}(x) + K_7^m \sigma''_{ot}^2(x), \tag{15}$$

127

where $K_i^m (i = 1, 8)$ are functions of the material properties and geometry, and are given in the appendix.

Variation of the complementary energy $\delta U_{(m)} = 0$ with the stresses satisfying the prescribed end traction yields the Euler's equation:

$$[A_1^m \frac{d^4}{dx^4} + A_2^m \frac{d^2}{dx^2} + A_3^m]\sigma_{ot}(x) = D_1^m, \tag{16}$$

where

$$A_1^m = 2K_7^m; \quad A_2^m = 2(K_6^m - K_4^m); \quad A_3^m = 2K_3^m$$
$$D_1^m = -K_2^m M_0.$$

The general solution of Eq. (16) has the form:

$$\sigma_{ot}(x) = \frac{D_1^m}{A_3^m} + \sum_{i=1}^{4} p_i^m (\exp)^{\alpha_i^m x}, \tag{17}$$

where $\alpha_i^m (i = 1, 4)$ are the roots of the characteristic equation

$$A_1^m (\alpha^m)^4 + A_2^m (\alpha^m)^2 + A_3^m = 0, \tag{18}$$

and $p_i^m (i = 1,4)$ are arbitrary constants to be determined by the stress free boundary condition at the actuator edges:

$$\sigma_{ot}(\pm l) = 0 \tag{19.1}$$
$$\sigma'_{ot}(\pm l) = 0. \tag{19.2}$$

128

The solutions obtained above for the external loading condition are to be superimposed to the solutions for the induced strain actuation to construct the complete solution of the original problem of Fig. 4.1. It is noted that the solutions are obtained for pure extension/contraction and pure bending mode. Nevertheless, a linear superposition of these solutions can yield the solution for a general loading condition.

4.3 Finite element analysis

In order to assist in verifying the current analysis, finite element analyses were performed. A typical finite element model with $b/a = 3$ thickness ratio and $l/a = 10$, $L/a = 20$ aspect ratio subjected to an external axial force and induced strain actuation by the actuators is depicted in Fig. 4.3. The model consists of 4×10 elements for each actuator and 24×20 elements for the beam.

Plane stress linear isoparametric elements were used for both the beam and the actuators. Since the characteristic induced strain of the actuator resembles the thermal expansion effects of a structural material, fictions thermal expansion coefficients were assigned to the actuators. The desired induced strain level was then obtained by applying a uniform temperature field on the model. The induced strain actuation and external loading were applied simultaneously in one loading step to model the combined effect of the two mechanisms. The analyses were performed using the ABAQUS finite element package for solution and IDEAS for pre- and post-processing.
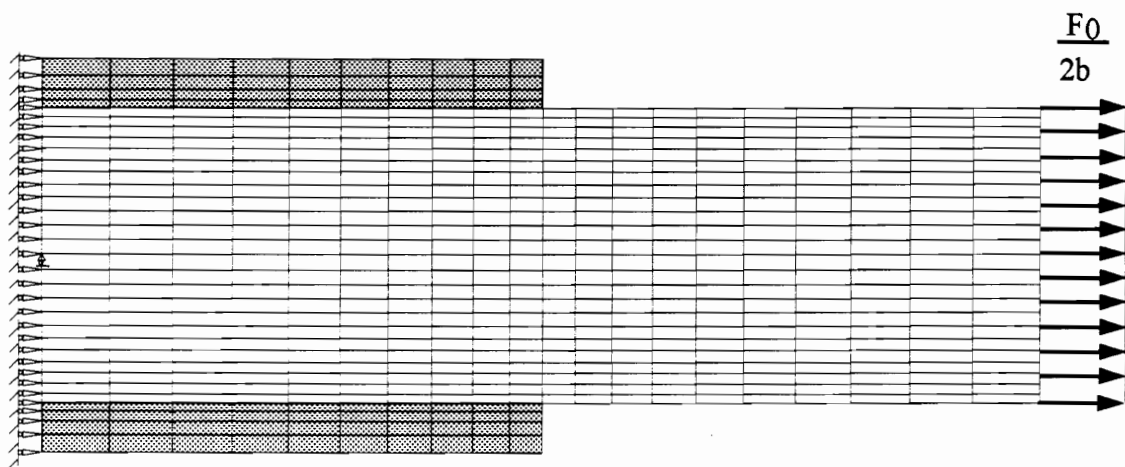
Figure 4.3. Finite element model of the actuator/beam substructure with applied axial force (modeled with edge pressure) and boundary restraints.

4.4 Results

The effective force/moment induced on the beam structure and the resulting interfacial stress distribution under the combined external loads and induced strain actuation of the actuators are presented. The geometric configurations of the integrated actuator/beam substructure selected are $b/a = 3$, $l/a = 10$, and $L/a = 20$, and the material properties of $E_s/E_a = 1.16$, and $v_s/v_a = 1$ are used, which are comparable to an aluminum beam with piezoceramic actuators.

Figure 4.4 shows the effective force distribution induced in the beam structure along the x-axis under pure extension activation, i.e., $\lambda_b = \lambda_t$, and applied external axial force of different magnitude. The magnitude of the applied axial force is normalized with the total blocking force of the actuators, i.e., $\overline{F} = F_0/(2aE_a\lambda_t)$, and the x-coordinate is nondimensionalized with respect to the thickness of the actuator. For comparison, the results obtained from the finite element analysis are included.

It is shown that results from the current analysis agree well with those of the FEM validating the superposition procedure used in the current analysis. A discrepancy is shown at the area near the ends of the actuator. At the ends of the actuator, i.e., at $r=10$, the effective force obtained by the analytical model exhibits a discontinuity. These are caused by the approximation made in the axial normal stress field in the analytical model. Nevertheless, the disagreement is confined within a length of one actuator thickness.
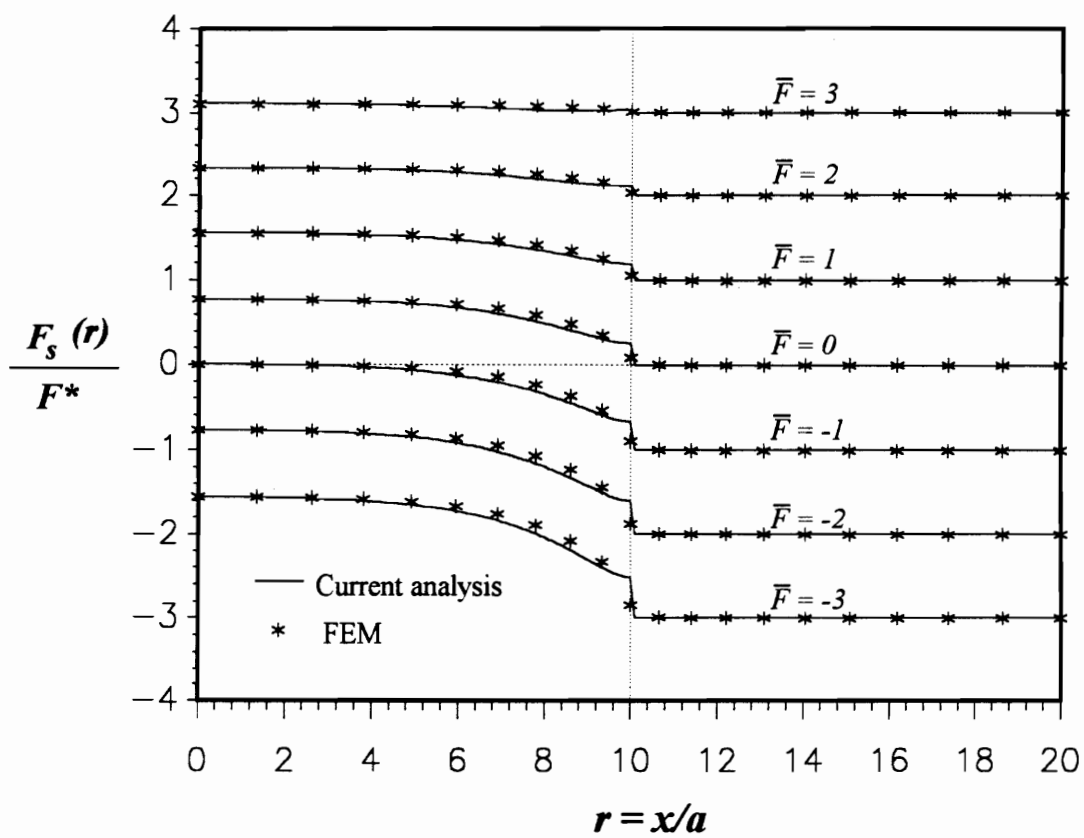
Figure 4.4. Effective force distributions induced in the beam structure along the x-axis under pure extension actuation, $\lambda_b = \lambda_t$, and applied external axial force of different magnitudes.

The corresponding interfacial shear stress distribution is illustrated in Fig. 4.5, where the magnitude of the shear stress is normalized with the blocking stress of the actuator, $E_a \lambda_t$. It is shown that the location and the level of the maximum shear stress are altered with the application of the external axial force. The maximum shear stress increases with the applied negative forces, i.e., compressive forces in the case of pure extension activation, and decreases with applied tensile forces. This is caused by the higher strain mismatch at the interface as a negative external force is applied. It is noted that increasing the positive forces, i.e., tensile forces, a high shear stress level will be induced in opposite direction.

Figure 4.6 shows the interfacial peeling stress distribution under pure extension activation and external axial force of different magnitude. The maximum peeling stress also exhibits the trend that increases with the applied negative forces, i.e., compressive forces, and decreases with the applied tensile forces. Further increase in tensile forces will also induced high peeling stress level in opposite direction.

The effective moment distribution induced in the beam structure along the x-axis under pure bending activation, i.e., $\lambda_b = -\lambda_t$, and applied bending moments is shown in Fig. 4.7. The magnitude of the external bending moment is normalized with the moment that the total blocking forces of the actuators produce about the neutral axis of the structure, i.e., $\overline{M} = M_0 / 2aE_a(a/2+b)$. It is shown that the results obtained from the current analysis and the FEM agree very well except at the location where the actuator ends. Again, the discrepancy is caused by the approximation in the axial normal stress field in the analytical model.
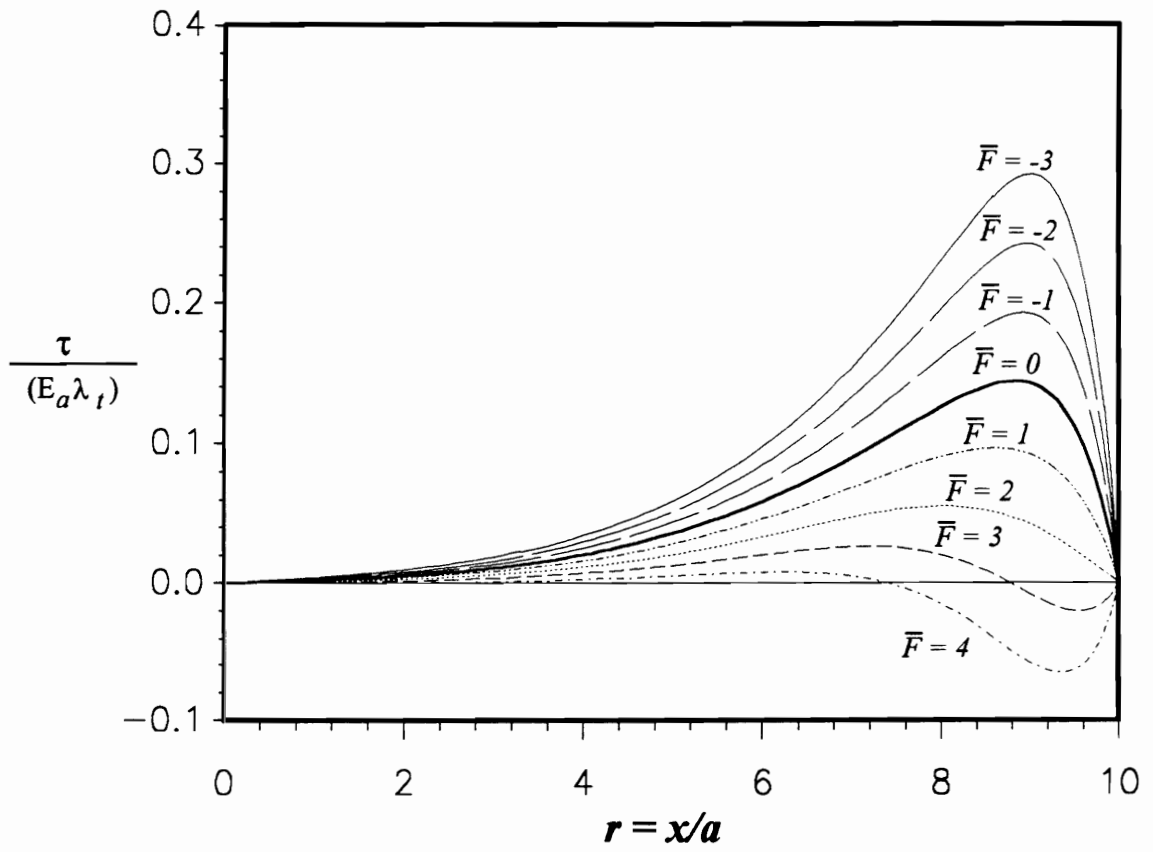
133

Figure 4.5. Interfacial shear stress distributions as the actuators are activated in pure extension and the beam is subjected to external axial force of different magnitudes.
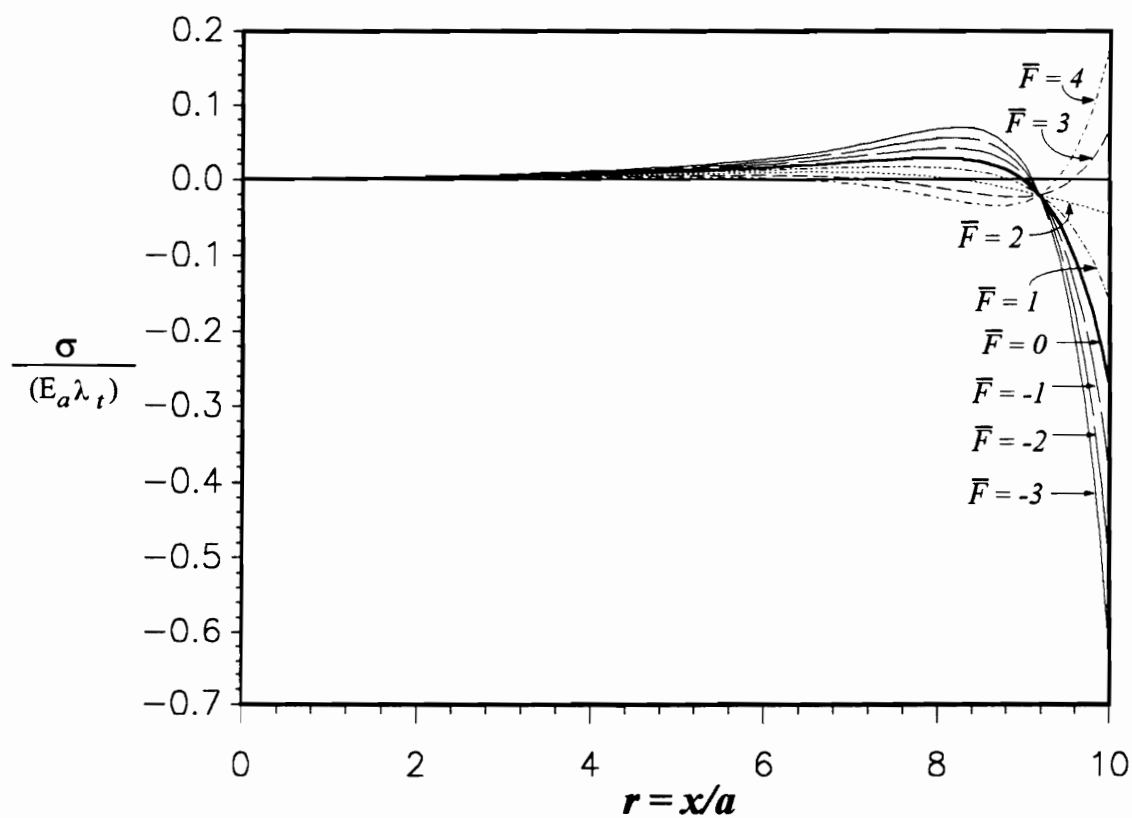
134

Figure 4.6. Interfacial peeling stress distributions as the actuators are activated in pure extension and the beam is subjected to external axial force of different magnitudes.
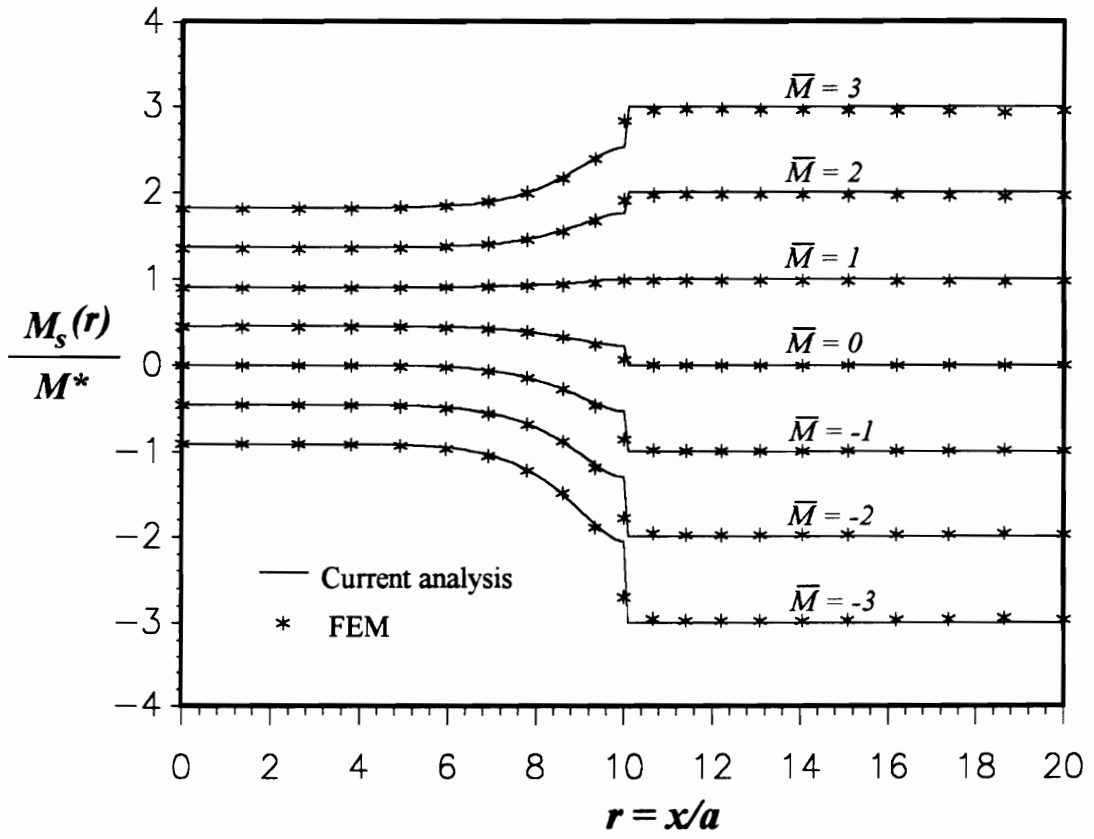
135

Figure 4.7. Effective moment distributions induced in the beam structure along the *x*-axis under pure bending actuation, $\lambda_b = -\lambda_t$, and applied bending moment of different magnitudes.

The corresponding interfacial shear and peeling stress distribution is shown in Figs. 4.8 and 4.9, respectively. It is apparent that the trend of the alternation on maximum interfacial shear and peeling stresses under the pure bending mode is the same as that of the pure extension mode. The maximum shear and peeling stress level increases with the applied negative moments, and decreases with positive moments. With high applied positive moments, high shear and peeling stress level will be induced in opposite direction.

The maximum interfacial shear and peeling stress as a function of external loads is depicted in Fig. 4.10. Under the pure extension mode, the actuators are activated with $\lambda_b = \lambda_t$ and F_o is the only external load, and under the pure bending mode, the actuators are activated with $\lambda_b = -\lambda_t$ and M_o is the only external load. It is evident that the maximum shear and peeling stresses vary linearly with the magnitude of the applied external loads for both pure extension and pure bending modes. The induced strain actuation of the actuators offsets the stress level in tension on shear stress and in compression on peeling stress.

It is well known that an optimum actuator/substructure thickness ratio exists as the structure is activated in pure bending by the actuators to deliver maximum actuation moment to the substrate. Superposition of the external bending moment M_o on the induced strain actuation will change the stress profile in both the actuator and beam substrate. This consequently alters the optimum thickness of the actuator. Figure 4.11 shows the optimum substructure-to-actuator thickness ratio as a function of applied external bending moments at different induced strain actuation levels, where the external

Figure 4.8. Interfacial shear stress distributions as the actuators are activated in pure bending and the beam is subjected to external bending moment of different magnitudes.
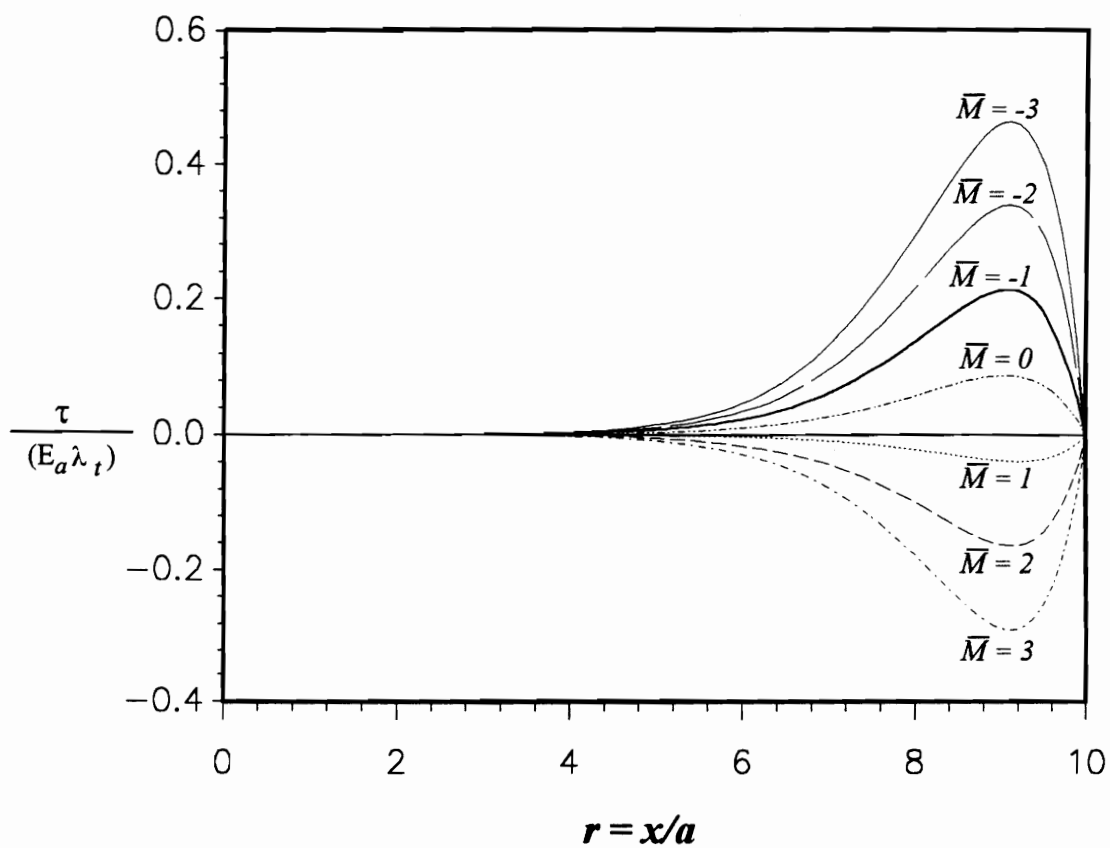
138
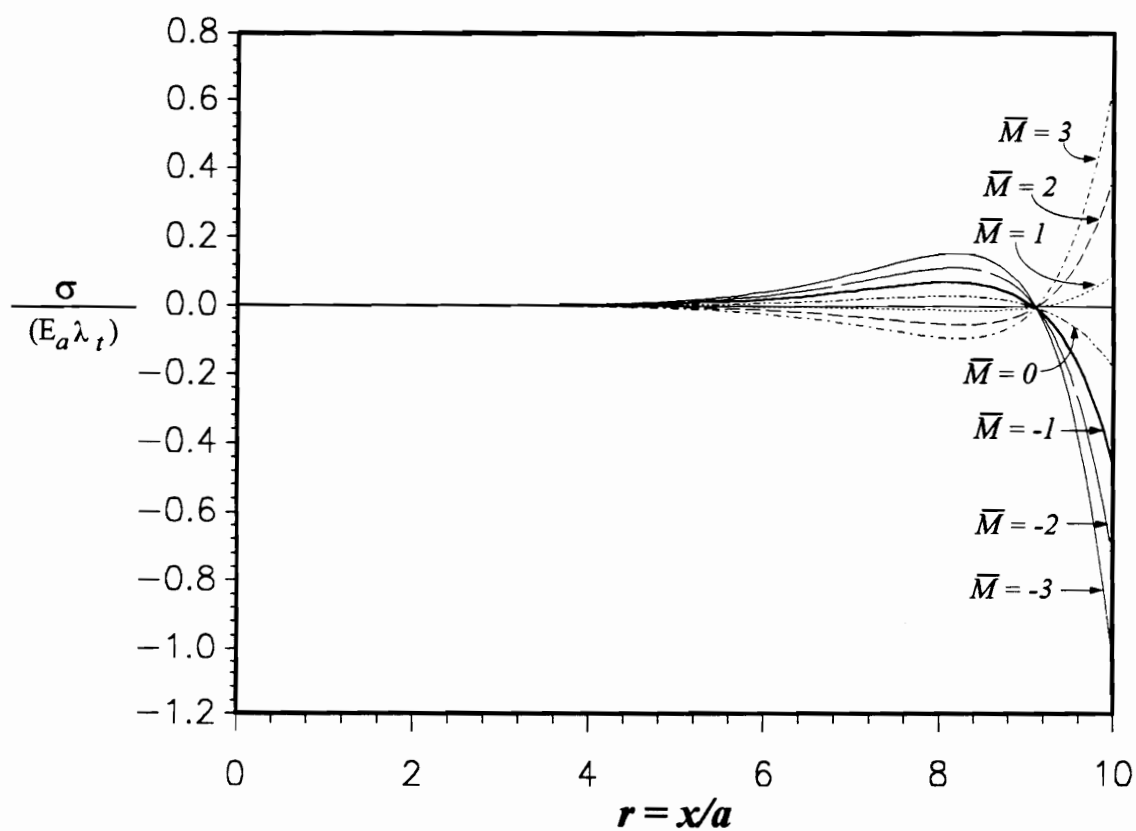
Figure 4.9. Interfacial peeling stress distributions as the actuators are activated in pure bending and the beam is subjected to external bending moment of different magnitudes.

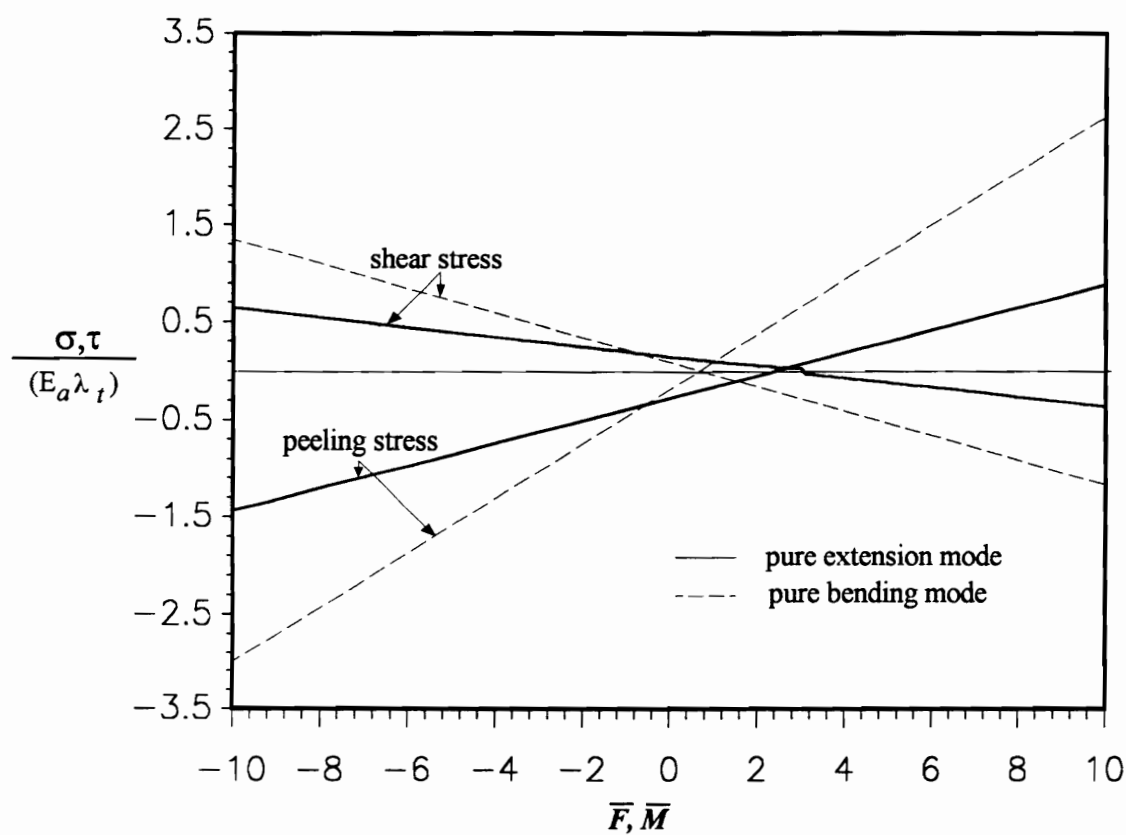**Figure 4.10.** Maximum interfacial shear and peeling stresses as a function of external loads in pure extension and pure bending modes.
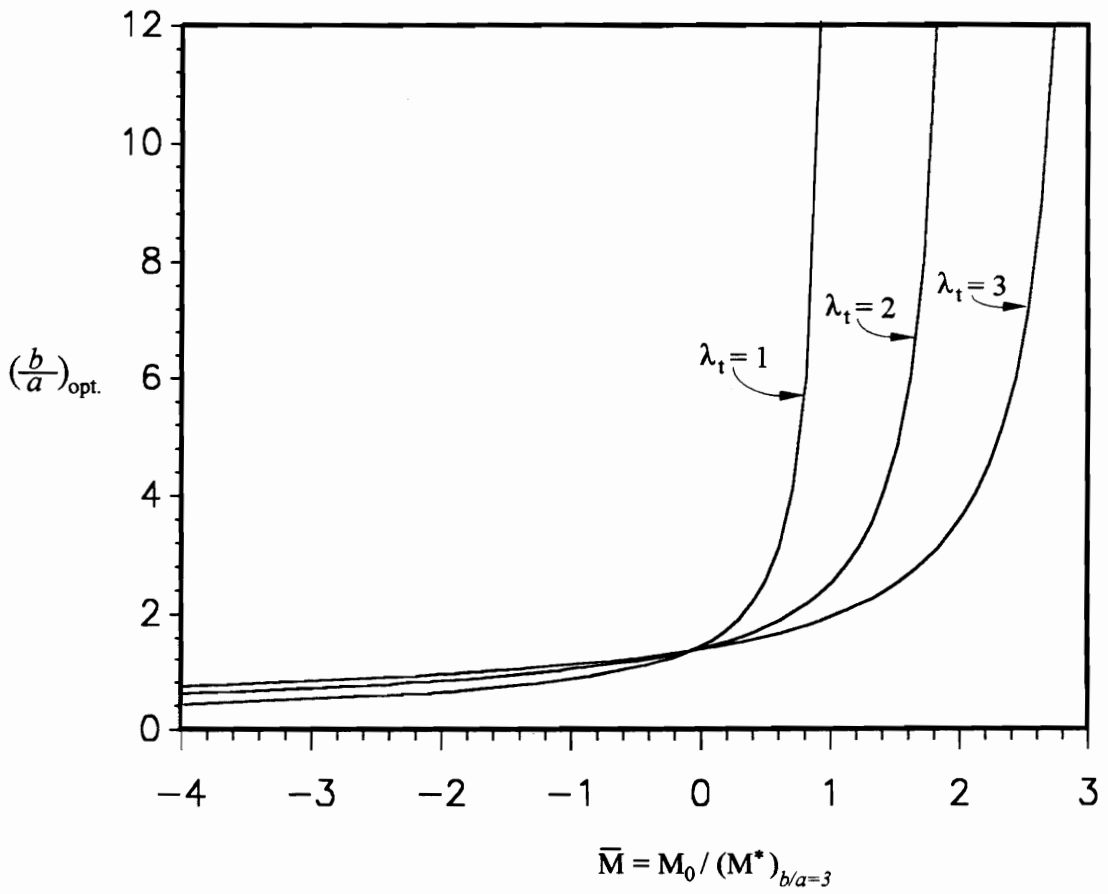
140

Figure 4.11. Optimum substrate-to-actuator thickness ratio as a function of applied bending moments at different induced strain actuation levels.

bending moments are normalized with the actuation moment induced by the actuators at $b/a = 3$.

It is shown that with negative bending moments, i.e., the bending moments with sign opposite to that of the actuation moment, a thicker actuator is desirable for the actuators to induce a maximum moment on the substrate. This result agrees with the conclusion of the study by Chaudhry and Rogers (1993). On the other hand, with positive bending moments a thinner actuator will deliver a higher moment to the substrate. It is evident that for a high positive bending moment, such as $\overline{M} = 1$ at $\lambda_t = 1$, the optimum thickness ratio approaches infinity. This suggests that no desired actuation moment on the beam substrate can be achieved. In other words, with a high positive bending moment, no actuation moment on the substrate can be added to the substrate using surface-bonded induced strain actuators.

4.5 Conclusion

The effect of external loads on a beam structure activated with surface-bonded induced strain actuators was modeled by extending the analytical scheme recently proposed by the authors (Lin and Rogers, 1993a). It was demonstrated that the mechanism of the external loads can be modeled using the same approach. The resulting stress field can be superimposed with the existing solution of the induced strain actuation mechanism obtained previously to yield a complete solution for the combined effects of the both mechanisms. The solution was obtained by the principle of complementary energy for

pure extension and pure bending mode separately which can be linearly superimposed to yield the solution for a general actuation and loading condition.

It was shown that the results obtained from the current analysis agree very well with those from the finite element analysis in the prediction of effective force/moment induced in the substrate. It was also demonstrated that the interfacial stress distribution is altered with external loads, and the maximum interfacial shear and peeling stresses are a linear function of external loads. Under the pure bending mode, parametric study showed that with bending moments with a sign opposite to that of the actuation moment, a low substructure-to-actuator thickness ratio is optimal. This result agrees with the conclusion of the study by Chaudhry and Rogers (1993). On the other hand, with bending moments with the same sign as that of the actuation moment, a high substrate-to-actuator thickness ratio is desirable. In the limit, with high positive bending moments, no actuation moment can be added to the substrate using surface-bonded induced strain actuators.

4.6 References

Bailey, T. and Hubbard Jr., J. E., 1985, "Distributed Piezoelectric-Polymer Active Vibration Control of a Cantilever Beam, "Journal of Guidance and Control, Vol. 8, No. 5, pp. 605-611.

Chaudhry, Z., and Rogers, C. A., 1991, "Bending and Shape Control of Beams Using SMA Actuators," Journal of Intelligent Material Systems and Structures, Vol. 2, No. 4, pp. 581-602.

Chaudhry, Z. and Rogers, C. A., 1993, "Performance and Optimization of Induced Strain Actuated Structures under the Action of External Loads," Proceedings of the AIAA/ASME/AHS/ASC 34th SDM Conference, La Jolla, CA, April 19-22, 1993.

Crawley, E. F. and de Luis, J., 1987, "Use of Piezoelectric Actuators as Elements of Intelligent Structures," AIAA Journal, Vol. 25, No. 10, pp. 1373-1385.
Crawley, E. F. and Lazarus, K. B., 1991, "Induced Strain Actuation of Isotropic and Anisotropic Plates," AIAA Journal, Vol. 29, No. 6, pp. 944-951.

Im, S,, and Atluri, S. N., 1989, "Effects of a Piezo-Actuator on a Finitely Deformed Beam Subjected to General Loading," AIAA Journal, Vol. 27, No. 12, p.p. 1801-1807.

Lin, M. W., and Rogers, C. A., 1993a, "Modeling of the Actuation Mechanism in a Beam Structure with Induced Strain Actuators," Proceedings of the AIAA/ASME/AHS/ASC 34th SDM Conference, La Jolla, CA, April 19-22, 1993.

Lin, M. W., and Rogers, C. A., 1993b, "Actuation Response of a Beam Structure with Induced Strain Actuators," Proceedings of the Adaptive Structures and Material Systems Symposium, ASME Winter Annual Meeting, New Orleans, LA, November 28-December 3, 1993.

Liang, C., Rogers, C. A. and Fuller, C. R., 1991, "Acoustic Transmission and Radiation Analysis of Adaptive Shape Memory Alloy Reinforced Laminated Plates," Journal of Sound and Vibration, Vol. 145, No. 1, pp. 23-41.

Rogers, C. A., Liang, C. and Li S., 1991, "Active Damage Control of Hybrid Material Systems Using Induced Strain Actuators," Proceedings of the AIAA/ASME/ASCE/AHS/ASC 32nd SDM Conference, Baltimore, MD, April 8-10, 1991,

4.7 Appendix

$$K_1^f = 81648 E_a E_s H G^2 \qquad (A.1)$$

$$K_2^f = -145152 b E_a E_s H G^2 \qquad (A.2)$$

$$K_3^f = 48384 b E_a H (2a E_a + 3b E_s) G^2 \qquad (A.3)$$

$$K_4^f = -145152 a E_a E_s H G^2 \qquad (A.4)$$

$$K_5^f = 96768abE_aE_sHG^2 \tag{a.5}$$

$$K_6^f = 48384aE_sH(3aE_a + 2bE_s)G^2 \tag{A.6}$$

$$K_7^f = 4608b^2E_aG^2[5a^3E_aE_s(1+v_a) + b(17a^2E_a^2 + 18abE_aE_s + 6bH^2E_s^2)(1+v_s)] \tag{A.7}$$

$$
\begin{aligned}
K_8^f = &-1152abE_aE_sG\{a^2[3a^2(3a+32b)E_a^2 + ab(39a+352b)E_aE_s \\
&+256b^3E_s^2](1+v_a) + b^2(8aE_a+3bE_s)[a(11a+32b)E_a \\
&+b(5a+32b)E_s](1+v_s)\}
\end{aligned}
\tag{A.8}
$$

$$
\begin{aligned}
K_9^f = &\ 72a^2\{2aE_s[3a^4(55a^2+416ab+1024b^2)E_a^4 + 6a^3b(69a^2+768ab \\
&+2560b^2)E_a^3E_s + a^2b^2(349a^2+6432ab+30208b^2)E_a^2E_s^2 \\
&+1024ab^4(3a+26b)E_aE_s^3 + 8704b^6E_s^4](1+v_a) + bE_a[315a^6E_a^4 \\
&+1680a^5bE_a^3E_s + 2a^2b^2(1979a^2+1760ab+2560b^2)E_a^2E_s^2 + 40ab^3(89a^2 \\
&+128ab+256B^2)E_aE_s^3 + 5b^4(235a^2+320ab+1024b^2)E_s^4](1+v_s)\}
\end{aligned}
\tag{A.9}
$$

$$K_{10}^f = 864bE_aE_sG^2[15a^3E_av_a + b(35a^2E_a + 32abE_a + 12b^2E_s)v_s] \tag{A.10}$$

$$K_{11}^f = 1152b^2E_aG^2\{-15a^2E_sv_a + [a^2(35a+68b)E_a^2 + 72ab^2E_aE_s + 24b^3E_s^2]v_s\} \tag{A.11}$$

$$K_{12}^f = -1152abE_aE_sG^2[3a^2(4aE_a - bE_s)v_a + b(35a^2E_a + 32abE_a + 12b^2E_s)v_s] \tag{A.12}$$

$$
\begin{aligned}
K_{13}^f = &\ 16b^2E_aG^2[a^2b(315a^2+1008ab+992b^2)E_a^2 \\
&+a(35a^4+504ab^3+1056b^4)E_aE_s + 228b^5E_s^2]
\end{aligned}
\tag{A.13}
$$

$$
\begin{aligned}
K_{14}^f = &-108aE_aE_sG\{3a^2[3a^2(31a+144b)E_a^2 + ab(123a+1024b)E_aE_s \\
&+592b^3E_s^2]v_a + 5b[21a^3(3a+16b)E_a^2 + ab(105a^2+940ab+128b^2)E_aE_s \\
&+4b^3(145a+32b)E_s^2]v_s\}
\end{aligned}
\tag{A.14}
$$

$$
\begin{aligned}
K_{15}^f = &\ 288abE_aG^2\{3a^2E_s(27aE_a+37bE_s)v_a \\
&-[105a^3E_{a2} + ab(175a+64b)E_aE_s + 24b^3E_s^2]v_s\}
\end{aligned}
\tag{A.15}
$$

$$
\begin{aligned}
K_{16}^f = &\ 288a^2E_sG^2[3a(16a^2E_a^2+13abE_aE_s - 13b^2E_s^2)v_a \\
&+5bE_a(21a^2E_a+35abE_s+8b^2E_s)v_s]
\end{aligned}
\tag{A.16}
$$

$$K_{17}^f = -8abE_aG^2[189a^3b(5a+8b)E_a^2 + a(165a^4 + 1575a^2b^2$$
$$+3780ab^3 + 928b^4)E_aE_s + 5b(47a^4 + 252ab^3 + 96b^4)E_s^2] \tag{A.17}$$

$$K_{18}^f = a^2[945a^6b(3a^2 + 24ab + 64b^2)E_a^5 + 9a^4(139a^5 + 1272a^4b + 4474a^3b^2$$
$$+11256a^2b^3 + 39648ab^4 + 7168b^5)E_a^4E_s + a^2b(3162a^6 + 40584a^5b$$
$$+152259a^4b^2 + 143640a^3b^3 + 736448a^2b^4 + 251392ab^5 + 20480b^6)E_a^3E_s^2$$
$$+ab^2(2051a^6 + 47944a^5b + 252736a^4b^2 + 63000a^3b^3 + 626400a^2b^4$$
$$+302080ab^5 + 40960b^6)E_a^2E_s^3 + 8b^4(2351a^5 + 24448a^4b + 23400a^2b^3$$
$$+14400ab^4 + 2560b^5)E_aE_s^4 + 56416a^3b^6E_s^5] \tag{A.18}$$

$$K_1^m = 435456E_aE_sH^2(3aE_a + 5bE_s) \tag{A.19}$$
$$K_2^m = -145152aE_aE_sH^2[a(13a+16b)E_a + b(25a+32b)E_s] \tag{A.20}$$

$$K_3^m = 12096aE_sH^2[3a^2(21a^2 + 64ab + 64b^2)E_a^2$$
$$+ab(125a^2 + 384ab + 448b^2)E_aE_s + 128b^4E_s^2] \tag{A.21}$$
$$K_4^m = 72a^2\{2aE_s[3a^4(67a^2 + 224ab + 1024b^2)E_a^4$$
$$+6a^3b(65a^2 + 256ab + 2560b^2)E_a^3E_s + a^2b^2(209a^2 + 1376ab$$
$$+30208b^2)E_a^2E_s^2 + 512ab^4(a+52b)E_aE_s^3 + 8704b^6E_s^4](1+v_a)$$
$$+bE_a[2835a^6E_a^4 + 15120a^5bE_a^3E_s + 2a^2b^2(15839a^2 + 3808ab$$
$$+3584b^2)E_a^2E_s^2 + 8ab^3(3615a^2 + 1792ab + 1792b^2)E_aE_s^3$$
$$+b^4(9575a^2 + 6720ab + 7168b^2)E_s^4](1+v_s)\} \tag{A.22}$$

$$K_5^m = -3456aE_aE_sH^2\{3a^2(3a^2E_a + 27abE_a + 37b^2E_s)v_a$$
$$+7b^2(15a^2E_a + 30abE_s + 8b^2E_s)v_s\} \tag{A.23}$$

$$K_6^m = 576a^2E_sH^2\{3a[a\ (11a^2 + 121ab + 128b^2)E_a^2 + 13ab^2(11a+8b)E_aE_s$$
$$-104b^4E_s^2]v_a + 7bH2(5a+8b)E_a(15a^2E_a + 30abE_s + 8b^2E_s)v_s\} \tag{A.24}$$

$$K_7^m = a^2 [945a^6 b(3a^2 + 24ab + 64b^2)E_a^5 + 9a^4(139a^5 + 1272a^4 b + 4474a^3 b^2$$
$$+ 11256a^2 b^3 + 39648ab^4 + 7168b^5)E_a^4 E_s + a^2 b(3162a^6 + 40584a^5 b$$
$$+ 152259a^4 b^2 + 143640a^3 b^3 + 736448a^2 b^4 + 251392ab^5 + 20480b^6)E_a^3 E_s^2$$
$$+ ab^2(2051a^6 + 47944a^5 b + 252736a^4 b^2 + 63000a^3 b^3 + 626400a^2 b^4$$
$$+ 302080ab^5 + 40960b^6)E_a^2 E_s^3 + 8b^4(2351a^5 + 24448a^4 b + 23400a^2 b^3$$
$$+ 14400ab^4 + 2560b^5)E_a E_s^4 + 56416a^3 b^6 E_s^5]$$

(A.25)

where

$$G = a^2 E_a + 4abE_a + 4b^2 E_s$$
$$H = aE_a + bE_s$$

Chapter 5

A Mechanical Approach to Interfacial Stress Alleviation in an Integrated Induced Strain Actuator/Substructure System

5.1 Introduction

Recent developments in the implementation of intelligent material systems and structures generally involve highly integrated, surface-bonded or embedded induced strain actuators as energy input devices or actuating elements in various engineering applications (Bailey and Hubbard, 1985; Crawley and de Luis, 1987; Chaudhry and Rogers, 1991). The means of integrating the actuators and the host substructures is primarily by bonding. The bonding interfaces, therefore, serve as the media for transferring the actuation mechanism. Thus, desirable interfaces must have a high efficiency in transferring the induced actuation strains of the actuators to the substructures, and have a sufficiently high fatigue endurance limit to provide a strong bond to ensure structural integrity.

Two vastly different approaches can be used to achieve these objectives. The first is within the context of material science and engineering, which focuses on methods to increase the stiffness and strength of the interfacial bonds. This approach generally involves the study of the chemical mechanisms the adhesion between heterogeneous

148

materials. The second approach involves a mechanical approach which seeks the design criteria for optimum configuration of the actuators to increase the efficiency of the actuation transfer and reduce the interfacial stresses. This approach requires an understanding of the mechanics of the mechanical interaction between the actuators and the substructures. The present study will be confined to the mechanical approach to designing an actuator configuration that can alleviate the high stress intensity at the interfaces and the free edges of the actuator.

The mechanism of the mechanical interaction between the actuators and the substructures has been modeled analytically by Crawley and de Luis (1987) and Im and Atluri (1989) using one-dimensional analysis based on the shear lag assumption. It was shown that the actuation forces/moments are transferred solely by the interfacial shear stresses localized near the end zones of the actuators. It was concluded that in order to achieve effective induced strain transfer from the actuator to the substructure, a high interfacial shear stress state is desirable. Thus, the issue of interfacial failure due to high intensity of this stress component has never been addressed.

A refined model based on a two-dimensional elasticity formulation was recently presented by Lin and Rogers (1993a, 1993b). This model more accurately describes the stress field in both the actuator and the substructure, particularly near the end zones or the free edges of the actuator. The interfacial shear and peeling stress distributions were correctly predicted. It was shown that the presence of the free edges of the actuator raises the intensity of the interfacial shear and peeling stresses near the actuator end zones.

Recently, Walkers et al. (1993) conducted a finite element analysis on various actuator edge configurations in an attempt to reduce interfacial shear and peeling stress intensity. It was demonstrated that using various designs of end caps and partial electrode configurations at the ends of the actuators can noticeably reduce the interfacial shear and peeling stresses. Nevertheless, the mechanics underlying this alleviation has not been discussed.

The objective of the present study is to develop the theoretical basis for the mechanics of the interfacial stress alleviation mechanism. The rationale on the design of reconfigured actuator free edges to alleviate interfacial shear and peeling stresses is first presented. A new actuator configuration with "inactive" edges is proposed. The issues related to the actuator efficiency brought about by the addition of inactive edges are discussed. Finally, the effectiveness of this new actuator configuration is characterized by analytical modeling and finite element analysis.

5.2 Theory

Consider a beam structure of length $2L$ with induced strain actuators of length $2l$ symmetrically bonded on the outer surfaces of the beam as shown in Fig. 5.1. The thickness of the actuator and beam are denoted by a and $2b$, respectively. The actuation mechanism transferred from the actuator to the beam substructure can be easily illustrated
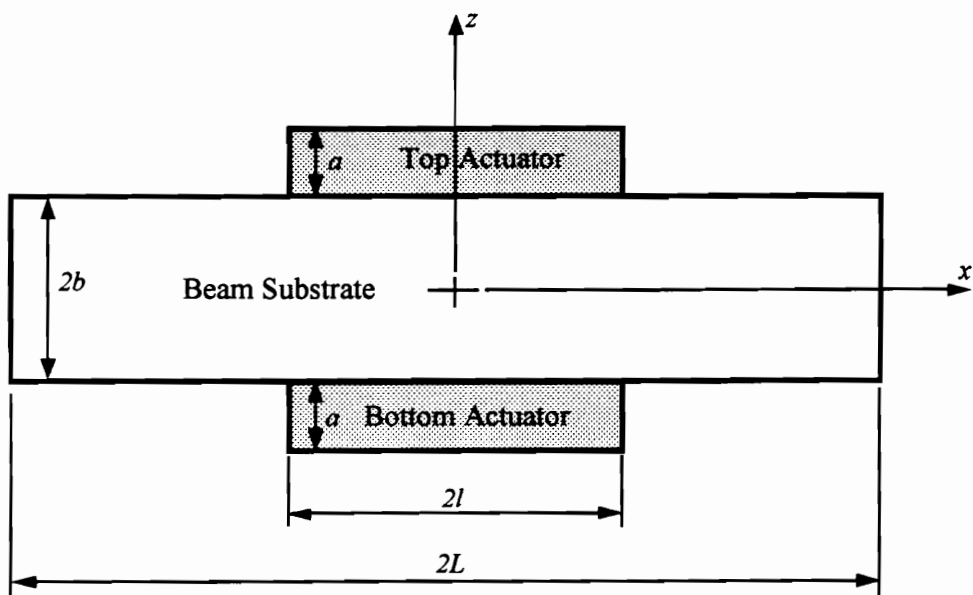
Figure 5.1. Schematic configuration of the induced strain actuator/beam substructure system.

using one-dimensional analytical scheme based on the shear lag assumption.

Consider a free body diagram cut from the top actuator as the actuators are activated. Based on the framework of the one-dimensional shear lag theory, the forces acting on this free body are depicted in Fig. 5.2(a), where F_a indicates the resulting normal force in the actuator, and S is the shear force on the interface. Note that the normal force F_a is equal in magnitude and opposite in sign to the effective force transferred to the beam substructure. Thus, the quantity F_a can equivalently represent the resulting actuation force in the beam substructure. In this configuration, the free edge effect is apparent, where the ends of the actuator have a force-free boundary condition and the actuation force F_a is solely transferred by the interfacial shear force S. In order to achieve a higher effective force level, a larger interfacial shear force is needed.

Now, if the free edge of the actuator is by some means reconfigured to reduce the free edge effect, the interfacial shear force can be correspondingly reduced, see Fig. 5.2(b). In other words, part of the force transfer can be accomplished through the ends of the actuator in addition to the interface. In this configuration, the actuation force is transferred not only by the interfacial shear force, S^*, but also the normal force on the ends of the actuator, F_e. Therefore, a lower interfacial shear force level is needed, i.e., $S^* < S$, to achieve the same level of effective force on the beam substructure F_a as that depicted in Fig. 5.2(a).
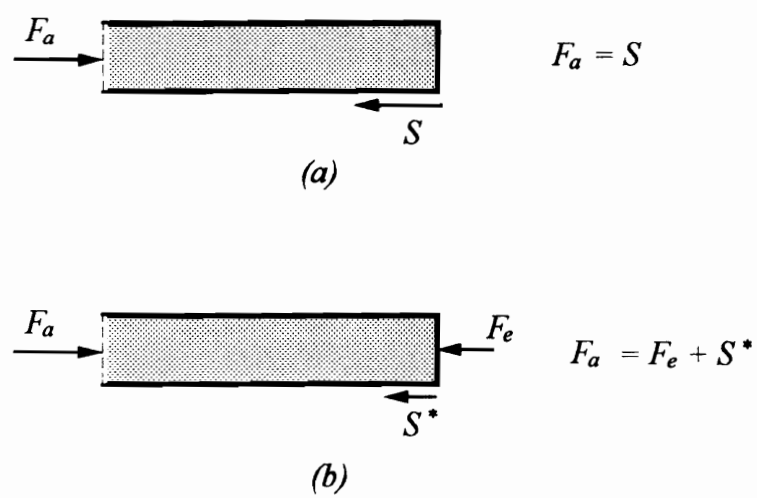
Figure 5.2. Free-body diagram of the top actuator: (*a*) with free edge effect, (*b*) with reduced free edge effect.

The mechanism of alleviating the interfacial stresses by reducing the degree of the free edge effect can be more vigorously analyzed based on equilibrium considerations using a two-dimensional analytical scheme. Consider the integrated induced strain actuator/beam substructure system of Fig. 5.1. The interfacial stress distributions along the x-axis which satisfy the stress-free boundary condition at the ends of the actuator are illustrated in Fig. 5.3.

The axial normal stress in the top actuator in general can be expressed as:

$$\sigma_{x(at)}(x,z) = f(z)g(x), \tag{1}$$

where subscript (at) denotes the quantity of the top actuator, and $f(z)$ and $g(x)$ are arbitrary functions depending solely on z and x, respectively. The first equation of equilibrium requires:

$$\sigma_{x,x} + \tau_{xz,z} = 0. \tag{2}$$

Substituting Eq. (1) into (2) for σ_x and integrating with respect to z, the shear stress field is obtained:

$$\tau_{xz(at)}(x,z) = -g'(x)\int f(z)dz + c_1(x), \tag{3}$$

where $c_1(x)$ is an arbitrary function depending on x to be determined by the boundary conditions.
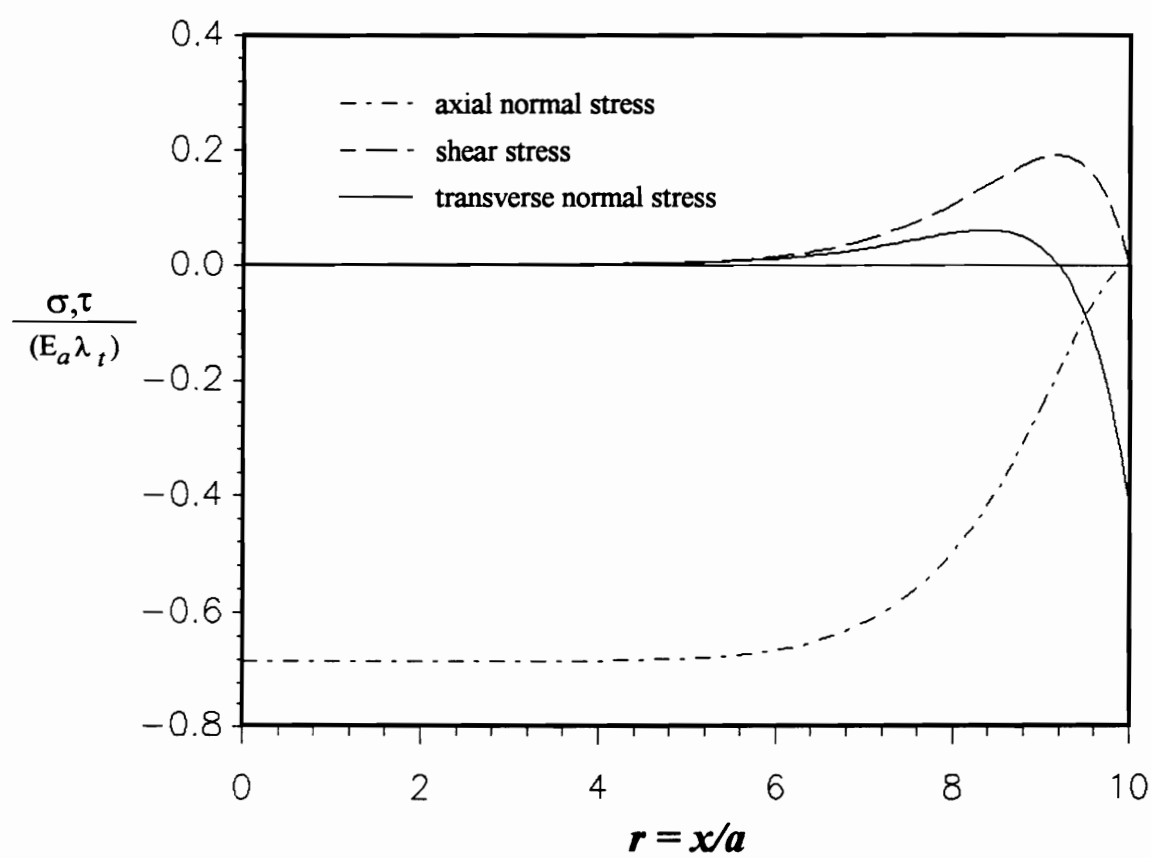
154

Figure 5.3. Stress distribution along the x axis at the interface.

The shear stress free boundary condition on the outer lateral surface of the top actuator yields:

$$\tau_{xz(at)}(x, a+b) = 0. \tag{4}$$

Imposing this boundary condition, the shear stress field is defined by:

$$\tau_{xz(at)}(x,z) = g'(x)\{[\int f(z)dz]_{z=a+b} - \int f(z)dz\} = g'(x)F(z). \tag{5}$$

The expression of the shear stress at the interface is then obtained:

$$\tau_{xz(at)}(x,b) = g'(x)F(b). \tag{6}$$

In the above, $g'(x)$, which represents the slope of the axial normal stress in the x direction, can be regarded as a factor that contributes to the variation of the interfacial shear stress in the x axis and its magnitude. It is apparent that the variation of the axial normal stress in the x axis, or more precisely the slope, controls the magnitude and distribution of the interfacial shear stress. In the case of an actuator with free edges, the slope of the axial normal stress increases dramatically near the end zones of the actuator due to the free edge effect. The interfacial shear stress, therefore, yields a noticeable intensity localized at the free end zones. Now, if the increase of the axial normal stress near the actuator edges can be minimized by some means, the intensity of the interfacial shear stress can then be accordingly alleviated. In the extreme, the interfacial shear stress will vanish in the case in which the axial normal stress is uniform in x, i.e., $g'(x) = 0$.

The transverse normal stress field can be obtained likewise by considering the second equilibrium equation:

$$\tau_{xz,x} + \sigma_{z,z} = 0. \tag{7}$$

Substituting Eq. (5) into (7) for τ_{xz} and integrating with respect to z, the transverse normal stress field is obtained:

$$\sigma_{z(at)}(x,z) = -g''(x)\int F(z)dz + c_2(x). \tag{8}$$

Imposing the transverse normal stress free boundary condition on the top outer lateral surface,

$$\sigma_{z(at)}(x,a+b) = 0, \tag{9}$$

the final expression of the transverse normal stress field becomes:

$$\sigma_{z(at)}(x,z) = g''(x)\{[\int F(z)dz]_{z=a+b} - \int F(z)dz\} = g''(x)H(z). \tag{10}$$

The transverse normal stress at the interface, or the peeling stress, is given by:

$$\sigma_{z(at)}(x,b) = g''(x)H(b). \tag{11}$$

Similarly, the slope of the shear stress with respect to x, $g''(x)$, controls the magnitude and variation of the peeling stress in the x direction. As shown in Fig. 5.3, the interfacial shear stress has the highest slope at the actuator edges, yielding a maximum interfacial peeling stress right at the ends of the actuator. By the same argument, if the free edge effect can be somehow diminished, resulting in a less dramatic change in the slope of the interfacial shear stress, the intensity of the interfacial peeling stress can then be alleviated.

Based on the above analysis, the interfacial shear and peeling stresses can be reduced as the axial normal stress becomes more uniform with respect to x. The non-uniform field of the axial normal stress is shown localized near the end zones of the actuator due to the free edge effect. Thus, as the degree of the free edge effect is reduced, the desired interfacial shear and peeling stress alleviation can be achieved.

One of the most direct approaches is to incorporate inactive edges at the ends of the actuators, as shown in Fig. 5.4. The inactive edges have the same thickness as the actuators and a length of e. These inactive edges provide a path for part of the actuation mechanism to be transferred from the ends of the actuators to the beam substructure from a force-transferring point of view. Alternatively, they also can be regarded as blocking elements which will exert axial normal stresses on the actuator edges to reduce the free edge effect.

Actuators with inactive edges can be easily manufactured. The inactive edges can be composed of different material from the actuator with comparable or higher stiffness, but insensitive to the activation stimulus. The inactive edges can also be created by blocking the activation stimulus from the areas near the actuators' edges. For example, in the case of piezoelectric actuators, the inactive edges can be implemented simply by removing the electrode on the surfaces near the end zones of the actuators.

With the addition of inactive edges, the efficiency of the actuators needs to be characterized. In particular, the issues concerning the effectiveness of the actuation
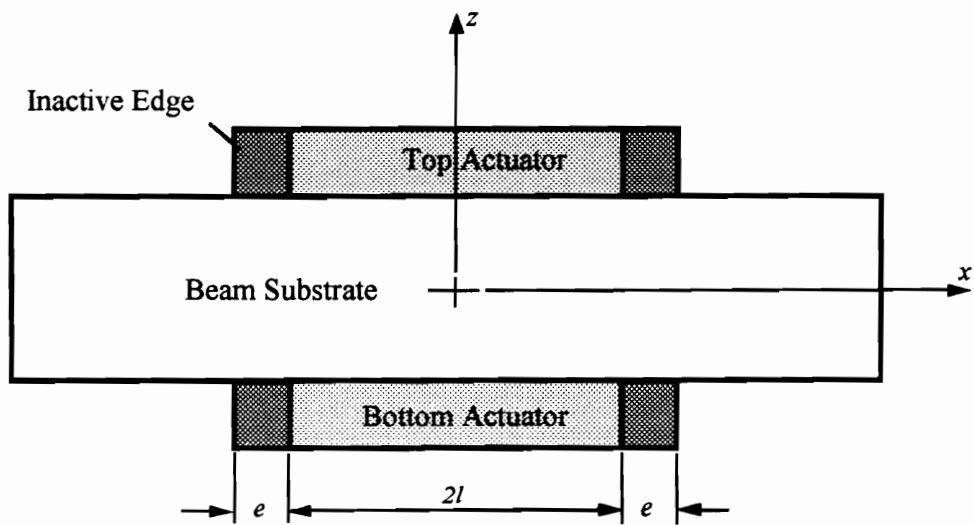
158

Figure 5.4. Schematic configuration of the proposed actuator with inactive edges.

force/moment transfer and the efficiency of the interfacial shear and peeling stress alleviation need to be addressed. Performance characterization of the proposed actuator configuration using both analytical and finite element models is discussed in the following sections.

5.3 Analytical modeling

In order to characterize the effectiveness of the proposed actuator configuration, the refined analytical model by Lin and Rogers (1993a) is used. The model was developed based on the plane stress formulation of the theory of elasticity for a beam structure with symmetrically surface-bonded actuator patches, as shown in Fig. 5.1. The whole-field stress distribution in each constituent was obtained in an approximate manner in closed form by the principle of complementary energy. The model is capable of describing the edge effect and determining the interfacial shear and peeling stress distribution.

The stress field in the top actuator was derived and has the form:

$$\sigma_{x(at)}(x,z) = -E_a \lambda_t + (\frac{a+b-z}{a})^2 \frac{E_a}{E_s} \sigma_{its}(x)$$
$$-\frac{(b-z)(2a+b-z)}{a^2} \sigma_{ot}(x)$$

$$(12.1)$$

$$\tau_{xz(at)}(x,z) = \frac{1}{3a^2} \{ \frac{E_a(a+b-z)^3}{E_s} \sigma'_{its}(x)$$
$$+(a+b-z)[2a^2 - 2ab - b^2 + 2(a+b)z - z^2]\sigma'_{ot}(x)\}$$

$$(12.2)$$

$$\sigma_{z(at)}(x,z) = \frac{1}{12a^2} \{ \frac{E_a(a+b-z)^4}{E_s} \sigma_{its}''(x) + (a+b$$
$$-z)^2 [5a^2 - 2ab - b^2 + 2(a+b)z - z^2] \sigma_{ot}''(x) \}, \tag{12.3}$$

where

$$\sigma_{its}(x) = \frac{1}{2(aE_a + bE_s)[aE_a(a+4b) + 4b^2 E_s]} \{ -3a^2 E_a E_s (aE_a + 2bE_s) \lambda_b$$
$$+ 3aE_a E_s [aE_a(3a+8b) + 2bE_s(a+4b)] \lambda_t$$
$$- 3a^2 E_a E_s (aE_a + 2bE_s) \lambda_b - 4bE_s [aE_a(a+4b) + 4b^2 E_s] \sigma_c(x)$$
$$- aE_s [aE_a(7a+16b) + bE_s(5a+16b)] \sigma_{ot}(x) + a^2 E_s (3aE_a + 5bE_s) \sigma_{ob}(x) \}$$

In the above, E_a and E_s are the Young's modulus of the actuator and the beam substructure, respectively, and λ_t and λ_b are the free induced strains in the top and bottom actuators, respectively. The quantities $\sigma_{ot}(x)$, $\sigma_{ob}(x)$, and $\sigma_c(x)$ are the axial normal stress at the outer fiber of the top and bottom actuator and at the center of the beam, respectively; $\sigma_{its}(x)$ is the axial normal stress of the beam at the top interface; and the prime indicates the derivative with respect to x.

The only unknown quantities in the stress field of Eq. (12) are $\sigma_{ot}(x)$ and its derivatives for the case of pure bending actuation, i.e., $\lambda_b = -\lambda_t$, and has the solution given by:

$$\sigma_{ot}(x) = \frac{D_1^b}{A_3^b} + \sum_{i=1}^{4} p_i^b (\exp)^{\alpha_i^b x}, \tag{13}$$

where A_i^b $(i = 1,3)$ and D_1^b are constants related to the material properties and geometry of the actuator and beam, and have been described by Lin and Rogers (1993a). In the above, α_i^b $(i = 1,4)$ are the roots of the characteristic equation:

$$A_1^b (\alpha^b)^4 + A_2^b (\alpha^b)^2 + A_3^b = 0, \tag{14}$$

and $P_i^b (i = 1, 4)$ are arbitrary constants to be determined by the end traction condition at the edges of the actuator.

Since the inactive edges of the actuator were not included in the model, their presence is simulated by prescribing different boundary traction conditions at the actuators' edges, i.e., $x = \pm l$. Three boundary traction conditions (B.C.) are used:

$$(1) \quad \sigma_{x(at)}(\pm l, a+b) = 0, \qquad\qquad \tau_{x(at)}(\pm l, z) = 0 \tag{15.1}$$

$$(2) \quad \sigma_{x(at)}(\pm l, a+b) = 0.5\sigma_{x(at)}(0, a+b), \quad \tau_{x(at)}(\pm l, z) = 0 \tag{15.2}$$

$$(3) \quad \sigma_{x(at)}(\pm l, a+b) = \sigma_{x(at)}(0, a+b), \qquad \tau_{x(at)}(\pm l, z) = 0. \tag{15.3}$$

B.C. (1) represents the actuator without inactive edges, where the free edge effect is present. B.C. (3) simulates the actuator with inactive edges which have a stiffness capable of transferring the maximum fraction of the actuator's induced strain to the beam substructure over the entire length of the actuator. In other words, the free edge effect is totally eliminated in this case. Finally, B.C. (2) models the actuator with inactive edges which have a stiffness resulting in an average effect of the extreme cases of B.C. (1) and (3).

The effective moments transferred from the actuators to the beam substrate under pure bending actuation for the three cases of boundary traction are shown in Fig. 5.5. The
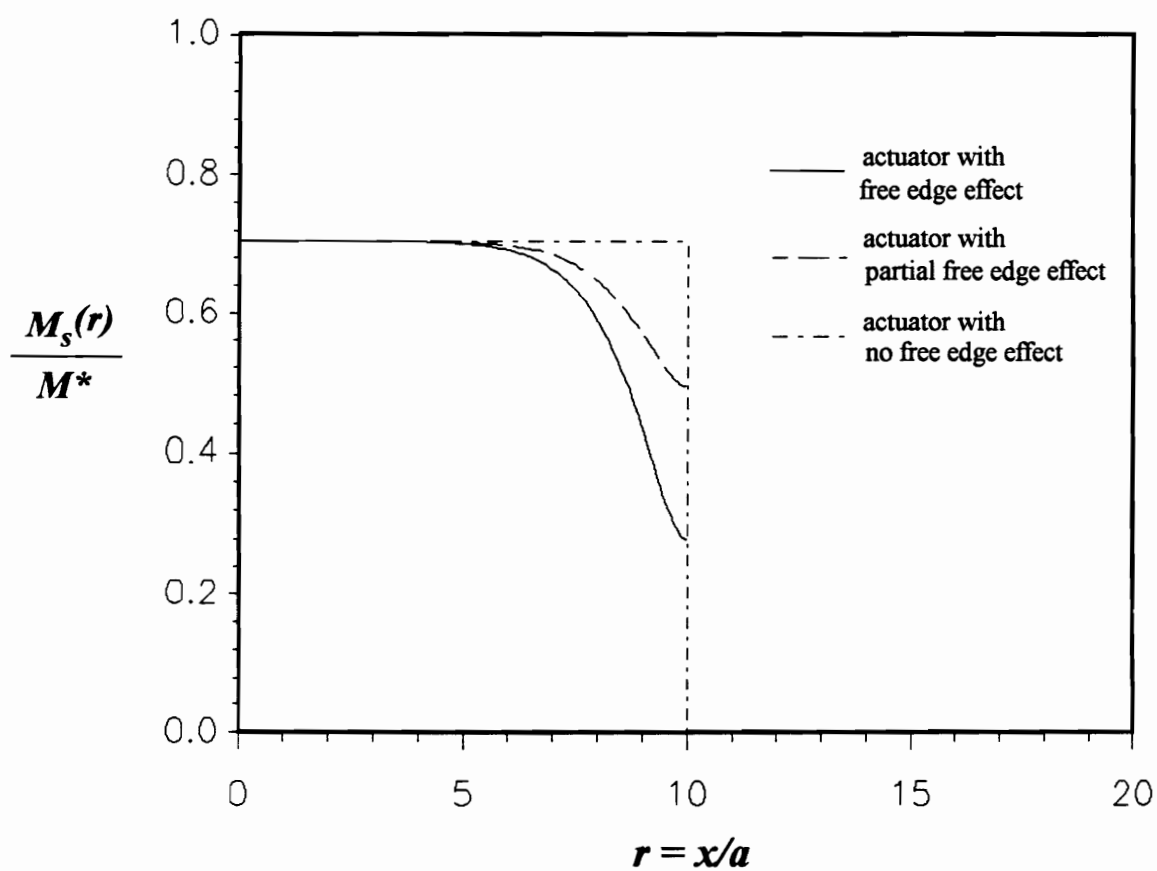
162

Figure 5.5. Effective moment distribution along the x axis under different boundary traction conditions as obtained from the analytical model.

actuator/beam structure geometric configuration of $b/a = 3$, $l/a = 10$, and $L/a = 20$ is used. The material properties are selected to be $v_s/v_a = 0.73$ and $E_s/E_a = 3.29$, which are comparable to a steel beam with piezoceramic actuators. The quantity of the effective moment is normalized with respect to the moment that the total blocking force of the actuators produce about the neutral axis, i.e., $M^* = 2aE_a\lambda_t(a/2+b)$, and the x axis is nondimensionalized with respect to the thickness of the actuator.

It is evident that the magnitude of the effective moment is not affected with the addition of inactive edges in a location away from the ends of the actuator. However, a higher level of the effective moment is shown near the end zones. In the extreme case, i.e., B.C. (3), the free edge effect is totally reduced, resulting in a uniform effective moment along the entire length of the actuator, which represents the maximum achievable actuation transfer mechanism.

Figure 5.6 shows the corresponding interfacial shear and peeling stress distribution along the x axis. The magnitude of the stresses is normalized with respect to the blocking stress of the actuators, i.e., $E_a\lambda_t$. It is shown that with the inactive edges, the interfacial shear and peeling stresses can be significantly reduced. In the case where a uniform axial normal stress field along the x axis is obtained, the interfacial shear and peeling stresses vanish through the entire interface.
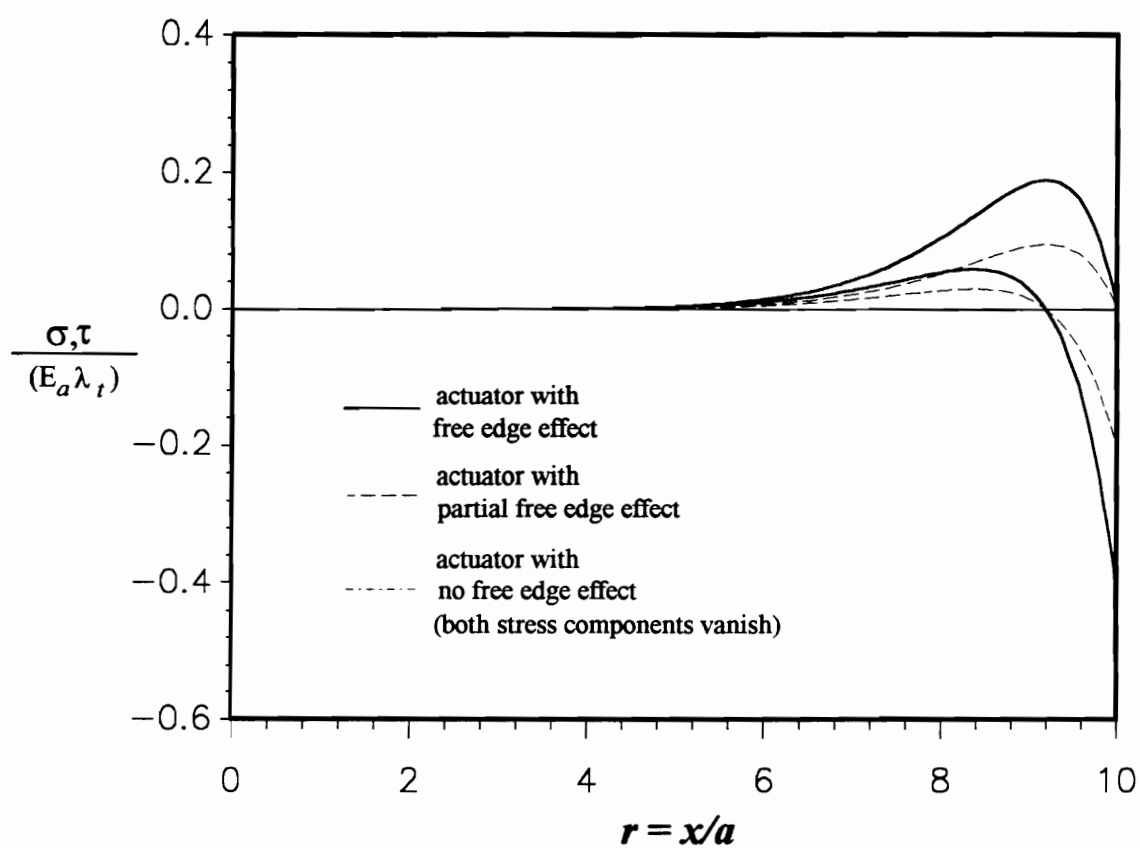
Figure 5.6. Interfacial shear and peeling stress distribution under different boundary traction conditions as obtained from the analytical model.

165

In summary, the analytical modeling demonstrates that inactive edges can significantly reduce the interfacial shear and peeling stresses and slightly increase the actuation transfer mechanism near the actuator ends. The free edge effect can be reduced by the proposed actuator configuration in which relatively stiffer inactive edges are desirable.
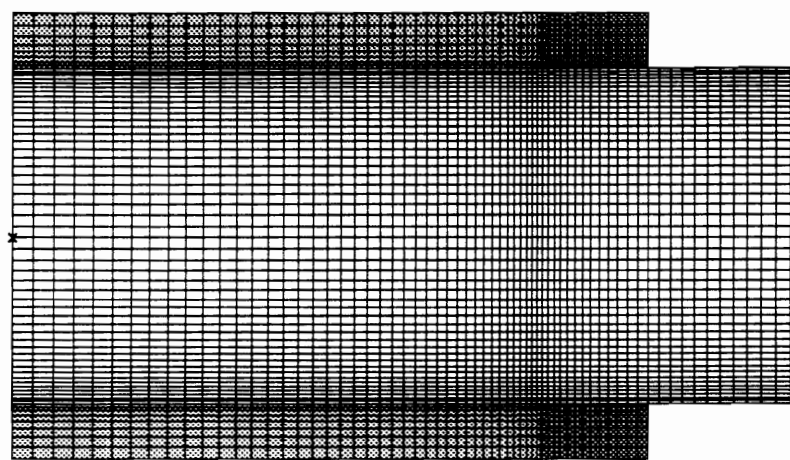
5.4 Finite element modeling

The effectiveness of actuators with inactive edges is also characterized using finite element models. Specifically, the geometric effect of the inactive edges is investigated. Figure 5.7 shows the finite element meshes used to model the actuators with and without inactive edges of length $2a$, where the geometric configuration of $b/a = 3$, $l/a = 10$, and $L/a = 15$ is used. The material properties chosen are $v_s / v_a = 0.73$ and $E_a / E_s = 3.29$. The same material properties as those of the actuator are assigned for the inactive edges. The influence of three different lengths of inactive edges, i.e., $e = a$, $e = 2a$, and $e = 3a$, are investigated. Note that the same element size bias is used for all the models to eliminate mesh and element size effects in the finite element model.

The plane stress linear isoparametric elements were used for all the constituents. Since the characteristic induced strains of the actuator resemble the thermal expansion effects of a structural material, a "fictitious" thermal expansion coefficient was assigned to the actuators, while the beam and inactive edges are insensitive to thermal effects. The desired induced strain level was then obtained by applying a uniform temperature field on
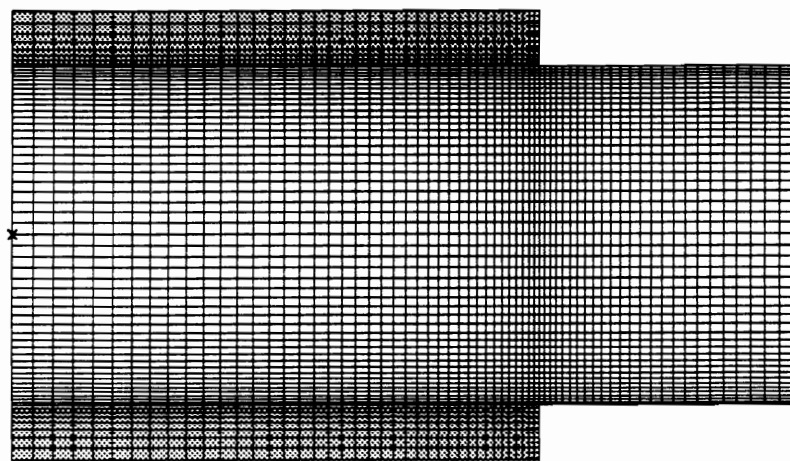
Figure 5.7. Finite element models for the actuator/beam substructure: (*a*) without inactive edges, (*b*) with inactive edges of length 2*a*.

the model. The analyses were performed using the ABAQUS finite element package for solution and IDEAS for pre- and post-processing.

The effective moments transferred from the actuators to the beam substructure under pure bending actuation are shown in Fig. 5.8. No effect is evident for the effective moment level in the area away from the actuator end zones, while the magnitude of the effective moment increases near the actuator ends for the actuators with inactive edges. Further increase of the effective moment is not shown by increasing the length of e from $2a$ to $3a$, indicating an optimum length of the inactive edge.

Figure 5.9 depicts the corresponding interfacial shear and peeling stress distribution. It should be noted that the shear stress distribution obtained from the current finite element models does not satisfy the stress-free boundary condition. Nevertheless, for the current study the relative stress level induced by different actuator configurations is of the primary interest. The results should therefore indicate the effectiveness of the interfacial shear stress alleviation. It was shown that both the interfacial shear and peeling stresses are significantly reduced for actuators with inactive edges. Increasing the length of the inactive edges longer than $2a$ does not further reduce the shear stress level. Although further decrease is shown in the peeling stress, the stress level is low enough to be neglected.
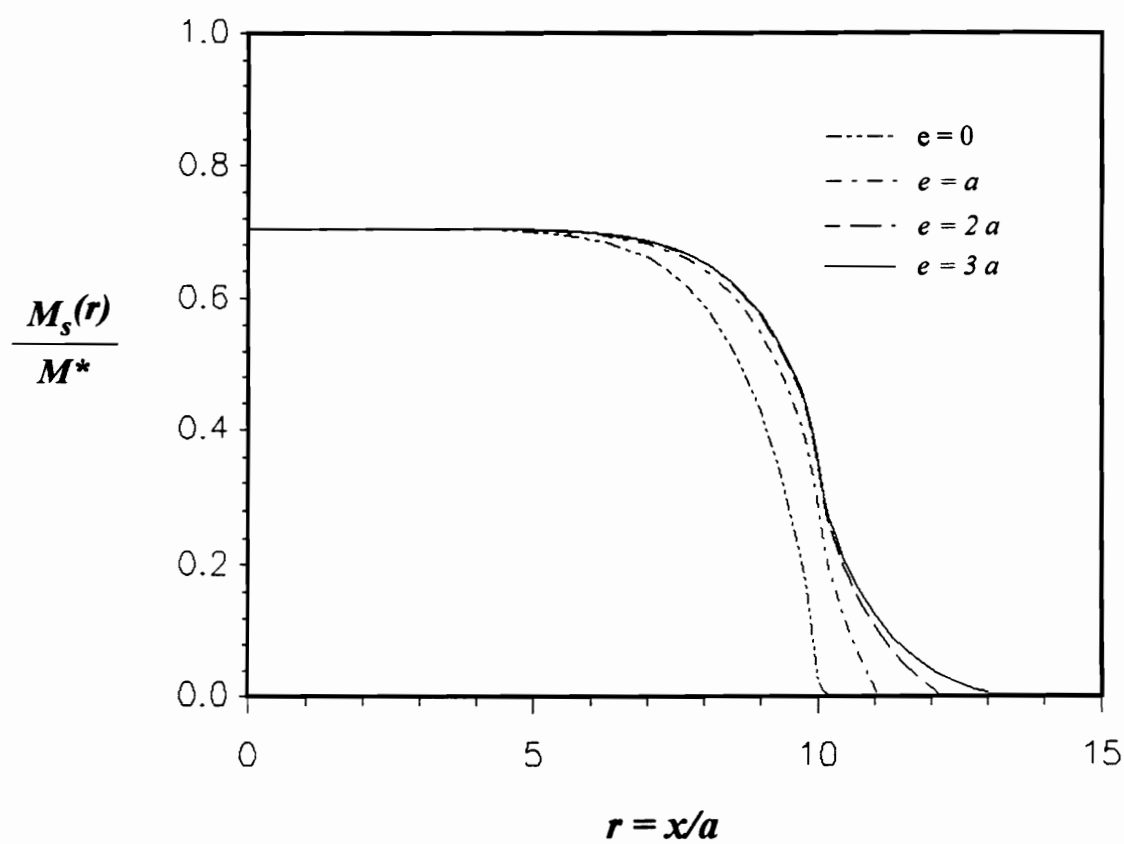
Figure 5.8. Effective moment distribution along the x axis for cases of different inactive edge lengths as obtained from finite element analysis.
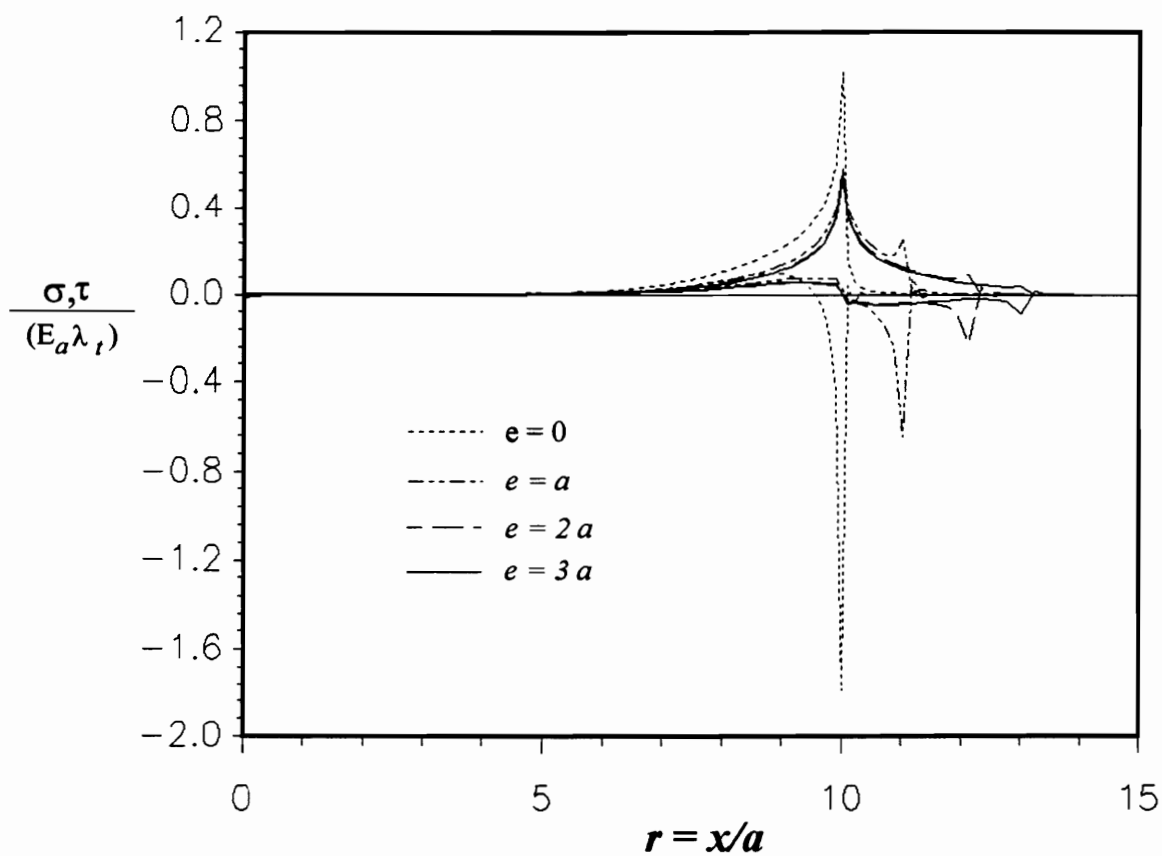
Figure 5.9. Interfacial shear and peeling stress distribution for cases of different inactive edge lengths as obtained from finite element analysis.

It can be concluded from this analysis that inactive edges on actuators can significantly reduce the interfacial shear and peeling stresses and slightly increase the effective moment in the actuator end zones. An optimum length of the inactive edge is found to be about a two actuator thickness for the present actuator/beam substructure configuration.

5.5 Conclusion

The basis of the mechanism underlying interfacial stress alleviation is discussed. It is demonstrated that the interfacial shear and peeling stress concentration localized at the ends of induced strain actuators can be alleviated by reducing the degree of the free edge effect. A new actuator configuration is proposed to eliminate the free edge effect by including inactive edges on the actuators. Both analytical and finite element modeling of the suggested actuator configuration show that the interfacial shear and peeling stresses can be significantly reduced without sacrificing the effectiveness of the transfer of the actuation mechanism. An optimum length of the inactive edges is found from finite element analysis to be about a two-actuator thickness, and inactive edges with a relatively higher stiffness than the actuator are desirable, as shown in the analytical model.

5.6 References

Bailey, T. and Hubbard Jr., J. E., 1985, "Distributed Piezoelectric-Polymer Active Vibration Control of a Cantilever Beam, "Journal of Guidance and Control, Vol. 8, No. 5, pp. 605-611.

Chaudhry, Z., and Rogers, C. A., 1991, "Bending and Shape Control of Beams Using SMA Actuators," Journal of Intelligent Material Systems and Structures, Vol. 2, No. 4, pp. 581-602.

Crawley, E. F., and de Luis, J., 1987, "Use of Piezoelectric Actuators as Elements of Intelligent Structures," AIAA Journal, Vol. 25, No. 10, pp. 1373-1385.

Im, S,, and Atluri, S. N., 1989, "Effects of a Piezo-Actuator on a Finitely Deformed Beam Subjected to General Loading," AIAA Journal, Vol. 27, No. 12, p.p. 1801-1807.

Lin, M. W., and Rogers, C. A., 1993a, "Modeling of the Actuation Mechanism in a Beam Structure with Induced Strain Actuators," Proceedings of the AIAA/ASME/AHS/ASC 34th SDM Conference, La Jolla, CA, April 19-22, 1993.

Lin, M. W., and Rogers, C. A., 1993b, "Actuation Response of a Beam Structure with Induced Strain Actuators," Proceedings of the Adaptive Structures and Material Systems Symposium, ASME Winter Annual Meeting, New Orleans, LA, November 28-December 3, 1993; in press.

Walker, J., Liang, C., and Rogers, C. A., 1993, "Finite Element Analysis of Adhesively-Bonded Piezoceramic Patches Implementing Modeling Techniques and Design Consideration to Reduce Critical Stresses," Proceedings of the AIAA/ASME/AHS/ASC 34th SDM Conference, La Jolla, CA, April 19-22, 1993.

Chapter 6

Conclusions and Recommendations

6.1 Conclusions

In this study, a theoretical elasticity model has been developed to correctly describe the transfer of the actuation mechanism in a surface-bonded induced strain actuator/beam substructure system. The model is based on the plane stress formulation of the theory of elasticity, and closed-form solutions were obtained by introducing some approximations and using the principle of stationary complimentary energy. The model was developed without reference to a specific induced strain and therefore can be used for different types of induced strain actuators, such as piezoelectrics, electrostrictors, magnetostrictors, shape memory alloys, etc. The model has also been extended to include the presence of adhesive bonding layers and applied external loads. This model correctly predicts the transfer of the actuation mechanism from the actuator to the host substructure and the resulting interfacial stress distributions; thus, the model can be used for efficient design of integrated structural systems. In addition, a new induced strain actuator configuration, which includes inactive edges on the ends of the actuators, has been proposed to alleviate the intensity of interfacial shear and peeling stresses.

The major conclusions from the study are summarized as follows:

- The model is capable of describing the effective actuation force/moment attenuation near the actuator edges which existing mechanical models, such as the pin-force and the Euler-Bernoulli models, fail to describe. The results obtained from the current model in predicting the effective force/moment transferred from the actuator to the substructure agree very well with those of finite element analysis.

- The interfacial shear stress distribution obtained from the current model satisfies stress-free boundary conditions at the ends of the actuator, which the finite element results using four-node linear isoparametric elements are not able to satisfy. The existing mechanical models provide no information on these quantities. Thus, the current model gives the best approximation in determining the interfacial stress intensity.

- A relatively thick and/or compliant adhesive layer is less effective in the transfer of the actuation mechanism. However, such an adhesive layer can alleviate the intensity of the interfacial shear and peeling stresses that is beneficial to the structural integrity. It is evident that these factors need to be taken into account in design considerations of adhesive material and thickness.

- The influence of the applied external loads can be modeled separately from the actuation mechanism and the results can be superimposed with those of the induced strain actuation to yield the solution of the combined effects. The external loads alter the magnitude and distribution of the interfacial stresses and affect the performance and optimal actuator/substructure thickness ratio under induced bending actuation mode.

- The proposed actuator configuration, which includes inactive edges on the ends of the actuators to reduce the degree of free edge effect, can significantly alleviate intensive interfacial shear and peeling stresses localized in the actuator end zones without sacrificing the effectiveness the actuation mechanism. An optimum length for the

inactive edges, which have the same material properties as the actuator, was found to be about the thickness of two actuators.

6.2 Recommendations

The present analytical model describes quantitatively the mechanical interaction between the actuator and the substructure in an integrated induced strain actuator/substructure system. The model can be used to efficiently design such a structural system. In order to establish a wider scope of applicability of the model, further study and research efforts are recommended:

- Many applications implementing intelligent material systems and structures concepts involve the control of structural dynamic response; thus, consideration of the current formulation to model structural dynamic response should receive foremost attention in future studies.

- The characteristic induced strains of most actuators usually exhibit some degree of stress and field dependence and/or nonlinearity in a highly activated field state. Moreover, material anisotropy is a common characteristic found in many actuators. The constitutive laws including these effects need to be incorporated into the model.

- Extension of the model for laminate composite beams, plates, and shell host substructures, in which the anisotropic structural properties and the in-plane Poisson's effects need to be considered, should also be considered.

- Different actuator configurations and integrating schemes, such as embedding actuator patches, fibrous actuators, and particulate microactuators, are currently under

175

investigation in the development of intelligent material systems. Modification of the model to account for various geometries is needed for the various types of integrated structural systems.

- Experimental measurements of the induced stress fields in both the actuator and the host substructure are also recommended for the verification of the accuracy of the present analytical model, particularly on the prediction of interfacial stress distributions.

- For the proposed actuator configuration, which includes inactive edges at the ends of the actuators, experiments need to be carried out to determine the effect of the configuration on the fatigue life of adhesive bonds.

Vita

Mark W. Lin was born on November 13, 1959 in Pyng-Dong, Taiwan, The Republic of China. He started his undergraduate study in mechanical engineering at National Kaoshiung Institute of Technology, Kaohsiung, in September 1975, and received his diploma in June 1980. He subsequently entered Tamkang University, Taipei, and received the degree of B.S. in mechanical engineering in June 1982. After graduating, he worked at Kwang-Wu Institute of Technology, Taipei, as a teaching assistant for three years. In September 1985, he started his graduate study in the Department of Engineering Science and Mechanics at Virginia Tech, Virginia, U.S.A. and earned his Master's degree in engineering mechanics in August 1987. He then continued to pursue a doctoral degree in the Engineering Science and Mechanics Department. In the fall of 1988, he transferred to the Mechanical Engineering Department and started working in the area of intelligent materials systems. He graduated with a Ph.D. in mechanical engineering in July 1993.